UNIVERSITY OF CALIFORNIA

Santa Barbara

Influence of Large-Scale Circulation on the Dynamics of Extratropical Cyclones and Orographic Precipitation in High Mountain Asia

A dissertation submitted in partial satisfaction of the

requirements for the degree Doctor of Philosophy

in Geography

by

Forest Glen Cannon

Committee in charge:

Professor Leila M.V. Carvalho, Chair

Professor Charles Jones

Professor Bodo Bookhagen

Dr. George N. Kiladis

December 2016

The dissertation of Forest Glen Cannon is approved.

George N. Kiladis

Bodo Bookhagen

Charles Jones

Leila M.V. Carvalho, Committee Chair

October 2016

Influence of Large-Scale Circulation on the Dynamics of Extratropical Cyclones and Orographic Precipitation in High Mountain Asia

Forest Glen Cannon

ACKNOWLEDGEMENTS

I would like to express the deepest appreciation to my committee chair, Professor Leila M.V. Carvalho, who has continually supported my education, as well as the education of many others, with great enthusiasm. Without her guidance and persistent help, this dissertation would not have been possible. She is a true friend and incredible mentor.

I would like to thank my committee members, Professor Charles Jones, Professor Bodo Bookhagen, and Dr. George Kiladis, whose time, comments, and direction are greatly appreciated.

I would like to thank my friends, Dr. Rodrigo Bombardi, Dr. Jesse Norris and Dr. Andrew Hoell, for their support and mentorship throughout my graduate career. I would also like to acknowledge my brother, Doug, whose own accomplishments are a source of inspiration.

I am especially grateful to my parents, Patricia and Phil, who instilled in me a passion for science and nature, and taught me to take pride in hard work. Their endless support is the greatest reason for my accomplishments.

Finally, I am deeply thankful to Genelle for her love and patience.

Curriculum Vitae: Forest Glen Cannon
October 2016

Education

P.h.D. Geography - University of California, Santa Barbara, October 2016 (expected). Influence of Large-Scale Circulation on the Dynamics of Extratropical Cyclones and Orographic Precipitation in High Mountain Asia

M.A. Geography - University of California, Santa Barbara, September 2013. Himalayan Wintertime Climate Variability: Large-Scale Atmospheric Circulation and Regional Precipitation

B.A. Geography - University of California, Santa Barbara, September 2010

Research Experience

National Aeronautics and Space Administration - Earth and Space Science Fellowship. *Western Himalaya Climate Variability: Recent Trends in Large-Scale Circulation and Local Precipitation Impacts.* (Sept. 2013 - present)

Research Assistant - Earth Research Institute - University of California, Santa Barbara. *Climate Variability and Impacts on Regional Surface Runoff in High Asia Mountains.* (June 2012 - present)

Teaching Experience

Teaching Associate (Instructor of Record) – UC Santa Barbara Dept. of Geography

- Oceans and Atmosphere – Geog 3A (2016)

Teaching Assistant – UC Santa Barbara Dept. of Geography

- Oceans and Atmosphere – Geog 3A (2012)
- Maps and Spatial Reasoning – Geog 12 (2012)
- Tropical Meteorology – Geog 133 (2011)

Publications

Hoell, A., M. Barlow, **F. Cannon** 2016: The Oceanic Origins of Historical Southwest Asia Precipitation During the Boreal Cold Season. *Journal of Climate (*submitted*)*

Cannon, F., L.M.V. Carvalho, C. Jones, T. Hall, D. Gomberg, J. Dumas, M. Jackson 2016: WRF simulation of downslope wind events in coastal Santa Barbara County. *Atmospheric Research* (in review)

Norris, J. L.M.V. Carvalho, C. Jones, **F. Cannon**, B. Bookhagen, E. Palazzi, AA. Tahir, 2015: The Spatiotemporal Variability of Precipitation over the Himalaya: Validation of One-Year WRF Model Simulation. *Climate Dynamics* (in review)

Hoell, A., C. Funk, S. Shukla, **F. Cannon**, M. Barlow, 2016: Pacific Climate Mode Synchrony, the West Pacific Sea Surface Temperature Gradient, and Southwest Asia During the Boreal Cold Season. *Journal of Climate* (in review)

Cannon, F., L.M.V. Carvalho, C. Jones, A. Hoell, G. Kiladis, J. Norris, E. Palazzi, AA. Tahir. 2016: The Influence of Tropical Forcing on Extreme Precipitation in the Western Himalaya. *Climate Dynamics* DOI: 10.1007/s00382-016-3137-0

Carvalho L.M.V., C. Jones, **F. Cannon**, J. Norris, 2015: Intraseasonal-to-Interannual Variability of the Indian Monsoon Identified with the Large-scale Index for the Indian Monsoon System (LIMS). *Journal of Climate*, 29:2941-2962

Cannon, F., L.M.V. Carvalho, C. Jones, J. Norris, 2015: Winter Westerly Disturbance Dynamics and Precipitation in the Western Himalaya and Karakoram: A Wave Tracking Approach. *Theoretical and Applied Climatology*, 125:27-44

Hoell, A., S. Shukla, M. Barlow, **F. Cannon**, C. Kelley, C. Funk, 2015: The Forcing of Monthly Precipitation Variability over Southwest Asia During the Boreal Cold Season. *Journal of Climate*, 28: 7038-7056

Norris, J., L.M.V. Carvalho, C. Jones, **F. Cannon**, 2015: WRF Simulations of Two Extreme Snowfall Events Associated with Contrasting Extratropical Cyclones over the Western and Central Himalaya. *Geophysical Research – Atmosphere*, 120: 3114-3138

Smith, T., B. Bookhagen, **F. Cannon**, 2015: Improving Semi-Automated Glacial Mapping with a Multi-Method Approach: Applications in Central Asia. *The Cryosphere*, 9: 1747-1759

Cannon, F., L. M. V. Carvalho, C. Jones, B. Bookhagen, 2014: Multi-Annual Variations in Winter Westerly Disturbance Activity Affecting the Himalaya. *Climate Dynamics*, 44: 441-455

Peer Reviewed Book Chapters

Hoell, A., C. Funk, M. Barlow, **F. Cannon**, 2015: A Physical Model for Extreme Drought over Southwest Asia. *Patterns of Climate Extremes: Trends and Mechanisms*, editors: C.Y. Wang, J.H. Yoon, C. Funk, AGU Monogram, Wiley (in press)

Publications in Preparation

Cannon, F., L.M.V. Carvalho, C. Jones, J. Norris 2016: WRF Modified Topography Experiments of Extreme Winter Precipitation in Western High Asia. *JGR Atmos*

Awards

University Corporation for Atmospheric Research – PACE Postdoctoral Fellowship (2016: Declined)

UCSB Earth Research Institute – Summer Research Fellowship (2016)

American Geophysical Union Annual Meeting – Outstanding Student Presentation Award: Atmospheric Sciences (2014)

American Meteorological Society 94th Annual Meeting - 3rd Place Award: Climate Variation and Change Poster Presentations (2014)

Earth Research Institute Travel Scholarship (2013, 2014, 2015)

NASA NESSF Doctoral Fellowship (2013) & Renewal (2014, 2015) ($90,000)

UCSB Graduate USAP Fellowship (2013, 2014, 2015)

Jack and Laura Dangermond Travel Scholarship (2012, 2013, 2014, 2015)

UC Santa Barbara Golden Eagle Award (2009) – High GPA among student athletes

Big West Athletic Conference All-Academic Team (2009)

Service

Journal Referee: Bulletin of the American Meteorological Society; Journal of Climate; Earth System Dynamics; Atmospheric Research; Advances in Meteorology; Atmospheric Science Letters; Geomatics, Natural Hazards and Risk; Meteorological Applications

Earth Research Institute UCSB, Faculty Search Committee (Jan. 2016) *Student Representative for tenure track faculty search for professor of climate dynamics*

High Asia Climate and Water Resources Website (Apr. 2015 – Current) *Built and currently maintain a website dedicated to sharing our group's research activities to a broad audience for educational purposes – clivac.geog.ucsb.edu/HASIA*

Dept. of Geography UCSB, Volunteer Teacher (Aug. 2013 – Oct. 2013) *Weekly lectures on logical programming in IDL for graduate students*

Dept. of Geography UCSB, Graduate Student Representative (2012-2014) *Represenative at department faculty meetings*

Dept. of Geography UCSB, Community Outreach Presentation (2011, 2016) *Climate change awareness presentation at local area high school*

Volunteer - Ty Warner Sea Center, Santa Barbara, CA (2011) *Community education on the local marine environment*

Conference and Workshop Participation

International Atmospheric Rivers Conference – La Jolla, CA (Aug. 8-11, 2016)

American Geophysical Union: Annual Meeting – San Francisco, CA (2012, 2013, 2014, 2015)

Jet Propulsion Laboratory, Center for Climate Sciences Summer School – Pasadena, CA (Aug. 31- Sep. 4, 2015)

Weather Research and Forecasting Model Tutorial: National Center for Atmospheric Research – Boulder, CO (Jul. 21-25, 2014)

American Meteorological Society: Annual Meeting – Atlanta, GA (Feb. 2-6, 2014)

Alpine Summer School: Climate Change and the Mountain Environment – Valsavarenche, Valle d'Aosta, Italy (June 18-28, 2013)

@Spatial – Santa Barbara, CA (June 5, 2012)

ABSTRACT

Influence of Large-Scale Circulation on the Dynamics of Extratropical Cyclones and Orographic Precipitation in High Mountain Asia

By

Forest Glen Cannon

Westerly disturbances are the primary climatic influence within High Mountain Asia during winter, producing over half of annual precipitation in 4-6 events per winter season and supplying essential water resources for large populations across Asia. This research examines High Mountain Asia's hydroclimate, focusing on the relationship between westerly disturbance dynamics, the mechanisms that drive orographic precipitation, and their variability on intraseasonal and interannual scales. The first chapter establishes that extreme winter precipitation events in High Mountain Asia are primarily attributable to combined contributions from dynamical forcing and moisture availability during westerly disturbance interaction with regional topography. A novel wave-tracking algorithm was developed to provide an inventory of location, timing, intensity, and duration of westerly disturbance events, allowing for a comprehensive study of the mechanisms that drive orographic precipitation, on an individual event basis and in the aggregate. In the second chapter, westerly disturbances are investigated using extreme event composites to identify significant influence of global atmospheric variability over westerly disturbance dynamics and moisture availability, focusing on tropical forcing by the Madden Julian Oscillation on intraseasonal

timescales and the El Nino Southern Oscillation on interannual scales. This work demonstrates that El Nino simultaneously enhances the strength of the storm track and moisture availability to westerly disturbances. Contrastingly, during Madden Julian Oscillation propagation there is a transition in the balance of contributions from moisture availability and dynamical forcing to orographic precipitation. The third chapter of this dissertation employs a mesoscale model to perform a set of modified topography experiments in which extreme precipitation events in High Mountain Asia that were related to westerly disturbances are simulated at 6km resolution with native model topography and with smoothed topography taken from a global circulation model. These experiments illustrate that topographic smoothing fundamentally alters the dynamic and thermodynamic mechanisms that produce orographic precipitation during westerly disturbances, and identifies important deficiencies in the ability of models with coarse topographic resolution to simulate High Mountain Asia weather and climate. Collectively, the three chapters of this dissertation give novel insight into the dynamics of westerly disturbances, how these systems generate extreme precipitation events in High Mountain Asia, and their relationships with global atmospheric variability. These findings advance the scientific community's understanding of weather and climate in High Mountain Asia and improve the potential for evaluating the current state and future fate of regional water resources.

TABLE OF CONTENTS

Introduction

High Mountain Asia, defined as the region of elevated topography in central Asia encompassing the Tibetan Plateau and surrounding mountain ranges, is the source of Asia's largest and most depended upon rivers, including the Indus, Ganges, and Brahmaputra, which provide water for power generation and agriculture throughout central Asia (Bookhagen and Burbank, 2010). Snowfall accumulation within these watersheds has constructed the world's largest and densest network of alpine glaciers, which melt seasonally to sustain the region's hydrology through the dry months. Increasingly, but not uniformly, rising temperatures associated with climate change are contributing to decreases in the mass-balance of these high-elevation reservoirs and raising concern over the future of Asia's water resources (Bolch et al. 2012; Kaab et al. 2012).

Glacier records in the majority of High Mountain Asia, including the Himalaya, yield some of the world's most rapid retreat rates (Scherler et al. 2011). However, contrary to the Intergovernmental Panel on Climate Change's Fourth Assessment, there are in fact a number of steady state or positive mass-balance glaciers in the Karakoram and western Himalaya regions, often referred to as the "Karakoram Anomaly" (Bookhagen and Burbank, 2010; Kaab et al. 2012; Bolch et al. 2012). Furthermore, dominant controls on the region's glaciers' mass balance are not well understood. The future state of high-elevation freshwater reservoirs in the Himalaya is of critical importance to the security of water for consumption, agriculture, and power generation throughout densely populated regions of south, east, and central Asia (Archer and Fowler, 2004; Tahir et al. 2011; Kaab et al 2012; Sharif et al. 2013).

Evidence of positive trends in glacier mass-balance in the western Himalaya and Karakoram has motivated recent studies on climate variation and change in this region

(Archer and Fowler 2004; Bhutiyani et al. 2010; Dimri and Dash 2012; Palazzi et al. 2013). Dimri and Dash (2012) investigated trends in temperature and precipitation using historical wintertime measurements (1975-2007). Their results indicated that most of the western Himalaya and Karakoram show significant increasing trends in the lower and higher percentile of the daily maximum, minimum and average temperatures, and more warm events compared to fewer cold events. Their study also observed a general decreasing trend in precipitation at most stations, but these trends were not spatially coherent. Preceding station data analysis in the upper Indus Basin (Archer and Fowler 2004) indicated similar temperature trends, but significant increases in winter precipitation from 1961-99. Furthermore, Palazzi et al. (2013) illustrated numerous complexities in discerning precipitation trends within the Hindu-Kush Karakoram in recent decades using satellite rainfall estimates, reanalyses, and gridded in situ rain gauge data as well as in future climate scenarios using a global climate model. Because temperature and precipitation exhibit a high degree of spatial heterogeneity within the region's complex topography, there remain substantial questions regarding the region's climate and its relationship with the global atmosphere. In the context of a changing climate, it is prudent to define the large-scale mechanisms that characterize the region's climate and to investigate the relationship between precipitation in the mountains and the global atmosphere (Provenzale and Palazzi, 2015). Without identifying climatic influences, the observation, understanding, and prediction of terrestrial water fluxes in this region are not possible. This dissertation seeks to characterize wintertime climatic variability over High Mountain Asia in terms of local precipitation, regional circulation and atmospheric teleconnections using observational and modeling methods.

Overview of Western High Mountain Asia Climate

The focus of this dissertation is on the climate of the western extent of High Mountain Asia, where the Hindu Kush, Karakoram and Himalaya converge (Fig. 1a). This is the region that has registered anomalous positive glacier mass balance in recent decades, and we seek to understand atmospheric influences that may have contributed to the observed trends in the cryosphere. Two large-scale mechanisms, the Indian Summer Monsoon, and Winter Westerly Disturbances (WD) dominate regional climate (Fig. 1a) (Cannon et al. 2014). In the boreal summer the Indian Monsoon, driven by differential heating between the Indian subcontinent and adjacent Indian Ocean, generates some of the highest precipitation totals on Earth (Gadgil, 2003). At High Mountain Asia's orographic barrier, moisture-laden air is forced upwards, triggering intense convection along the windward side of topography. Moisture advection during the monsoon rarely experiences sufficient mechanical forcing to reach the orogen's interior (Barros et al. 2004; Wulf et al. 2010), where the Karakoram and its vast glaciers are situated. Consequently, despite the considerable influence of the monsoon across much of the Himalaya, within the Karakoram the majority of precipitation is associated with wintertime extratropical cyclones, which are colloquially termed "Westerly Disturbances" (Lang and Barros, 2004).

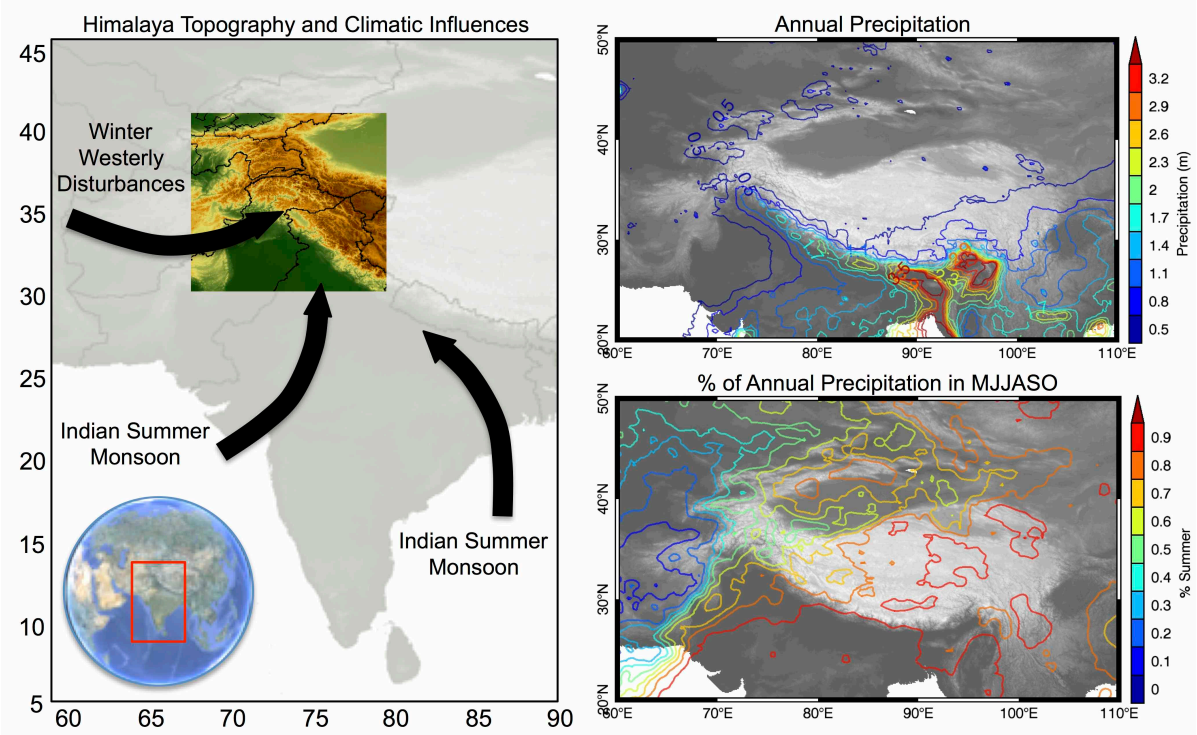

Figure 1 – Primary climatic influences on the Karakoram and Western Himalaya (colored region) are identified in the left panel. Total annual precipitation is shown in the top right, and the percentage of annual precipitation falling during summer (monsoon) months is shown in the bottom right.

Background on Westerly Disturbances

Extratropical cyclones, including WD, are fundamental features of the atmosphere that redistribute energy, momentum, and moisture at global scales while intimately linking large-scale circulation to regional-scale meteorology (Carlson, 1998; Neu et al. 2013). In the western Himalaya and Karakoram and to a lesser degree the central Himalaya, WD are the primary climatic influence during non-monsoon months (Singh et al. 1995; Lang and Barros, 2004; Barlow et al. 2005), as identified in fig. 1. The link between the atmosphere and glacial trends has motivated numerous studies on wintertime climate variability (Archer and Fowler 2004; Bhutiyani et al. 2010; Dimri and Dash 2012; Palazzi et al. 2013). In the western Himalaya and Karakoram, in excess of 50% of the total annual precipitation is delivered by

only a few WD between the months of November and April (Fig. 1b,c) (Archer and Fowler, 2004; Palazzi et al. 2013).

WD are characteristically eastward propagating extra-tropical cyclones (Lang and Barros, 2004; Barlow et al. 2005). Lag-composite analysis of WD events producing heavy precipitation in the KH display a deep upper-level trough, propagating along a Rossby wave guide (Hoskins and Ambrizzi, 1993), stationed several degrees to the west of the KH during the maximum in precipitation (Fig. 2) (Cannon et al. 2014). Their associated frontal systems interact with High Mountain Asia topography and warm tropical air masses over the Indian subcontinent to produce heavy orographic precipitation in the western Himalaya and Karakoram during winter and spring (Ridley et al. 2013; Cannon et al. 2014; Cannon et al. 2015). These systems derive their moisture from the Mediterranean, Red, Persian and Arabian Seas (Singh et al. 1995; Barlow et al. 2005, Filippi et al. 2014), though during the event moisture advection is typically observed from the Arabian Sea toward the western Himalaya and Karakoram, along the frontal boundary. Within the stable wintertime environment, precipitation is primarily mechanically forced by moist air impinging on terrain (Roe, 2005). The environmental lapse rate ensures that the majority of precipitation within the western Himalaya and Karakoram's high topography falls as snow (Immerzeel et al. 2009; Tahir et al. 2011), which contributes to glacial mass-balance (Hewitt, 2005; Bolch et al. 2012).

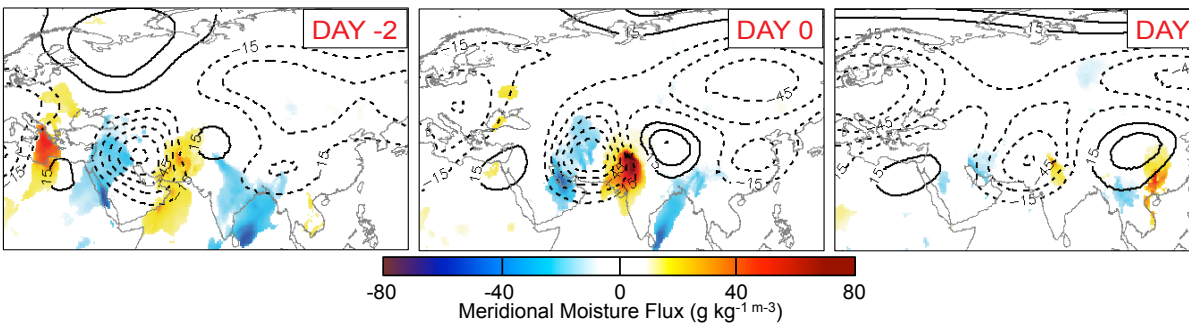

Figure 2 – Lag composites of 200-hPa geopotential height (contour; m) and 95th percentile significant vertically integrated meridional moisture flux anomalies during extreme precipitation events in the Karakoram and western Himalaya.

Orographic Influence on Westerly Disturbances

Orographic effects are the dominant influence on climatology within mountain environments (Roe, 2005). High Mountain Asia's extreme elevation and topographic complexity produce precipitation gradients that are stronger here than perhaps anywhere else on Earth (Anders et al. 2006; Bookhagen and Burbank, 2010). The remarkable south-north precipitation gradient (Fig. 1) across the Himalaya is attributable to enhancement over southern/windward slopes, where moisture-laden flows from the south encounter High Mountain Asia's steep topography. Both the summer monsoon and winter westerly disturbances interact with topography, though the ultimate precipitation distribution from any given event is influenced by more than just the underlying topography. The vertical profiles of temperature and moisture and the velocity of the incoming flow, which is variable between systems, modify how the atmosphere interacts with mountains (Houze, 1993; Roe, 2005).

Precipitation in High Mountain Asia is attributable to either convective clouds or frontal systems, both of which are fundamentally unrelated to the underlying topography but strongly modified by it. Effectively, orographic precipitation is the reorganization of one of these systems as it encounters topography (Houze, 2012). Its effects are shaped by a myriad of non-linear processes, of which the most fundamental are relatively well understood (Roe, 2005). Orographic influences principally occur as a result of rising and descending motions of air forced by topography. These forcings can be mechanical, thermal or a combination of the two. Germane to High Mountain Asia, they are principally mechanical as southerly flow

along WD fronts impinges on topography to force vertical motion (Lang and Barros, 2004), while, thermodynamic processes play a secondary (but important) role in modifying orographic ascent (Cannon et al. 2016).

Smith (1979) presented an idealized and physically based model, which predicts precipitation based on the moisture content and speed of a flow and the obstructing topography. This model characterizes the spatial distribution of precipitation according to elevation as a simple relationship between the adiabatic cooling of a rising air-parcel as forced by topography and the rate of condensation. As the parcel elevation increases, adiabatic cooling occurs and saturation vapor pressure decreases, eventually leading to condensation. Though this model oversimplifies relevant physical processes by assuming that condensation and precipitation fallout are instantaneous, it demonstrates the underlying principal of precipitation as a function of moisture flux and topography.

Beyond the simplicity of the upslope model, atmospheric density and temperature stratification play an influential role in modifying flow. As topography forces a moisture-laden air parcel upwards, the ambient air temperature, as defined by the environmental lapse rate, may be greater than that of the air-parcel, causing the flow to become negatively buoyant or stable. This relationship can be explained by the Brunt-Vaisala buoyancy frequency equation in which, the temperature, observed lapse rate of the air parcel, and dry adiabatic lapse rate are considered. The buoyancy restoring force causes airflow over mountains to take the form of waves, which in the case of the Himalaya modify large-scale climate. On a local scale, oscillations according to the buoyancy frequency can limit or enhance precipitation depending on the strength of incoming flow and stratification relative to mountain width (Roe, 2005). If the incoming flow is weak, or the mountains are high, the

effects of stratification can block the flow and the parcel will oscillate between negative and positive buoyancy. Differences in the atmospheric stability between WD events can modify the velocity of orographic updrafts and consequently influence precipitation rates and drying of the moist flow. Alternatively, less significant topography or a stronger flow will overcome topographic blocking. In such cases buoyantly unstable flow triggers convection as the air parcel passes over topography. Seasonal changes in the importance of dynamic and thermodynamic contributions to precipitation are investigated in the first chapter of this dissertation, while the second chapter investigates how global atmospheric variability modifies these factors at intraseasonal and interannual scales. The third chapter focuses specifically on the simulation of dynamic and thermodynamic contributions to orographic precipitation during WD events affecting High Mountain Asia, and how model topography influences their representation.

Previous Research on Multiannual Variations in Westerly Disturbance Activity

Studies of long-term changes in the frequency and intensity of WD have typically analyzed upper-level variability of geopotential height over several decades on account of the deep synoptic trough associated with the cyclone (Lang and Barros, 2004; Hatwar et al. 2005; Syed et al. 2006; Fillipi et al. 2014), which is strongly related to the generation of moist cross-barrier winds and consequent orographic precipitation. Lang and Barros (2004) identified a significant relationship between mid-troposphere geopotential height and heavy precipitation events in the central Himalaya, and used this relationship to evaluate WD activity over several decades of reanalysis. Increased variability of 500-hPa height indicated more frequent troughs and was positively correlated to increased precipitation at seasonal

scales. Accordingly, modes of global atmospheric variability, including the Arctic Oscillation, Siberian High, Polar/Eurasian Pattern and the El Niño-Southern Oscillation, play an important role in the interannual climatic variability of the western Himalaya and Karakoram by modulating the strength or position of geopotential height anomalies at seasonal to interannual scales (Barlow et al. 2005; Syed et al. 2006; Yadav et al. 2010). Much interest has been garnered by the use of teleconnective indices to explain western Himalaya and Karakoram precipitation variability, however, feedbacks between modes and associated lags create additional difficulties in attributing a climate signal in High Mountain Asia to any one mode (Palazzi et al. 2013, Dimri et al. 2015).

Ridley et al. (2013) examined regional modeling projections of synoptic pressure variability and concluded that WD activity will increase through the 21st century, producing increased winter precipitation for the western Himalaya and Karakoram and buffering glacial loss to global warming. However, studies regarding the prognosis of WD activity and High Mountain Asia winter precipitation using global and regional climate models must accurately represent the known modes of atmospheric variability to effectively project the future status of WD (Syed et al. 2010). Previous work by Cannon et al. (2014) and research presented in this dissertation focus on investigating the mechanisms that drive WD and their relationship with orographic precipitation in High Mountain Asia, defining the influence of large-scale atmospheric variability on their relationship, and identifying trends in their frequency and intensity.

Cannon et al. (2014) used satellite precipitation estimates, rain-gauge data, and reanalysis to examine variations and changes in synoptic activity affecting High Mountain Asia in recent decades (1979-2010). The focus of their analysis was on extreme precipitation

events associated with the propagation of synoptic systems from midlatitudes toward the Himalaya. That study primarily investigated the differences between WD affecting the western Himalaya and the central Himalaya, long term trends in their behavior, and their respective multiannual variations.

Wavelet power spectrum analysis of 200-hPa geopotential height anomalies in Cannon et al. (2014) indicated differing trends in synoptic scale variability across High Mountain Asia (Fig. 3). The zonal track of WD to the west of the Himalaya experienced an increase in the magnitude of individual events since 1979. Specifically, the synoptic power spectrum for the region corresponding to the center of the WD trough affecting the western Himalaya and Karakoram during day-0 of lag composite analysis (see Fig. 2) experienced an intensification of activity for the period 1979-2010 with the strongest increase elicited by several high-magnitude events occurring between 2003 and 2010. In contrast, the region corresponding to central Himalaya WD activity observed a significant negative trend since 1979. The dipole in WD activity across the Himalaya (Fig. 3) was likely attributable to changes in large-scale circulation, with potential impacts on regional precipitation.

In addition to changes in synoptic variability of geopotential height, Cannon et al. (2014) observed the wintertime subtropical jet to have intensified in the late 80s, 90s and early 00s, and to have shifted northward. The intensification of the jet appears to have increased WD activity in the Karakoram, while the northward shift has altered the geometry of these systems to be more prone to orographic blocking by western Himalaya and Karakoram mountain ranges. The central Himalaya appears to have been increasingly shadowed from enhanced WD activity in recent decades.

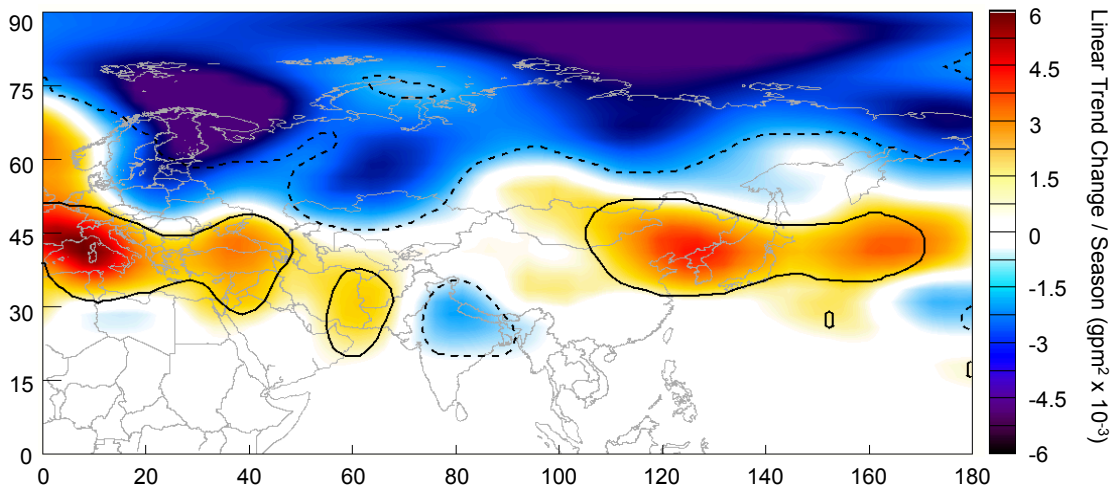

Figure 3 – Linear trend coefficients of DJFM seasonal averages (1979-2010) of total daily 200-hPa geopotential height synoptic power (5-15 day). Contours show statistically significant trends ant the 90th percentile confidence interval.

Cannon et al. (2014) further examined linkages between synoptic power of the upper-level geopotential height field, precipitation, and large-scale circulation as modified by the main modes of climate variability affecting Asia on interannual timescales, including the Arctic Oscillation, the Siberian High, the Polar/Eurasia Pattern and the El Nino Southern Oscillation. Although the relationships between these modes and WD propagation are complex, their signatures in the upper-level jet and regional precipitation clearly evidence the importance of their multiannual variability for the observed trends in western Himalaya and Karakoram and central Himalaya synoptic power. One notable finding was that composites of precipitation during El Niño events indicated increased precipitation and the delayed northward migration of the jet during the index's warm-phase. This association was not readily apparent through a comparison between WD synoptic power based on geopotential height variability and the ENSO index, which indicated the importance of continued investigation of how ENSO cascades into higher frequency variations as well as the spatially differing responses during ENSO events and their influence amongst different atmospheric

variables. This dissertation expands the work of Cannon et al. (2014). Chapter 1 investigates the relationship between WD and orographic precipitation generation, and Chapter 2 specifically addresses how global modes of variability manifest their influence at the synoptic scale, thereby influencing individual WD and High Mountain Asia precipitation.

Dissertation Objectives

This research seeks to advance the scientific community's understanding of weather and climate in High Mountain Asia and improve the potential for evaluating the current state and future fate of regional water resources. ***The objectives of this dissertation are:***

1) Investigate the dynamics of westerly disturbances (WD) and define how these systems generate extreme precipitation events in High Mountain Asia (Chapter 1).
2) Establish the relationships between WD and global atmospheric variability, emphasizing the role of tropical forcing in event-to-event variability (Chapter 2).
3) Use a mesoscale model to evaluate the importance of resolving High Mountain Asia's topography in simulating the relationships between orographic precipitation, WD and global circulation (Chapter 3).

The first paper of this dissertation focuses on intraseasonal variability of WD and the respective contributions of mechanical instability and moisture content in the atmosphere to orographic precipitation in the KH (Cannon et al. 2015). A novel wave-tracking algorithm was developed to provide an inventory of location, timing, intensity, and duration of WD events, allowing for a comprehensive study of the mechanisms within WD that drive orographic precipitation, on an individual event basis and in the aggregate. This work

identified the relationship between the strength of disturbances, the state of the background environment during their propagation, and precipitation totals in western High Mountain Asia, throughout individual months of the winter season.

The second chapter builds on earlier work that had identified teleconnections with High Asia (Cannon et al. 2014) by focusing on the role of tropical forcing in modifying the background state of the atmosphere through which WD propagate (Cannon et al. 2016). This work found both the El Nino Southern Oscillation and the Madden Julian Oscillation to strongly modulate the dynamic and thermodynamic mechanisms that drive orographic precipitation during WD interaction with High Mountain Asia. This research is unique relative to previous studies because of its focus on extreme events, rather than monthly or seasonal averages (e.g. Barlow et al. 2005; Hoell et al. 2012). The study's findings give insight into the dynamics and predictability of extreme precipitation events in the KH through their relationship with global atmospheric variability, and are an important consideration in evaluating Asia's water resources.

The dissertation also builds upon two coauthored publications with the Climate Variations and Change group at UCSB, which performed dynamical downscaling of reanalysis to produce 35 years of publically available, high-resolution meteorological data over High Mountain Asia (Norris et al. 2015; 2016). In those studies, the Weather Research and Forecasting model was tuned to simulate mesoscale precipitation patterns in High Mountain Asia by evaluating the model against available in-situ observations and remotely sensed data. Weather Research and Forecasting model simulation enabled investigations of High Mountain Asia climate that were not possible based on observations or coarse resolution reanalyses. In the third chapter of this dissertation, the optimal model

configuration from Norris et al. (2015; 2016) is utilized to perform a set of modified topography experiments in which extreme precipitation events in High Mountain Asia that are related to WD are simulated at 6km resolution with native model topography and with smoothed topography taken from a global circulation model. These experiments illustrated that topographic smoothing fundamentally alters the simulation of the dynamic and thermodynamic mechanisms that drive orographic precipitation during westerly disturbance events. This work identified important biases and deficiencies in the ability of models with coarse topographic resolution to adequately simulate High Mountain Asia's climate. These biases have not previously been identified and are an important consideration for the application of global circulation models toward projecting regional hydroclimate in the 21st century.

References

Anders AM, Roe GH, Hallet B, Montgomery DR, Finnegan NJ, Putkonen J (2006) Spatial patterns of precipitation and topography in the Himalaya. Geological Society of America Bulletin 398Archer DR, Fowler HJ (2004) Spatial and temporal variations in precipitation in the Upper Indus Basin, global teleconnections and hydrological implications. Hydrol Earth Syst Sc 8:47-61

Barlow M, Wheeler M, Lyon B, Cullen H (2005) Modulation of daily precipitation over southwest Asia by the Madden-Julian oscillation. Mon Weather Rev 133:3579-3594

Barros AP, Kim G, Williams E, Nesbitt SW (2004) Probing orographic controls in the Himalayas during the monsoon using satellite imagery. Nat Hazards Earth Syst Sci 4:29-51

Bhutiyani MR, Kale VS, Pawar NJ (2010) Climate change and the precipitation variations in the northwestern Himalaya: 1866-2006. Int J Climatol 30:535-548

Bolch T, Kulkarni A, Kaab A, Huggel C, Paul F, Cogley JG, Frey H, Kargel JS, Fujita K, Scheel M, Bajracharya S, Stoffel M (2012) The state and fate of Himalayan glaciers. Science 336:310-314

Bookhagen B, Burbank DW (2006) Topography, relief, and TRMM-derived rainfall variations along the Himalaya. Geophys Res Lett 33, L08405

Bookhagen B, Burbank DW (2010) Towards a complete Himalayan hydrological budget: The spatiotemporal distribution of snow melt and rainfall and their impact on river discharge. J Geophys Res-Earth 115

Cannon F, Carvalho LMV, Jones C, Bookhagen B (2014) Multi-annual variations in winter westerly disturbance activity affecting the Himalaya. Clim Dyn doi:10.1007/s00382-014-2248-8

Cannon, F., L.M.V. Carvalho, C. Jones, J. Norris, 2015: Winter Westerly Disturbance Dynamics and Precipitation in the Western Himalaya and Karakoram: A Wave Tracking Approach. Theor Appl Clim doi:10.1007/s00704-015-1489-8

Cannon F, Carvalho LMV, Jones C, Hoell A, Norris J, Kiladis G, Tahir AA (2016) The influence of tropical forcing on extreme winter precipitation in the western Himalaya. Clim Dyn doi:10.1007/s00382-016-3137-0

Carlson TN (1998) Mid-latitude weather systems. American Meteorological Society, Boston

Dimri AP, Dash SK (2012) Wintertime climatic trends in the western Himalayas. Climatic Change 111:775-800

Dimri AP, Niyogi D, Barros AP, Ridley J, Mohanty UC, Yasunari T, Sikka DR (2015) Western disturbances: a review. Rev Geophys 53:225-246

Filippi L, Palazzi E, von Hardenberg J, Provenzale A (2014) Multidecadal variations in the relationship between the NAO and winter precipitation in the Hindu-Kush Karakoram. J Clim doi:10.1175/JCLI-D-14-00286.1

Gadgil S (2003) The Indian Monsoon and its variability. Auun Rev Earth Planet Sci 31:429-467

Hatwar HR, Yadav BP, Rama Rao YV (2005) Prediction of western disturbances and associated weather over western Himalayas. Curr Sci India 88:913-920

Hewitt K (2005) The Karakoram anomaly? Glacier expansion and the “elevation effect”, Karakoram Himalaya. Mountain Res Dev 25:332-340

Hoell A, Barlow M, Saini R (2012) The leading pattern of intraseasonal and interannual Indian Ocean precipitation variability and its relationship with Asian circulation during the Boreal cold season. J Climate 25:7509-7526

Houze RA (2012) Orographic effects on precipitating clouds. *Review of Geophysics*, 50

Houze RA (1993) Hailstorms in Switzerland – left movers, right movers, and false hooks. *Monthly Weather Review* 121:3345-3370

Immerzeel WW, Droogers P, de Jong SM, Bierkens MFP (2009) Large-scale monitoring of snow cover and runoff simulation in Himalayan river basins using remote sensing. Remote Sens Environ 113:40-49

Kaab A, Berthier E, Nuth C, Gardelle J, Arnaud Y (2012) Contrasting patterns of early twenty-first-century glacier mass change in the Himalayas. Nature 488:495-498

Lang TJ, Barros AP (2004): Winter storms in the central Himalayas. J Meteorol Soc Jpn 82:829-844

Norris J, Carvalho LMV, Jones C, Cannon F (2015) WRF simulations of two extreme snowfall events associated with contrasting extratropical cyclones over the Himalayas. doi:10.1002/2014JD022592

Palazzi E, von Hardenberg J, Provenzale A (2013) Precipitation in the Hindu-Kush Karakoram Himalaya: Observations and future scenarios. J Geophys Res-Atmos 118:85-100

Palazzi E, Tahir AA, Cristofanelli P, Vuillermoz E, Provenzale A (2015) Climatic characterization of Baltoro Glacier (Karakoram) and northern Pakistan from in-situ stations. Engineering Geoglogy for Society and Territory, Springer, Switzerland 33-37

Provenzale A, Palazzi E (2015) Assessing climate change risks under uncertain conditions. Engineering Geoglogy for Society and Territory, Springer, Switzerland 1-5

Ridley J, Wiltshire A, Mathison C (2013) More frequent occurrence of westerly disturbances in Karakoram up to 2100. Sci Total Environ. DOI:10.1016/j.scitotenv.2013.03.074

Roe GH (2005) Orographic Precipitation. Annu Rev Earth Planet Sci 33:647-671

Scherler, D., B. Bookhagen, M.R. Strecker (2011): Spatially variable response of Himalayan glaciers to climate change affected by debris cover, Nature Geoscience, 4, 156-159

Singh P, Ramasastri KS, Kumar N (1995) Topographical influence on precipitation distribution in different ranges of western Himalayas. Nord Hydrol 26:259-284

Smith RB (1979) The influence of mountains on the atmosphere. *Advances in Geophysics* 21:87-230

Syed FS, Giorgi F, Pal JS, King MP (2006) Effect of remote forcings on the winter precipitation of central southwest

Syed FS, Giorgi F, Pal JS, Keay K (2010) Regional climate model simulation of winter climate over Central-Southwest Asia, with emphasis on NAO and ENSO effects. Int J Climatol 30:220-235

Tahir AA, Chevallier P, Arnaud Y, Ahmad B (2011) Snow cover dynamics and hydrological regime of the Hunza River basin, Karakoram Range, Northern Pakistan. Hydrol Earth Syst Sci 15:2275-2290

Wu BY, Wang J (2002) Winter Arctic Oscillation, Siberian High and East Asian winter monsoon. Geophys Res Lett 29:1-4

Wulf H, Bookhagen B, Scherler D (2010) Seasonal precipitation gradients and their impact on fluvial sediment flux in the Northwest Himalaya. Geomorphology 118:13-21

Yadav RK, Yoo JH, Kucharski F, Abid MA (2010) Why is ENSO influencing northwest India winter precipitation in recent decades? J Climate 23:1979-1993

I. Chapter 1: Winter Westerly Disturbance Dynamics and Precipitation in the Western Himalaya and Karakoram: A Wave Tracking Approach

Forest Cannon[1,2], Leila M.V. Carvalho[1,2], Charles Jones [1,2], and Jesse Norris[2]

[1] Department of Geography, University of California, Santa Barbara

[2] Earth Research Institute, University of California, Santa Barbara

1.1 Abstract

Extra-tropical cyclones, including Winter Westerly Disturbances (WD) over central Asia, are fundamental features of the atmosphere that maintain energy, momentum, and moisture at global scales while intimately linking large-scale circulation to regional-scale meteorology. Within High Mountain Asia, WD are the primary contributor to regional precipitation during winter. In this work, we present a novel WD tracking methodology, which provides an inventory of location, timing, intensity and duration of events, allowing for a comprehensive study of the factors that relate WD to orographic precipitation, on an individual event basis and in the aggregate. We identify the relationship between the strength of disturbances, the state of the background environment during their propagation, and precipitation totals in the Karakoram/western Himalaya. We observe significant differences in convective and mechanical instability contributions to orographic precipitation as a function of the relationship between the intensity of WD and the background temperature and moisture fields, which exhibit strong intraseasonal variability. Precipitation is primarily orographically forced during intense WD with strong cross-barrier winds, while weaker WD with similar precipitation totals are observed to benefit from enhanced instability due to high moisture content and temperature at low-levels, occurring primarily in the late winter/pre-

monsoon. The contribution of these factors is observed to fluctuate on a per-case basis, indicating important influences of intraseasonal oscillations and tropical-extratropical interactions on regional precipitation.

1.2 Introduction

Water resources in High Mountain Asia (HMA) are important for hundreds of millions of people throughout southern and central Asia (Kaab et al. 2012). Recently, numerous studies have been undertaken to evaluate changes in glaciers across the region, as they are important storage reservoirs, which provide water for agriculture, power generation, and human consumption during low-precipitation months (Gardelle et al. 2005; Bookhagen and Burbank 2010; Bolch et al. 2012). In the western Himalaya and Karakoram (KH) and to a lesser degree the central Himalaya, winter westerly disturbances are the primary climatic influence during non-monsoon months (Singh et al. 1995; Lang and Barros, 2004; Barlow et al. 2005). The link between the atmosphere and glacial trends has also motivated studies on wintertime climate variability (Archer and Fowler 2004; Bhutiyani et al. 2010; Dimri and Dash 2012; Palazzi et al. 2013). In the KH, an excess of 50% of the total annual precipitation is delivered by only a few westerly disturbances occurring between the months of December and March (Barros et al. 2006). Winter Westerly Disturbances (WD) are characteristically eastward propagating extra-tropical cyclones (Lang and Barros, 2004; Barlow et al. 2005). Their associated frontal systems interact with HMA topography and warm tropical air masses over the Indian subcontinent to produce heavy precipitation in the KH during winter and spring (Ridley et al. 2013).

Precipitation produced by WD is supplied by advected moisture from the Mediterranean, Red, Persian and Arabian Seas (Singh et al. 1995; Barlow et al. 2005, Filippi et al. 2014). Within the convectively stable wintertime environment, precipitation is mechanically forced by air impinging on terrain (Roe, 2005). KH orography induces a significant blocking effect thereby modifying regional and large-scale circulation and the distribution of orographic precipitation. The environmental lapse rate ensures that the majority of precipitation within the KH's high topography falls as snow (Immerzeel et al. 2009; Tahir et al. 2011). Snowfall is a primary determinant of glacial mass-balance in HMA (Hewitt, 2005; Bolch et al. 2012).

WD are well associated with a baroclinic wave approaching HMA and exhibiting prototypical cold-frontal behavior (e.g. Holton, 2004). Lag-composite analysis of WD events producing heavy precipitation in the KH display a deep upper-level trough, propagating along a Rossby wave guide (Hoskins and Ambrizzi, 1993), stationed several degrees to the west of the KH during the maximum in precipitation and exhibiting vertical tilting (e.g. Cannon et al. 2014, their Fig. 3). Moisture is advected northward along the cold front and into a notch in the KH, which captures and orographically lifts the flow to produce precipitation. Long-term studies in the frequency and intensity of WD typically analyze upper-level variability of geopotential height over several decades because the deep synoptic trough associated with the cyclone exhibits a distinctive signature. Lang and Barros (2004) identified a significant relationship between 500-hPa geopotential height and heavy precipitation events in the central Himalaya, and used this relationship to evaluate WD activity over several decades of reanalysis. Increased variability of 500-hPa height indicated more frequent troughs and was positively correlated to increased precipitation. Similarly,

Cannon et al. (2014) used wavelet-derived synoptic variability of upper-level geopotential height to estimate WD activity between 1979 and 2010. Their work indicated increasing variability in 200-hPa geopotential height at synoptic scales and gave evidence of increased WD activity contributing to trends in glacier mass-balance across HMA.

Numerous studies found WD to be significantly influenced by the Madden-Julian Oscillation (Barlow et al. 2005; Hoell et al. 2012), the El Niño Southern Oscillation (Syed et al. 2006; Yadav et al. 2010), the Arctic Oscillation/North Atlantic Oscillation (Gong et al. 2001; Wu and Wang, 2002, Yadav et al. 2009; Syed et al. 2010; Filippi et al. 2014) and the Polar Eurasia Pattern (Lang and Barros, 2004). However, linkages between global modes of variability and upper-level geopotential height are complicated by competing influences between modes (Hoell and Funk, 2013; Cannon et al 2014) as well as documented feedbacks (Cohen et al. 2007). Additionally, there is not a linear relationship between the dynamics associated with the intensity of a disturbance and the amount of precipitation received in HMA (Lang and Barros, 2004). Factors including the location of the WD track, the depth of the trough, the duration of the disturbance, and moisture sources are all of necessary consideration.

Extratropical cyclones, including WD, are fundamental features of the atmosphere that redistribute energy, momentum, and moisture at global scales while intimately linking large-scale circulation to regional-scale processes (Carlson, 1998; Neu et al. 2013). Within HMA, there is no mechanism that is more important in contributing to water supply during winter, and therefore it is important that we create a baseline climatology of WD and further explore variability over time. Eulerian methods of investigating variance of fields related to WD at synoptic scales are typically employed as a general measure of storm track activity

(Lang and Barros, 2004; Barlow et al. 2005; Syed et al. 2006; Yadav et al. 2010; Cannon et al. 2014). However, Eulerian statistics cannot convey important information regarding the specifics of individual systems, nor can the attributes of a cyclone be taken directly (Hoskins and Hodges, 2002). Thus, a Lagrangian method of automatically tracking WD, which can provide complementary information about individual systems and allows us to investigate track activity, is desired (Syed et al. 2010).

Over recent decades, many diagnostic methods of objectively identifying extra-tropical cyclones have been developed (Murray and Simmonds 1991; Hodges 1995; Serreze 1995; Blender et al. 1997; Sinclair 1997; Simmonds et al. 1999; Lionello et al. 2002; Benestad and Chen 2006; Trigo 2006; Wernli and Schwierz 2006; Akperov et al. 2007; Rudeva and Gulev 2007; Inatsu 2009; Kew et al. 2010; Hewson and Titley 2010; Hanley and Caballero 2012). Depending on the definition of a cyclone, these automated algorithms utilize differing variables and tracking techniques (Hoskins and Hodges, 2002). Syed et al. (2010) first employed the tracking algorithm of Murray and Simmonds (1991), further refined by Simmonds and Keay (2000), to investigate WD behavior in relation to teleconnections. This study heralded the benefits of Lagrangian tracking in HMA, and here, we demonstrate a simplified, easily reproducible methodology to track WD, which often propagate along relatively low latitudes, encounter highly variable topography, exhibit strong tropical influences, and are highly asymmetric. Chen and Bromwich (1999) noted the difficulties of synoptic analysis in mountainous regions, the most complex of which is HMA on account of its vertical and horizontal extent, thus greatly reducing the number of observable pressure levels over a large area. Here, we propose a new tracking procedure for synoptic-scale disturbances based on the signature of WD in 500-hPa geopotential height.

500-hPa geopotential height is often employed to investigate the behavior of Rossby waves in subtropical and extratropical latitudes (Carlson, 1998), and is thus a commonly used variable in HMA wintertime climate studies (Subbaramayya and Raju, 1982; Lang and Barros, 2004; Hatwar et al. 2005; Syed et al. 2010).

The primary objective of this work is to investigate changes in WD behavior with respect to HMA precipitation during winter seasons from 1979-2013. In this study, we utilize negative 500-hPa geopotential height anomalies to identify individual WD responsible for KH precipitation and track their progression. Our novel WD tracking methodology, explicitly created to improve identification over high topography relative to other mid-latitude disturbance tracking procedures, provides an inventory of location, timing, intensity and duration of events, which are explored in depth with an emphasis on seasonal variability. This provides a valuable link between the large-scale climate, transient disturbances, and hydrologic processes within the KH, and allows us to evaluate WD on a per-case basis while considering all factors that relate these systems to precipitation in the mountains. These factors include the intensity of systems as defined by the depth of 500-hPa anomalies at their center, wind speed intersecting topography, and precipitable water throughout the winter season. Furthermore, how WD characteristics evolve over the course of a season in response to changes in the background climate is investigated, with the goal of understanding dynamic and thermodynamic influences on the relationship between these events and KH precipitation. Strong orographic forcing is known to reduce the efficiency of topography in converting advected moisture to precipitation, whereas convective events do not typically propagate as far into the orogenic interior (Bookhagen and Burbank, 2010; Wulf et al. 2010)

The manuscript is organized as follows. Section 1.3 introduces the data. Section 1.4 explains the tracking methodology and is followed by section 1.5, which validates the method's performance. Section 1.6 discusses the frequency of disturbances. Section 1.7 compares two sources of precipitation data during identified WD events and section 1.8 investigates the dynamics of these events. Section 1.9 concludes our manuscript.

1.3 Data

Meteorological data within topographically heterogeneous HMA is limited. In HMA, the observation network thins considerably due to increased elevation and remoteness. Furthermore, extant data is generally of poor quality due to sampling errors or biases. This research utilizes remotely sensed satellite precipitation estimates and reanalyses as the best available options for gridded meteorological data over recent decades.

Precipitation from the Tropical Rainfall Measurement Mission 3B42V7 (TRMM) (Huffman et al. 2007) and Climate Forecast System Reanalysis (CFSR), from the National Centers for Environmental Prediction (Saha et al. 2010), are used to identify heavy precipitation events in HMA. TRMM provides 3-hourly precipitation estimates at near-global 0.25° horizontal-resolution for the period 1998-2013. The product combines TRMM 2B31, TRMM 2A12, Special Sensor Microwave Imager, Advanced Microwave Scanning Radiometer, Advanced Microwave Sounding Unit and Climate Prediction Center infrared observations to estimate precipitation over low/mid-latitudes and is calibrated by station data. TRMM has documented deficiencies in capturing snowfall (TRMM Working Group Summaries, 2003), which are especially problematic in HMA during winter (Lang and Barros, 2004; Barros et al. 2006, Maussion et al. 2014). Because accurately quantifying total

precipitation accumulation is difficult, our focus is on the timing and the relative precipitation contribution of WD events, compared to all other dates. Under the assumption that low-elevation rainfall within the mountains is typically concomitant with high-elevation solid-state precipitation during WD events, we can identify the dates of heavy-precipitation events relative to all other dates by examining TRMM data. Similar procedure was performed in Cannon et al. (2014). We note that it is unlikely that the magnitude of precipitation in TRMM is accurate and that the proportion of high-elevation solid-state precipitation to low-elevation rainfall is not constant (Lang and Barros, 2004).

Daily CFSR precipitation is also used to identify the timing of heavy precipitation events with an extended temporal record. CFSR is available at 0.5° horizontal-resolution for the period 1979-2013. CFSR was chosen on account of its model coupling, spatial resolution, and modern assimilation system (Saha et al. 2010). For both TRMM and CFSR, we have aggregated to daily precipitation totals. Within the manuscript we compare TRMM and CFSR during WD events as independent indications of precipitation. Daily CFSR is also used to investigate the dynamics of WD. Analysis of geopotential height, wind, moisture, and temperature are performed at near-surface and 500-hPa levels. Both the total fields and anomalies are considered, with the anomalies being derived by removing the mean seasonal cycle 1979-2013.

1.4 Tracking Method

Extratropical cyclones, including WD, have a characteristic depression in the 500-hPa geopotential height field, which differentiates these systems from the background flow and facilitates detection. The approach of our WD tracking methodology is to apply the spatial

correlation of standardized 500-hPa geopotential-height-anomaly features to track synoptic-trough trajectories associated with extra-tropical cyclones. Similar methods have been used to track mesoscale convective systems based on cloud-top temperatures (Carvalho and Jones, 2001) and large-scale convective features based on outgoing long-wave radiation (Carvalho et al. 2002; Jones et al. 2004). Standardization of the 500-hPa geopotential height input field by monthly mean-variance accounts for increased variability in geopotential height with increasing latitude and allows for the identification of events based on the relative departure from normal. Standardized geopotential height has previously been used to investigate trough depth relative to typical conditions (Grumm and Hart, 2001). Our procedure facilitates the detection of WD in subtropical latitudes and in regions of high topography. Figure 1 exemplifies the tracking procedure and is used in the following paragraph as a visual aid to understanding the general principles on which our methodology is built. This is followed by a detailed discussion of the steps that comprise our algorithm.

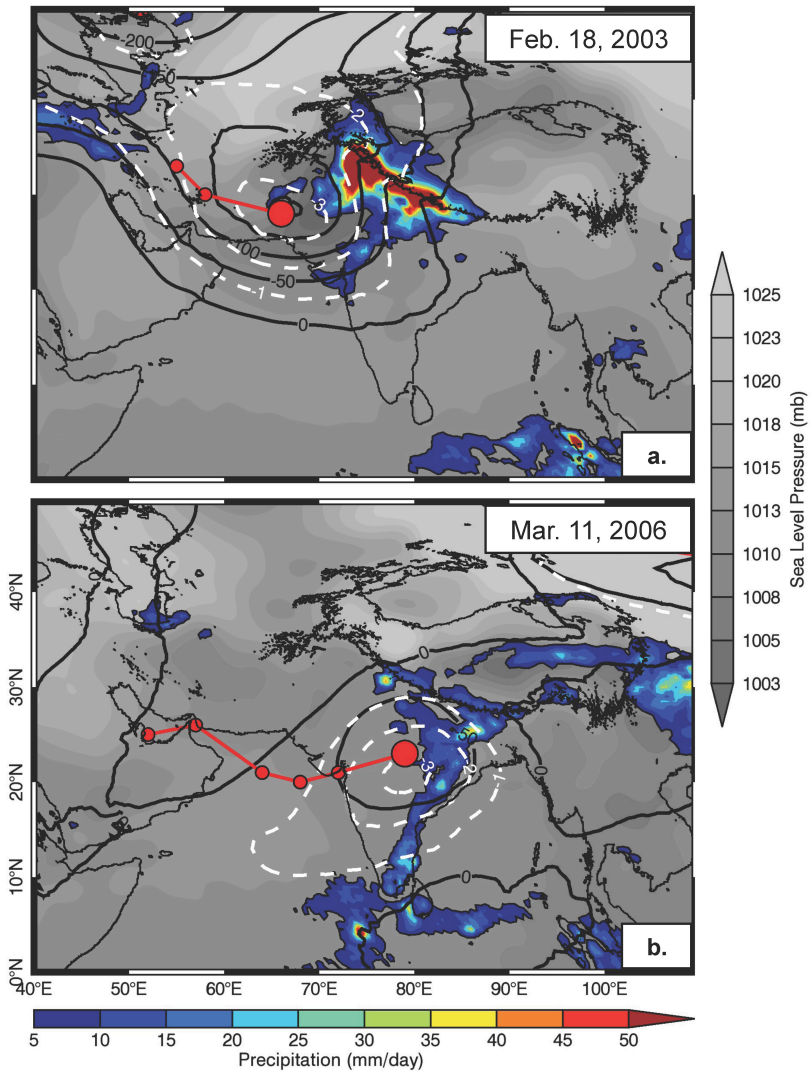

Figure 1 – Example of 500-hPa wave tracking methodology for two Westerly Disturbances. Black contour indicates 500-hPa geopotential height anomaly (m). White dashed contour indicates standardized 500-hPa geopotential height anomaly (interval is -1 standard deviations). Red line indicates disturbance trajectory. Red dots indicate location of center of disturbance on previous days. Large red dot indicates location of disturbance on current day. Sea level pressure (gray) and precipitation (color) shading apply only to current day.

Figure 1a and b show the relationship between 500-hPa geopotential height anomalies (black contours) and standardized geopotential-height anomalies (white dashed contours) for two WD events affecting HMA. Figure 1a shows a characteristic mid-winter WD occurring on February 18, 2003 and exhibiting a well-defined trough in 500-hPa anomalies, while the late-season March 2006 event in Figure 1b exhibits a comparatively shallow 500-hPa

anomaly. The use of standardized anomalies augments the signal of the features relative to the background flow and has enabled the tracking of both troughs, each of which represents a significant deviation from local average conditions. These WD produced 95th percentile precipitation (based on independent events in CFSR climatology) in the Karakoram (Fig. 1a) and central Himalaya (Fig. 1b). The large red dot indicates the position of the track center for the current day and smaller red dots, connected by a red line, indicate the position of the disturbance's center on preceding days, beginning with the first day of identification. The synoptic conditions that produced the events observed in Fig. 1, with respect to the benefits of our tracking method in identifying them, are discussed in Section 1.5. Our tracking methodology is detailed as follows.

1) Input data is CFSR 500-hPa geopotential height, aggregated to 1° horizontal resolution over the Northern Hemisphere. We consider daily maps of standardized 500-hPa geopotential height anomalies for the time period 1979-2013. For each daily map, we apply a series of standard deviation thresholds to retain only data exceeding the given threshold of standardized geopotential height anomaly. Our threshold procedure begins at -5 standard deviations and is incrementally relaxed by 0.25 per step toward -1 standard deviation. For each applied threshold, all data points not satisfying the threshold are set to null-value to create a background mask. The more restrictive the threshold, the smaller the area of geopotential height anomalies retained. Using maps of decreasing restrictiveness allows us to identify multiple centers within a single, large region of negative anomalies. For example, imagine a perturbation (wavenumber one or two) covering the majority of continental Asia, which propagates eastward very slowly relative to two or three embedded shortwaves that propagate eastward at a faster rate. In this scenario, incrementally relaxing

our thresholds allows for the identification of the centers of each individual disturbance, whereas using only a single threshold would likely have resulted in a single track, exhibiting unrealistic behavior as it skipped between shortwaves embedded within the longwave.

2) After we have identified disturbances in geopotential height for a given threshold, we filter out apparent small features by removing identified regions comprised of fewer than 5 pixels across (5 pixels, or 5° is roughly 450km at 35°N; the approximate latitude of the Karakoram). These features are common in the tropics where slight perturbations appear significant. This filtering, henceforth termed "the area threshold", ensures the presence of a spatially coherent mid-latitude disturbance. Also, it is worth noting that global CFSR 500-hPa data at 1° resolution intersects topography in only one gridpoint. Though this gridpoint is in our study area (containing K2 and the Gasherbrum Massif) and below the surface for roughly 17% of the year, it does not disrupt the general circulation and we do not address this minor issue in our application of the dataset.

3) At this point, we retain two datasets; daily maps of the location and spatial extent of anomalies surpassing the first standard deviation threshold, in which the identified area also exceeded the area threshold (to be referred to as "the max map"), and daily maps of the location and spatial extent of anomalies surpassing the least restrictive (-1) standard deviation threshold, in which the area threshold was also exceeded. We locate the center of disturbances by first selecting all non-null-value regions in the max map and then identifying the spatially-weighted center of the actual geopotential height anomalies within the active regions.

4) To track disturbances over time, we begin by calculating the spatial correlation of identified regions in the -1 standard deviation map between consecutive days. If the spatial correlation between two regions exceeds 0.3, we determine the disturbance at time t+1 to be a continuation of the disturbance at time t. The spatial correlation threshold of 0.3 was reached empirically in initial development of the algorithm. We use the -1 standard deviation map rather than the max map to determine spatiotemporal correlation because the deepest regions of anomalies are typically disjointed at high standard deviation levels.

5) Once the algorithm has identified regions of negative gopotential height anomalies that are connected in time, the trajectory of the trough is created by linking corresponding centers between consecutive days. If, within an identified region in the -1 standard deviation map of time t, which is spatially correlated with a region on the subsequent day, there exists only one identified center, the track will begin at time t at that location. If the spatially correlated region on the subsequent day also contains only one identified center, the disturbance's track will be created by linking corresponding centers at times t and t+1. If multiple centers exist within a region, multiple tracks will be created. Given multiple centers in either time t or t+1, tracks are created by linking centers that are in closer spatial proximity. If the number of centers within a region passing the -1 standard deviation threshold changes between time t and time t+1, a merging or splitting of tracks has occurred. For splitting, an independent track is created at t+1 for the center furthest from the original track. For merges, the track with the longest duration to date is retained. This procedure is performed for each consecutive day of the data set, while retaining all track information from the previous day. If an identified center is not related to a pre-existing

track, a new one is created. Similarly, if an existing track cannot be linked to a spatially correlated region on the subsequent day, the track ceases.

6) Daily temporal resolution allows for centers of synoptic systems to propagate large distances between images. To create continuous tracks, track centers for consecutive days were linked using shortest straight-line distance interpolation to connect adjacent grid-points between centers. The final product of our tracking procedure is daily-resolution 500-hPa trough tracks over the northern hemisphere for the time period 1979-2013.

1.5 Tracking Verification

In the previous section we detailed the methods by which we identify and track 500-hPa troughs. Here, we examine two troughs that produced large precipitation totals in the Himalaya to elucidate how the tracking method works in practice. The February 2003 event, shown in Fig. 1a, is characterized by a deep upper-level trough, exhibiting negative 500-hPa geopotential height anomalies in excess of 200m at the center. With respect to the climatology of WD this represents a strong, but archetypical event. This event developed two days prior, from an existing trough over the Caspian Sea. The March 2006 event (Fig. 1b) was caused by the interaction of a WD, exhibiting a shallow upper level trough (between -50 and -100 m on March 11th), with a moist tropical air mass over the Indian subcontinent. The track, observed over the Arabian Sea and India, originated on the 6th of March as a shortwave at approximately 50°E, 25°N and propagated zonally toward the central Himalaya. By the 11th (Fig. 1) the trough was positioned over central India and the resultant southerly moisture transport driven against the Himalaya was sufficient to produce an extreme precipitation event (Norris et al. 2015).

Neither event displayed changes in sea-level pressure that were remarkable or exclusive to extra-tropical cyclones, precluding their identification in many of the tracking algorithms discussed by Neu et al. (2013), which rely on well-structured features at lower levels. The general dissociation between pre-monsoon storms in this region and lower-tropospheric circulation was first observed by Ramaswamy (1956), in which the usefulness of upper-tropospheric charts for forecasting these events was also discussed. Furthermore, any methodology employing data below the 500-hPa-level would be significantly affected by high topography over much of central Asia and yield dubious results. It is also worth mentioning that a number of tracking algorithms, including that of Murray and Simmonds (1991) and Hodges (1995), which were originally designed to identify surface systems, can be modified to incorporate middle tropospheric variables, such as done by Keable et al. (2002), Hoskins and Hodges (2002), and Syed et al. (2010).

For both events, the standardized negative 500-hPa geopotential height anomalies were 3 to 4 standard deviations below normal, thus facilitating the tracking of WD using our methodology. This example of events occurring in different locations, during different times of the year, with varying trough depth was specifically chosen to demonstrate that the tracking methodology performs well irrespective of track latitude, intensity or timing. However, we note that not all systems are as well behaved, and there are rare instances where the methodology has difficulties. Notably, when stationary waves covering expanses of central Asia linger for many days with periodic extensions of their troughs toward HMA, or when multiple tracks are recorded in close proximity over several days. Uncommon cases such as these are observed to produce unrealistic tracks.

Figure 2 shows a global 500-hPa wave track density map for the Northern Hemisphere winter (November–April) for the time period 1979-2013. Density is defined as the total number of tracks recorded in a given grid-point through time, with minimum-distance interpolation performed between consecutive day's centers. Over southwest and central Asia, the region of WD activity, an appreciable maximum in track activity exists. This region of increased activity is co-located with the subtropical jet, which may act as a baroclinic-wave-guide (Krishnamurti, 1961; Hoskins and Ambrizzi, 1993; Ridley et al. 2013). Enhanced activity is also identifiable in the North Pacific, across the United States, and over the North Atlantic, co-located with the mean position of the maximum zonal wind in the mid-troposphere during winter. We note that as a result of using standardized 500-hPa anomalies, the regions of maximum track density appear to be shifted equatorwards compared to results from many other tracking methods, which employ low-troposphere variables. This work focuses on the propagation of troughs as identified by perturbations in 500-hPa geopotential height, which shows a characteristic response to WD, and not on replicating storm tracks as identified by other methods as reviewed by Neu et al. (2013). However, our maps of track density strongly resemble those of Hoskins and Hodges (2002), in which several variables at upper levels were used to investigate winter storm tracks. Notably, both our method and the established Hoskins and Hodges method as well as the analysis performed by Syed et al. (2010) identified a maximum in track density in the vicinity of the mid-latitude jet, where WD develop.

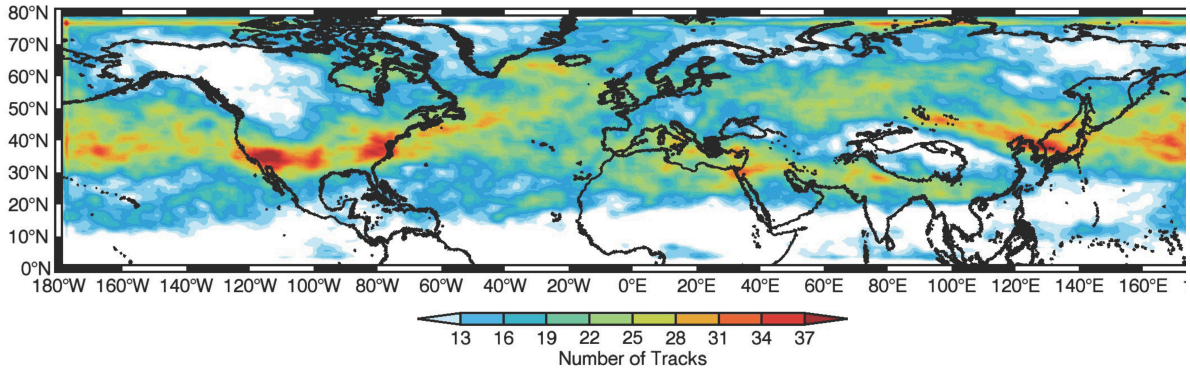

Figure 2 – Global 500-hPa wave track density map indicating trajectories of centers of disturbances recorded during winter seasons (Nov. to Apr.) 1979-2013. 3000m elevation contour of Tibetan Plateau is indicated as black line.

To demonstrate the relationship between disturbances identified by our method and precipitation, an index of extreme precipitation events was created for the western Himalaya/ Karakoram (74-78°E, 34-37°N) (KH) by spatially averaging CFSR daily precipitation estimates for the region and retaining the 95th percentile of independent (3 days between events) non-zero precipitation dates during winter (NDJFMA). Figure 3 displays the density of all tracks that recorded a segment concomitant with an extreme precipitation event. The 500-hPa geopotential height anomaly is also composited onto the index of extreme precipitation. A depression is observed centered several degrees to the west of the KH as demonstrated in Cannon et al. (2014). Track density in this figure indicates that extreme precipitation in the KH is associated with the propagation of WD across southwest/central Asia between 25°N and 35°N

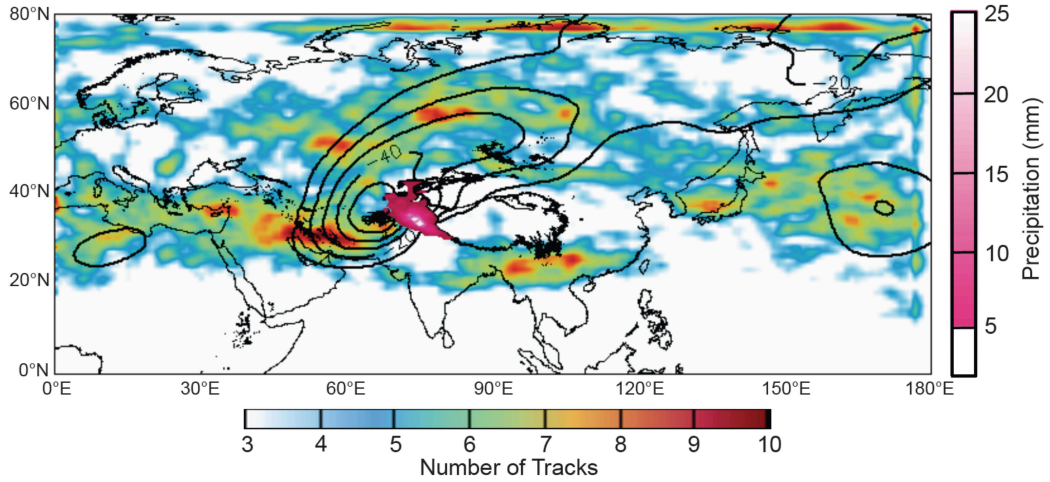

Figure 3 –500-hPa wave track density map indicating trajectories of centers of disturbances recorded during 95th percentile precipitation dates in the Karakoram (Nov. to Apr.) 1979-2013. Black Contours indicate negative 500-hPa geopotential height anomalies (m). Pink shade over Karakoram indicates precipitation intensity. 3000m elevation contour of Tibetan Plateau is also shown as a black line.

Our WD tracking method is proven to accurately identify the primary atmospheric circulation pattern that produces KH precipitation events. Heavy precipitation events are particularly well represented, as these are characteristically associated with the systems we are tracking. We note that many of the lighter precipitation events are not related to characteristic WD circulation and are not captured. Therefore, the average seasonal precipitation may not be accurately represented. Additionally, WD in our region of interest do not always produce precipitation. These issues are further discussed in the subsequent sections along with the statistics of trough depth, cross-barrier wind speed and precipitable water content of individual events.

1.6 Westerly Disturbance Properties

The average properties of WD, including their intensity, size, duration and associated precipitation, vary according to their location. The variability in latitude between

disturbances alters their interaction with High Mountain Asia by changing the angle of incidence between topography and circulation, thus it is necessary to investigate WD according to several sub-regions. We subdivided the greater region of WD activity into three sub-regions of varying latitude to explore the effect of storm track location on system dynamics and resulting KH precipitation. Figure 4 shows the regions in which we investigated WD events: the outer domain (50-80°E, 15-50°N), Region One (60-75°E, 25-40N), Region Two (60-75°E, 15-25°N) and Region Three (60-75°E, 40-50°N). Figure 5 indicates the number of track center trajectories intersecting each of the designated regions of WD propagation (Fig. 4) per winter season. The outer domain is the general region in which troughs propagating through will have a high probability of influencing weather in the KH. Region One indicates the region of maximum activity within the outer domain. Troughs entering this region are most frequent (5-6 per year, Fig. 5b), and affect the KH most directly. This region is also co-located with the mean position of the subtropical jet over southwest Asia during winter (Cannon et al. 2014, their Fig. 11a). Regions Two and Three represent areas that also experience WD, though their influence in the KH is less direct than Region One and generally less frequent, exhibiting an average of approximately 2 per year per region (Fig. 5c,d).

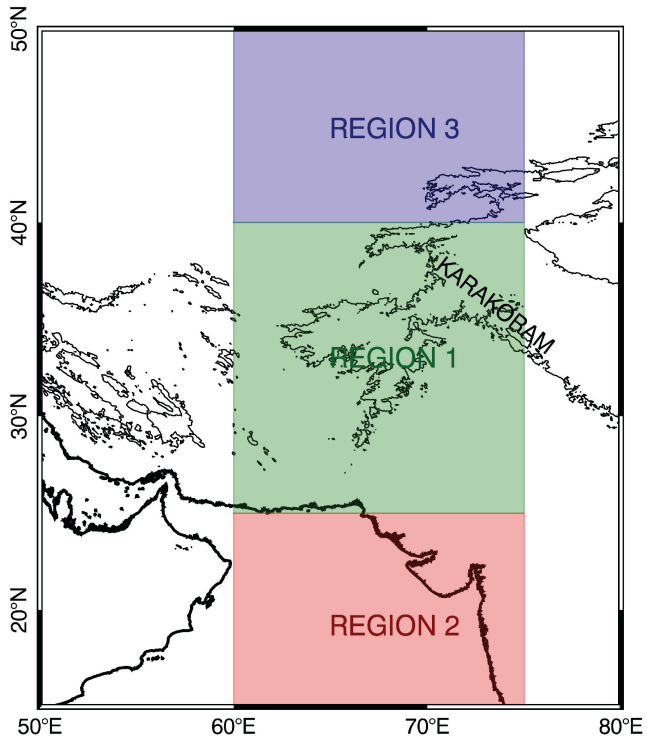

Figure 4 – Schematic map indicating regions used to index Westerly Disturbances. Thin black line indicates 3000m elevation contour.

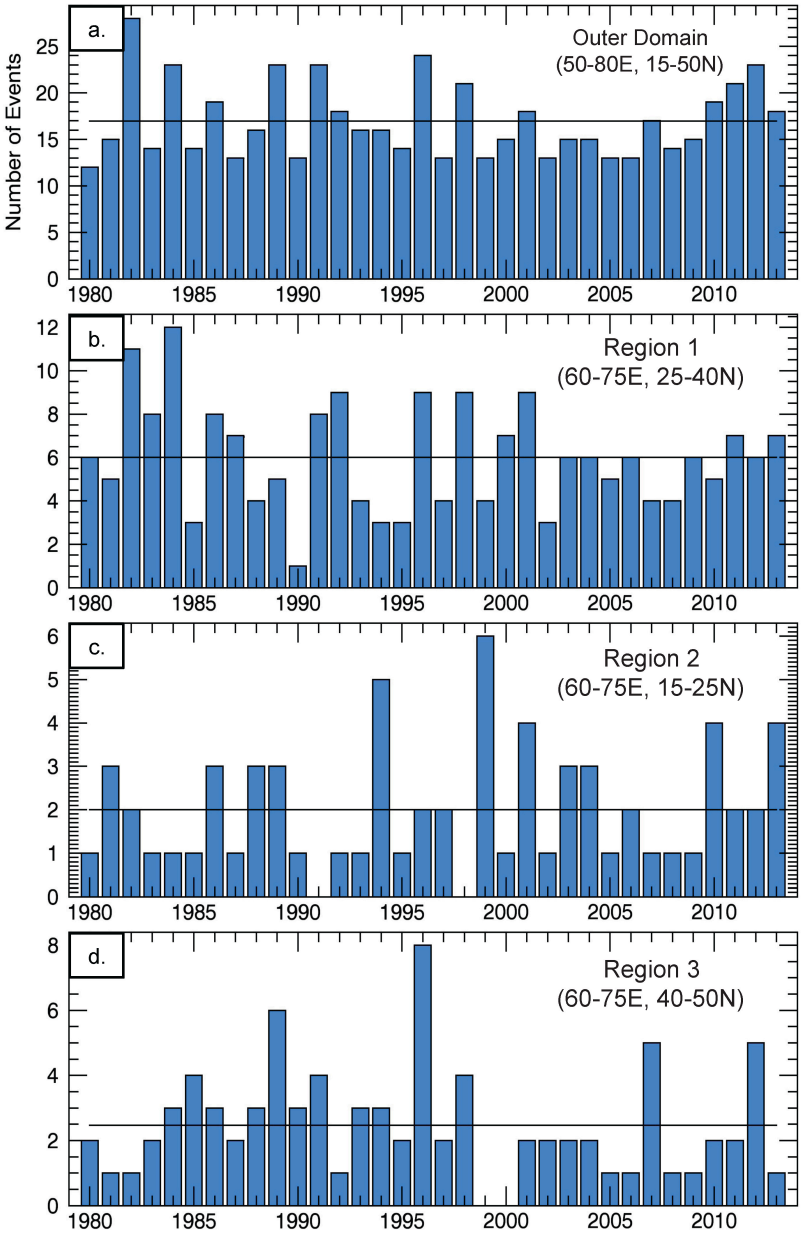

Figure 5 – Number of wave track center trajectories intersecting each of the regions displayed in Figure 4 per winter season. Black line indicates average number of disturbances in the given region per winter (Nov. to Apr), 1979-2013. Note that the Y-axis is not constant between panels.

The total number of recorded WD as well as the number of Region One WD shows interannual variability for the period 1979-2013, but a statistically significant trend in the number of these events per-season cannot be determined based on the short record. This is interesting because it indicates that the frequency of WD in the region of maximum activity

has not changed. With respect to the findings of Cannon et al. (2014), which indicated an increase in the synoptic variability in the upper-level geopotential height field for this region, this may signify an increase in the intensity rather than frequency of WD. It is also important to note that global modes of atmospheric variability, such as ENSO, likely play a role in the distribution of events per region. Previous studies have indicated a significant barotropic Rossby wave response of upper-level geopotential height over southwest-central Asia to ENSO, resulting in intensified westerly jet activity and a deepened trough during El Niño (Syed et al. 2006; Yadav et al. 2010; Hoell et al. 2013; Cannon et al. 2014). Using our tracking methodology, we also observed a drastic increase in the number of WD during El Niño events (not shown), as well as global influences of ENSO on geopotential height variability. The focus of this manuscript is on understanding the dynamics of WD and their variability through time. For the remainder of this work we concentrate on WD tracks recorded in Region One (60-75°E, 25-40°N), the region with the most events and strongest relationship with KH precipitation.

1.7 TRMM and CFSR Comparison of WD Precipitation in the Karakoram and Western Himalaya

Given the difficulties associated with estimating precipitation in mountainous regions using satellites (Barros et al. 2000; Anders et al. 2006; Bookhagen and Burbank 2006) and models, it is necessary to briefly compare the two precipitation products used in this study. In Section 1.3 we introduced some of the issues associated with CFSR and TRMM precipitation; here, we show the relationship between the two products during the maximum precipitation day of WD in Region One as indexed from CFSR data (Fig. 6). For this

analysis, TRMM is interpolated to the 0.5° CFSR grid. Figure 6a indicates the Pearson product-moment correlation between CFSR and TRMM for the maximum precipitation day of each event affecting Region One (2000-2013, 84 events). Correlation in the Karakoram and western Himalaya is between 0.5 and 0.8. Figure 6b is a regression of area-averaged TRMM and CFSR precipitation estimates for the Karakoram (74-77°E, 34-37°N) during those WD. The red dots indicate events where CFSR was more than three times greater than the TRMM estimate. This was observed most frequently in low-precipitation events. On an accumulated monthly precipitation basis, CFSR generally exceeds TRMM precipitation estimates during winter months in High Mountain Asia (not shown). We do not evaluate how much of this difference is attributable to TRMM's difficulty in estimating light and solid-state precipitation and how much is based on CFSR overestimation, though previous work by Maussion et al. (2014), which evaluated TRMM, station gauge, reanalysis, and dynamically downscaled precipitation products to find that differences between products vary on account of season, location and precipitation type, also identified issues in the ability of TRMM to properly represent high-elevation solid-state precipitation in regions of strong winter westerly disturbance influence.

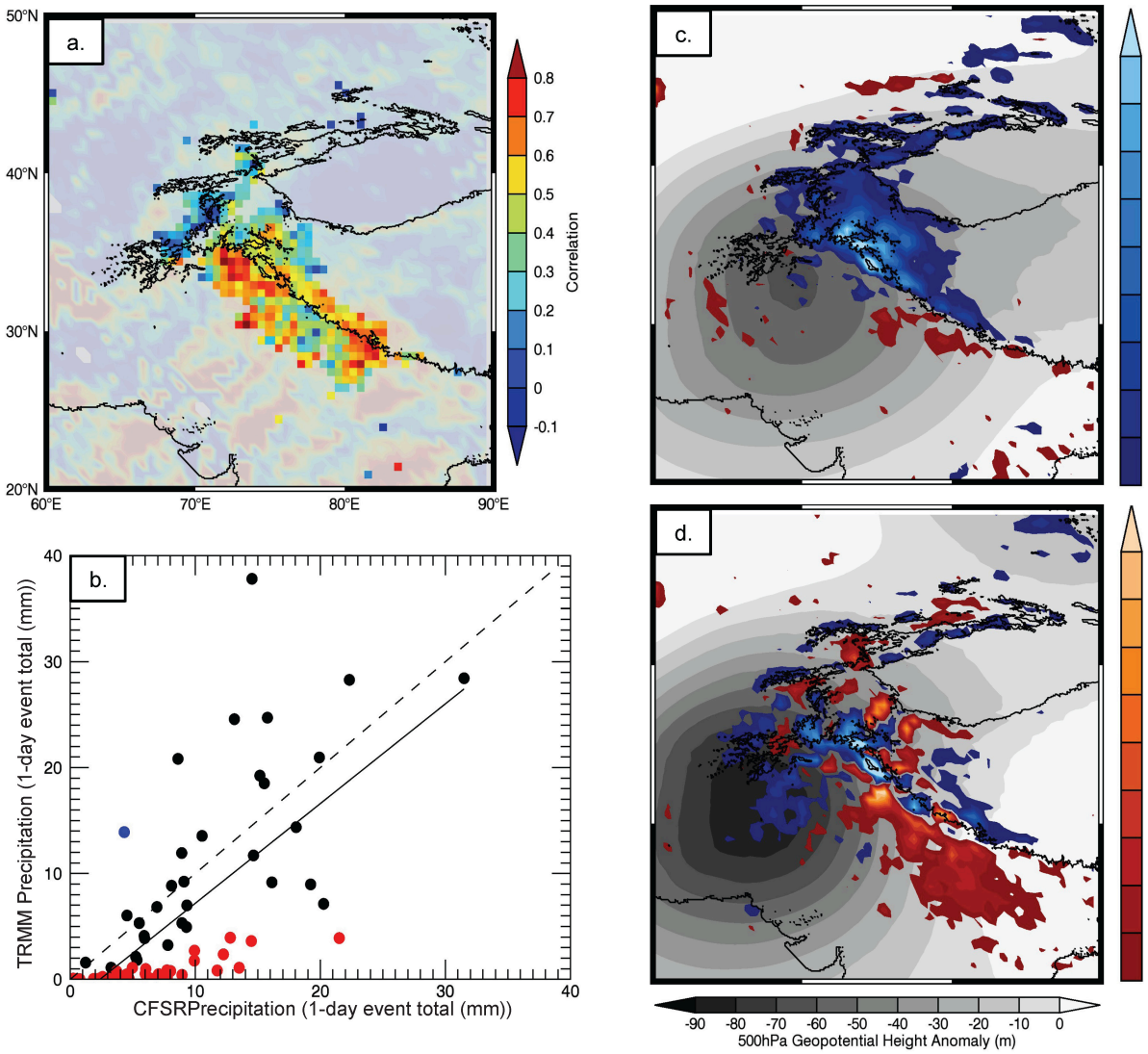

Figure 6 – Correlation between TRMM and CFSR precipitation delivered to Karakoram by Region One Westerly Disturbances 2000-2013 (a). The faded regions indicate that observed precipitation was less than 1mm. Panel (b) shows regression of 1-day precipitation totals delivered to Karakoram by Region One Westerly Disturbances. Red dot indicates event where CFSR precipitation recorded was more than three times greater than TRMM precipitation. Blue indicates the opposite and black is in between. Panel (c) is a composite of precipitation differences between CFSR and TRMM and geopotential height anomalies for red-dot events. Black-dot events are composited in Panel (d). Colorbars for Panels c and d apply to both figures.

A comparison of composites of 500-hPa geopotential height anomalies for WD where CFSR precipitation estimates in the KH were more than three times greater than TRMM (Fig. 6c), compared to all other events (Fig. 6d), indicated that deeper troughs are associated

with more similar precipitation estimates. Analysis of the centers of tracks for dates when CFSR was three times greater than TRMM (49 events) and dates when CFSR was less than three times greater than TRMM (35 events) indicated the mean depth of 500-hPa anomalies to be -96m for events when CFSR greatly exceeded TRMM and -117.6m for events when CFSR did not exceed TRMM by a factor of three. A t test determined the difference in WD depth to be significant at the 5% confidence level. This is likely attributable to deep troughs producing comparatively heavy precipitation, which should be more accurately represented by both products as the signal is stronger and covers a greater area.

Figure 7 shows the mean TRMM and CFSR precipitation amount for the single maximum precipitation day of 84 events (2000-2013; indexed using CFSR) for the Karakoram region. In both products, the maximum in precipitation is found on the southern (windward) slope of the western Himalaya, which protrudes abruptly from the Gangetic Plain. Additionally, there is consistency in indicating a secondary maximum in the Karakoram Mountains, which are further downwind, in the interior of the ranges. Though the spatial distribution is similar between CFSR and TRMM, it is again observed that CFSR has a higher mean value on both the primary and secondary peaks. For this work, we have confidence that the spatial and temporal distribution of precipitation during individual events is accurate, given the consistency between data sets. However, without dependable *in-situ* measurements, we are doubtful that the magnitude of precipitation is reliable. We employ CFSR precipitation for the majority of this manuscript on account of its extended temporal record, though additional research (not shown here) has indicated similar results using TRMM (1998-2013).

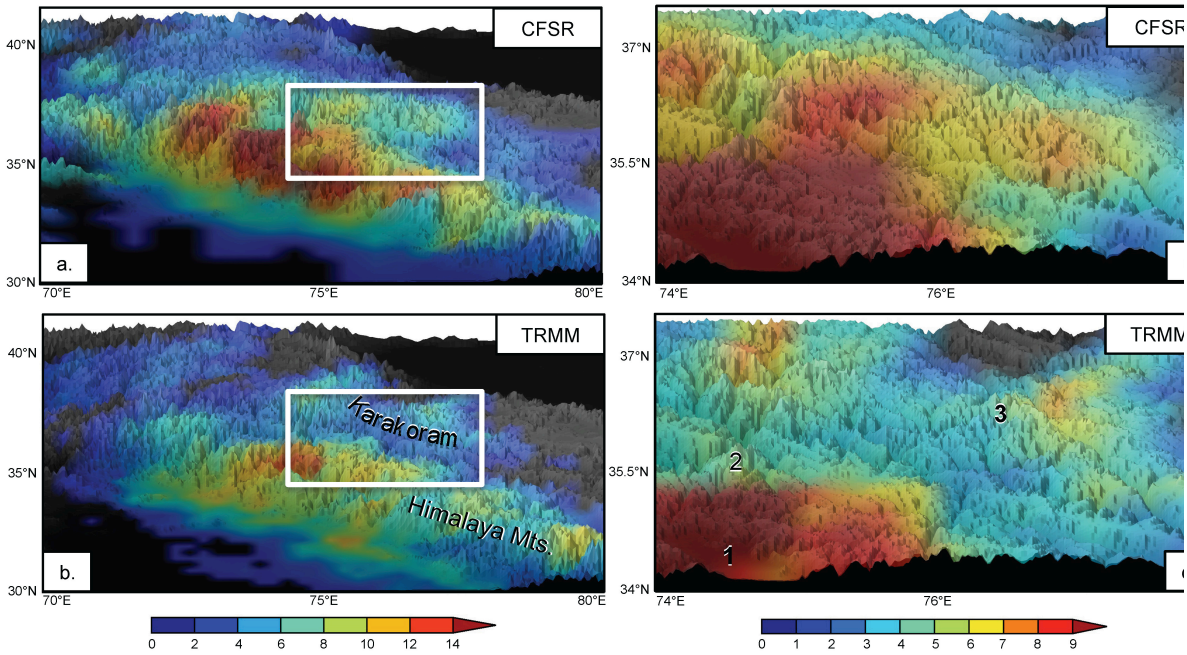

Figure 7 – Average Karakoram precipitation recorded during Westerly Disturbances in winter seasons when TRMM and CFSR data were available (1998-2013). Topography is shown in three dimensions. CFSR outer domain (a), inner domain (c) and TRMM outer domain (b) and inner domain (d). 1. Location of Kashmir Valley. 2. Nanga Parbat. 3. K2. White box in b indicates domain for c and d.

1.8 Seasonal Variability of WD and Precipitation Contribution

Tracking individual westerly disturbances and investigating their collective statistics illuminates the manner in which the mechanisms that drive orographic precipitation during these events change throughout the winter season. WD are primarily active November through April and exhibit strong seasonal variability (Lang and Barros, 2004). Additionally, general changes to the atmosphere due to the seasonal cycle create significant differences between individual disturbances according to when they occur in the winter season. Figures 8, 9 and 10 illustrate changes in WD over the winter season as identified through our tracking approach. Figure 8 indicates the number of Region One WD recorded in each month for each year of CFSR (1979-2013). We observe a large interannual variability in the number of WD

with some years exhibiting three or more events per month and others no event. The March timeseries in Fig. 8 is the best illustration of the year-to-year differences in the number of disturbances. Moreover, the environmental conditions in which WD develop vary throughout the winter season. To illustrate these differences, Fig. 9 shows composites of 500-hPa geopotential height anomalies, vertically integrated moisture transport, and precipitation, for WD events, as indexed by wave tracking, in each month of the winter season. In December, January and February the average geopotential height anomaly is up to 70m deeper than in March, April or November. December through February, the meridional temperature gradient across the northern hemisphere is at a maximum and thus, mid-latitude storm intensity peaks during this time (Ramaswamy, 1956). WD occurring during these months are dynamically more intense, with deeper troughs and stronger wind speeds than those occurring in March and April. However, through the Clausius-Clapeyron relationship, elevated temperatures in spring increase moisture content, as evidenced by the high precipitable water values observed over continental areas in March and April (Fig. 10). This produces a less thermodynamically stable atmosphere, in which reduced dynamical forcing may still trigger orographic precipitation in the KH. Figure 10 shows increased precipitable water along the Himalayan Arc in spring months relative to mid-winter months as well as weaker 500-hPa meridional wind speed for late season WD. March is the most variable month as WD transition from primarily orographic to orographic and convective forcing. After April and before the onset of the monsoon, large-scale convection is unlikely as the subtropical jet has migrated to the north of the Tibetan Plateau and upper-level divergence associated with waves in the jet is absent (Ramaswamy, 1956).

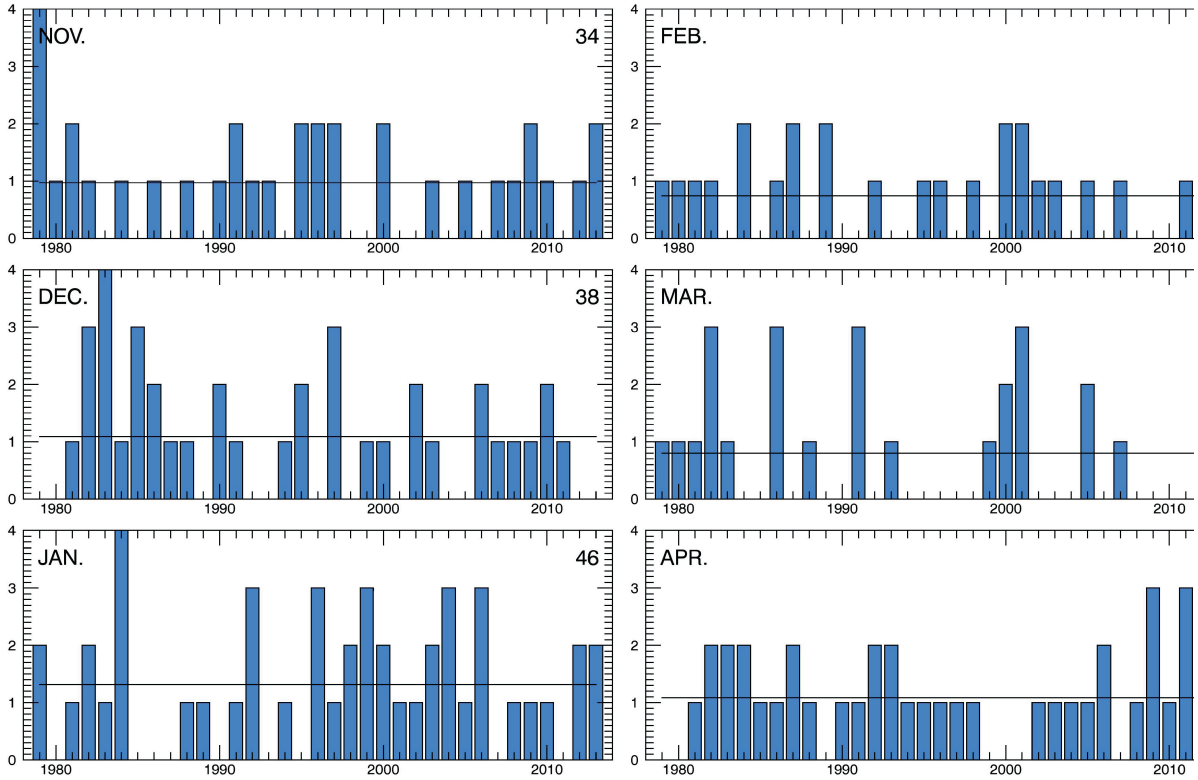

Figure 8 – Number of wave track center trajectories intersecting Region One per month. Black line indicates average number of disturbances in the given region per month, 1979-2013. Number in upper right indicates total number of disturbances.

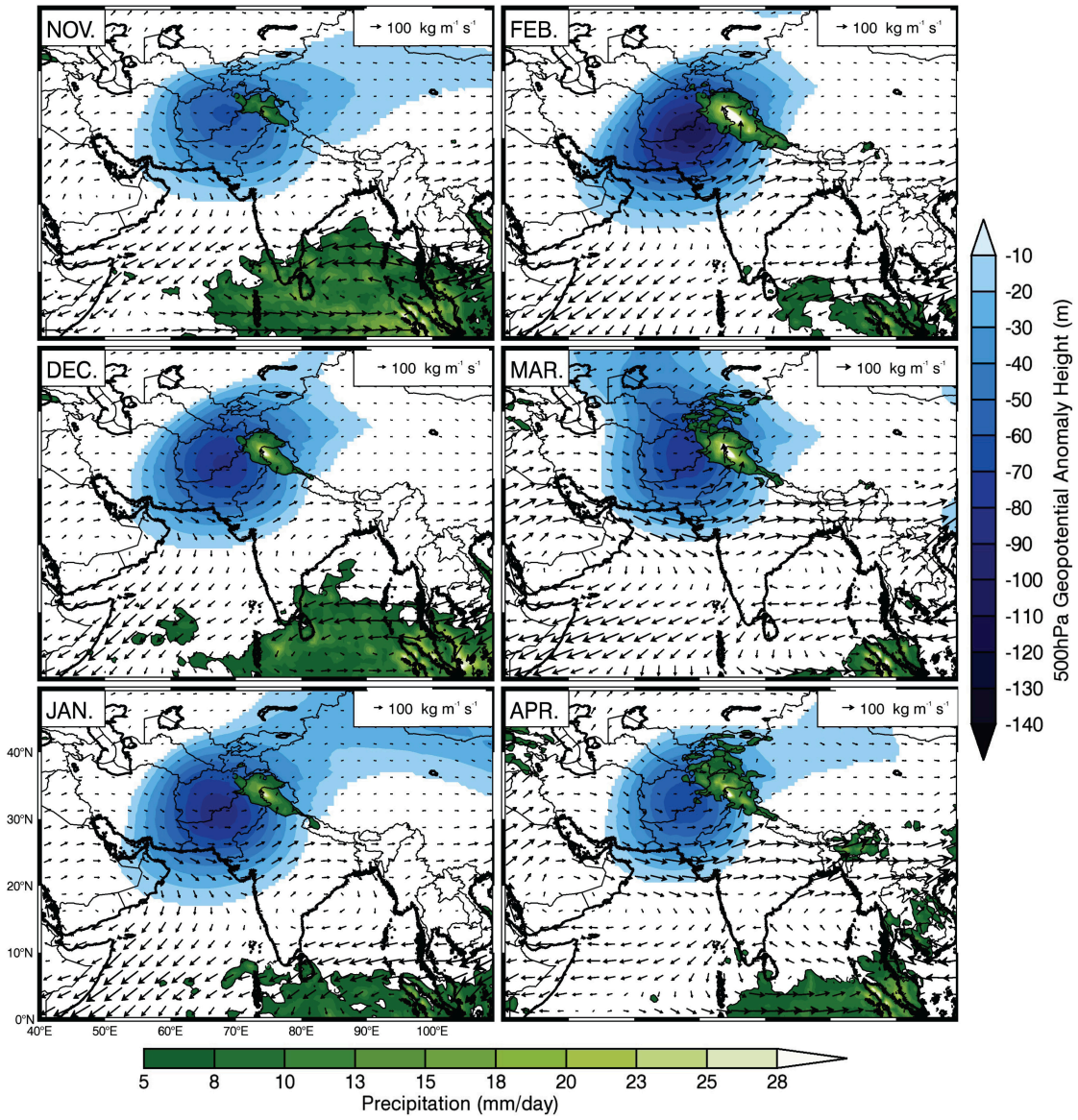

Figure 9 – Composites of Westerly Disturbance events as identified by the maximum Karakoram precipitation (CFSR) day of track trajectories intersecting Region One. Vectors indicate vertically integrated moisture flux.

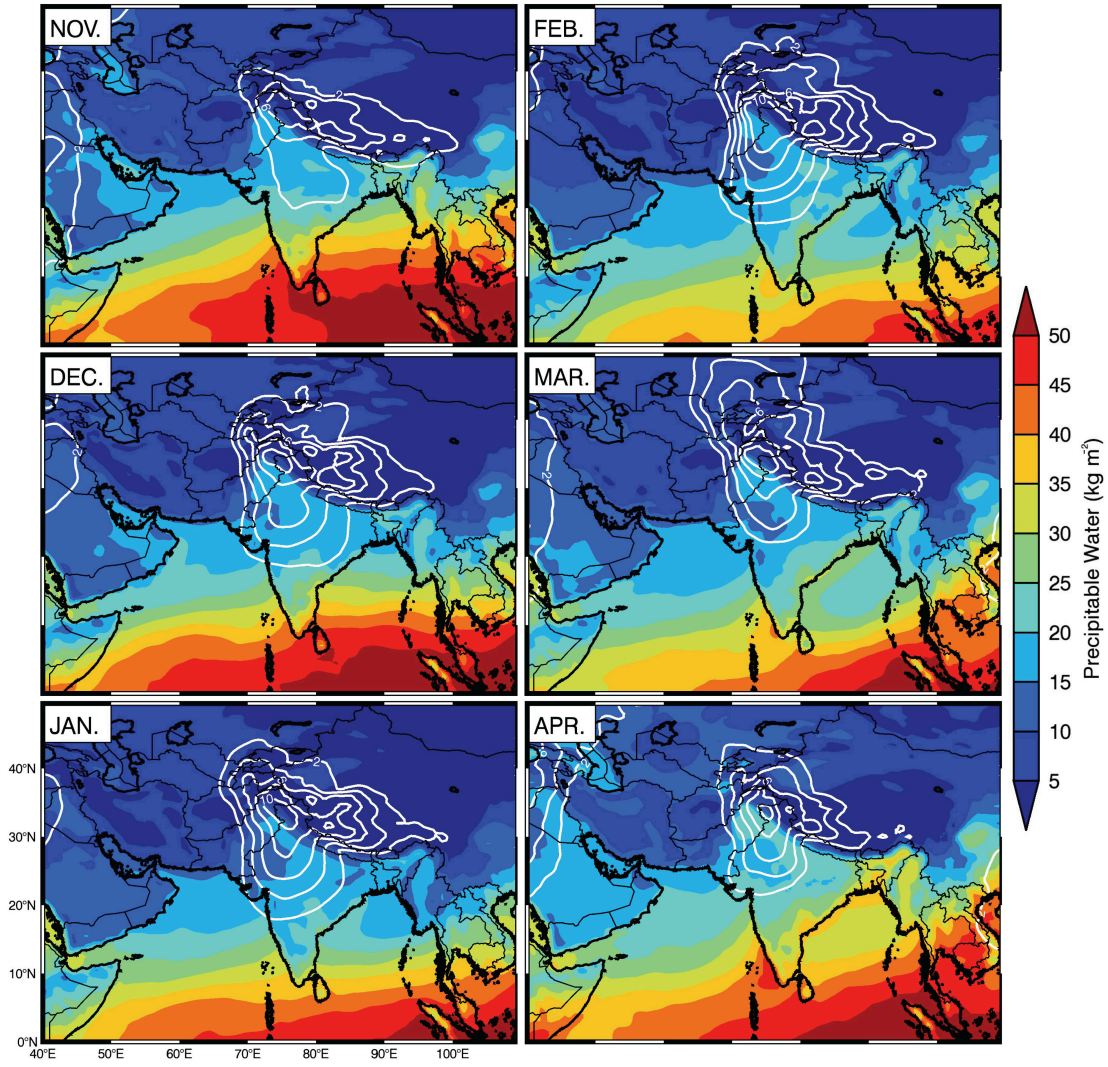

Figure 10 – Composites of Westerly Disturbance events as identified by the maximum Karakoram precipitation day (CFSR) of track trajectories intersecting Region One. White contour indicates the southerly 500-hPa wind speed (m s^{-1}).

Heavy precipitation events associated with WD can occur in any month during the winter season, but are driven by different processes according to their timing. As noted, the upper-level trough is, on average, deeper December through February and associated meridional wind velocities are stronger than in March and April, thus impinging on the KH with more intense orographic forcing. Figure 9 indicates little change in vertically integrated moisture flux (vectors) between these months, though the dominant term appears to change

from wind speed to precipitable water. Curio et al. (2015) discuss the mechanisms by which moisture is transported to the Tibetan Plateau and demonstrate that, in winter months westerly disturbances are the dominant source of moisture, while in warmer months the western Tibetan Plateau receives monsoon moisture in addition to advection from westerlies, while also benefiting from enhanced local evaporation, leading to moisture recycling.

In March and April, atmospheric moisture content is seen to increase due to rising temperatures, which increase saturation vapor pressure. Amplified moisture and temperature at low levels are a primary condition for convective instability, as measured by moist static energy change with height (not shown), during these events. In this pre-monsoon environment, the interaction of an extratropical cyclone with a relatively warm, moisture-laden, tropical air mass provides strong moisture transport towards the mountains. Figure 10 shows average precipitable water during April WD events to be 25% higher over the Gangetic Plain than during January events, while 500-hPa southerly winds are generally $2ms^{-1}$ slower. Heavy precipitation in the Himalaya via orographic lifting experiences stronger contribution from thermodynamic instability, as the atmosphere is less stable than in the middle of winter (Norris et al. 2015). It is worth noting that Simmons et al. (2010) show that surface temperature and humidity trends from two reanalysis products are in excellent agreement with estimates from climatological land data, and the work of Lu et al. (2014) and Curio et al. (2015) further support the ability of reanalyses to represent in situ moisture conditions at coarse spatiotemporal resolution over the Tibetan Plateau. At finer spatial and temporal scales, reanalyses may be less representative of moisture conditions given their inability to resolve individual mountain valleys (Curio et al. 2015), which serve as moisture conduits (Bookhagen and Burbank, 2010), but this is of minor importance with respect to our

study given the magnitude of differences between seasons relative to the magnitude of differences in moisture advection resulting from the smoothing of local valley systems.

To further investigate the dynamics of WD as well as the mechanisms that drive precipitation in the KH, and to substantiate the argument proposed to explain Figure 9, we performed a series of regressions between 500-hPa geopotential height anomalies at track centers, 500-hPa meridional wind in the KH (74-77°E, 34-37°N), total precipitable water in the KH, and precipitation in the KH (Fig. 11). Because the Karakoram is east-west oriented, meridional wind is perpendicular to the mountains and is the more important horizontal component of wind for orographic precipitation. These four variables have a complex relationship that defines winter weather in HMA. Additionally, moving away from composite analysis enables the identification of changes in the relative contribution of each variable to precipitation on a case-by-case basis. Though these figures delineate statistically significant patterns, they also demonstrate that the average values shown in the monthly WD composites (Figs. 9 & 10) are derived from strongly varying individual events.

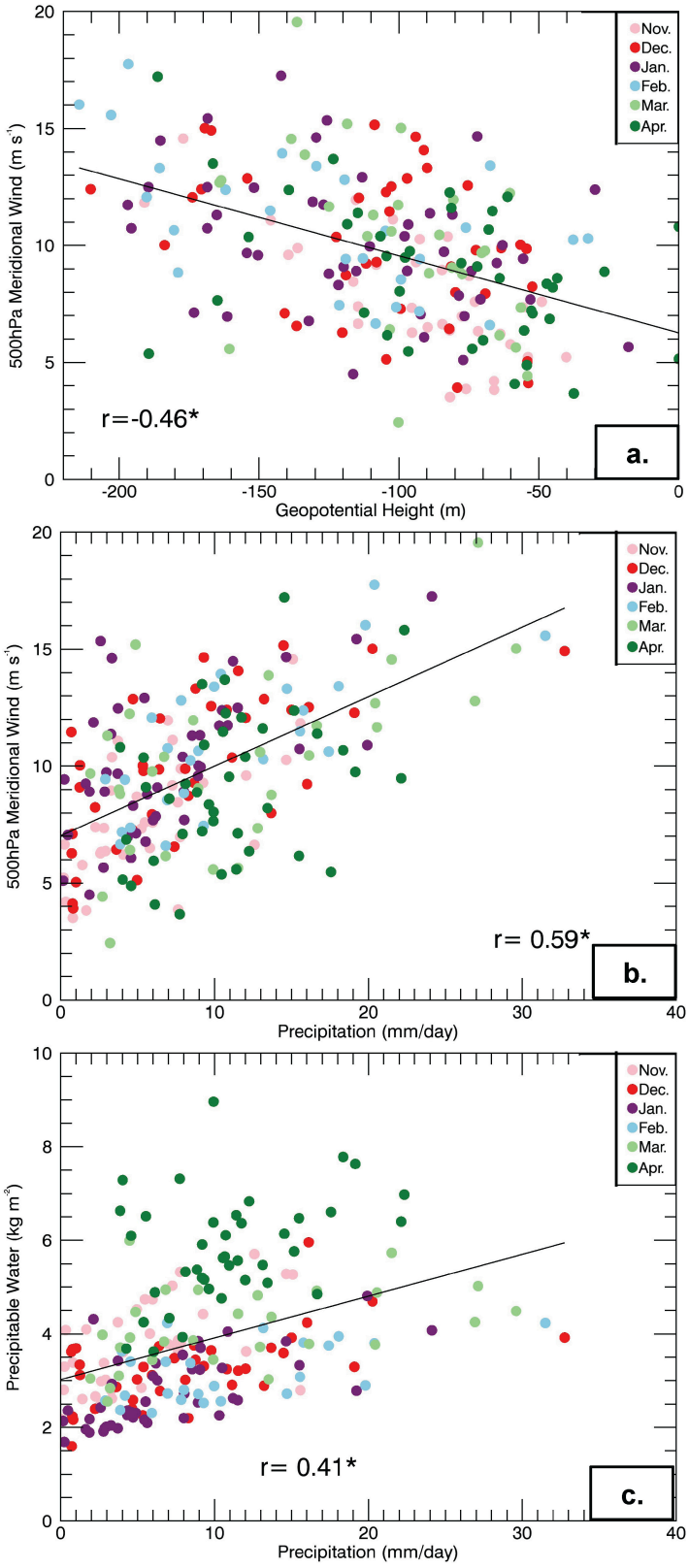

Figure 11 – Regression of variables during all Region One Westerly Disturbances. 500-hPa geopotential height anomalies at the trough center and 500-hPa meridional wind in the

Karakoram (a); 500-hPa meridional wind and Precipitation in the Karakoram (b); Precipitable water and precipitation in the Karakoram (c). Dot color indicates month (see legend). Black line indicates slope of regression. Number on graph indicates Pearson correlation coefficient. Star next to number indicates significance at 5% confidence interval.

Correlation between WD depth and 500-hPa meridional wind speed in the KH is 0.46 for 209 independent Region One events occurring November through April 1979-2013 (Fig. 11a). Figure 11a also demonstrates differences in trough depth according to month as previously illustrated in Fig. 9. In December, January and February, WD are at maximum intensity as the mid-latitude jet is at its peak; the average depth of geopotential height anomalies is -115m compared to -94m for March and April events. Consequently, wind speeds in the KH (maximum value two days before precipitation maximum through two days after, for the region 74-78°E, 34-37°N) also peak during events falling in these months. Figure 11b shows a regression between 500-hPa meridional wind in the KH and precipitation. The correlation is 0.59, which is statistically significant at the 5% level (p value for two-sided t test less than 0.05), indicating a positive relationship between the strength of the wind encountering topography and the amount of precipitation received, with high wind speeds enhancing precipitation over topography (Roe, 2005). Coincident with increasing trough depth, wind speeds are highest in December, January, and February, leading to the conclusion that the orographic forcing of precipitation associated with WD is at a maximum during these months. Interestingly though, precipitation accumulation is not necessarily highest at the same time, due largely to changes in available moisture.

Heavy precipitation events occurring in March and April have characteristically slower meridional wind speeds at upper levels (The average for 66 March and April events is 9.4m s^{-1} compared to 10.5m s^{-1} for 110 events occurring December through February),

though the decrease in orographic forcing is compensated for by enhanced precipitable water, as noted earlier (5kg m^{-2} compared to 3kg m^{-2} for December through February events). Figure 11c indicates highest precipitable water in the KH to have occurred primarily during March and April WD. Increased convective instability, slower storm propagation, and increased moisture all contribute to heavy precipitation despite reduced wind speed compared to middle-of-winter events.

Figure 12 delineates the relationship between precipitable water, 500-hPa meridional wind and precipitation during region one WD for December through February (Fig. 12a; 110 events) compared to March and April (Fig. 12b; 66 events). November is omitted in this analysis, as precipitation during this month is minimal. The intensification of negative geopotential-height anomalies is associated with a strengthening of the pressure gradient, which yields southerly wind along the eastern edge of the disturbance and draws moisture from the Arabian Sea toward HMA. This can be observed in Fig. 12a by the significant positive correlation (0.35) between 500-hPa meridional wind and Precipitable water. Additionally, the largest precipitation totals (greater than 24mm/day) are recorded during strong wind and high precipitable water events. The well-balanced relationship deteriorates in March and April, when precipitable water is enhanced irrespective of the disturbance (Fig. 12b; $r = -0.01$). This is further illustrated by multiple regression analysis using precipitable water and 500-hPa wind as estimators of precipitation during past events, which yields an R^2 value of 0.56 for the December through February events, but only 0.31 for March and April.

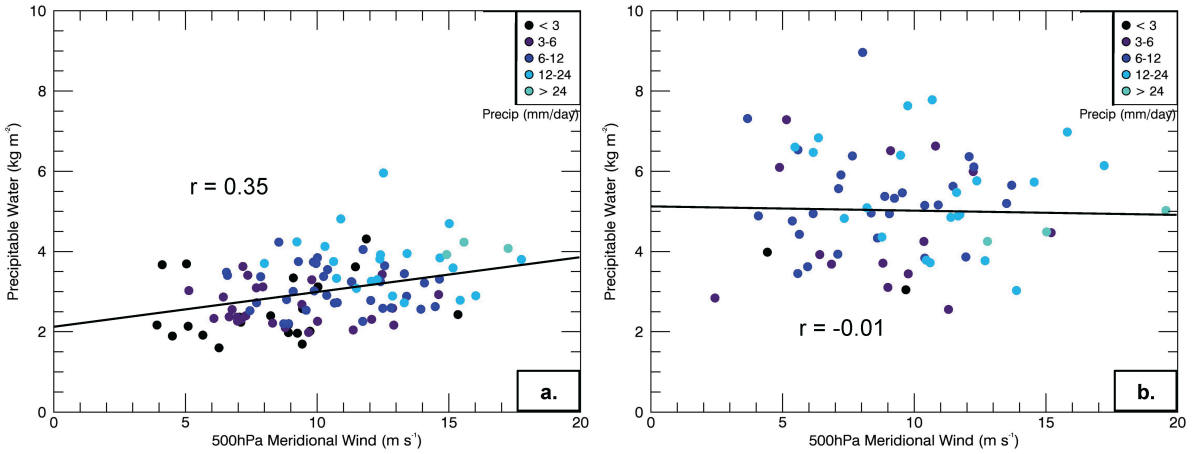

Figure 12 – Regression of 500-hPa meridional wind and precipitable water in the Karakoram region for Westerly Disturbances in the months of DJF (left) and MA (right), 1979-2013. Color indicates the amount of precipitation received in the Karakoram on the maximum precipitation day during each event.

Table 1 is introduced to summarize the results shown in Figs. 11 and 12, and to characterize the combined relationships amongst the investigated variables, which are not entirely independent. This table lists correlation values between all variables for December through February and March through April events. In agreement with Fig. 12, both 500-hPa meridional wind and precipitable water are better correlated to precipitation in mid-winter than early spring, and they are not independent at this time (r = 0.35). The considerable weakening of the relationship between precipitable water and precipitation, from r = 0.57 in mid-winter to 0.28 in spring, and precipitable water and meridional wind, from r = 0.35 to 0.02, apparently results from a reduction in the dependency on WD to provide sufficient moisture for precipitation, on account of the higher moisture content in the atmosphere irrespective of WD occurrence. The relatively minor reduction in the correlation between 500-hPa wind and precipitation indicates that orographic forcing remains the primary precipitation mechanism, while the consistent relationship between the depth of the trough and meridional wind indicates that the relationship between orographic forcing and WD is

unchanged, despite their reduced intensities in spring. Furthermore, a similar correlation matrix using TRMM precipitation for 50 WD events in the December through February period and 29 in March and April, 1998-2013, (not shown) displays an even larger reduction in the correlation between precipitable water and precipitation from mid-winter to spring, but no reduction in the correlation between 500-hPa meridional wind and precipitation.

r	H5	V5	PW	Cp
H5	1	**0.43**	0.03	**0.41**
V5	**0.45**	1	**0.35**	**0.65**
PW	0.08	0.02	1	**0.57**
Cp	**0.37**	**0.49**	**0.28**	1

KEY: H5 = Depth of 500-hPa Geopotential Height Anomaly at Track Center
V5 = 500-hPa Meridional Wind over the Karakoram
PW = Precipitable Water over the Karakoram
Cp = CFSR Precipitation over the Karakoram
Black Values = December through February Events
Red Values = March and April Events

Table 1 – Correlation matrix of westerly disturbance 500-hPa geopotential height anomaly at the trough center, and Karakoram/western Himalaya precipitation, 500-hPa meridional wind, and precipitable water during 110 independent events occurring December through February (black) and 66 events occurring in March and April (red) 1979-2010. Bold values indicate significance.

These analyses give additional evidence that orographic precipitation during WD events occurring December through February are strongly dependent on moisture that is advected by cyclonic winds associated with the disturbance, while March and April events are characterized by a strong dependence on cross-barrier wind, but a weakened relationship with moisture anomalies. By tracking individual WD events we are able to illustrate that dynamical forcing alone does not determine precipitation quantity. The fact that there is significant correlation between precipitable water and precipitation, even in spring when the relationship is considerably weaker, indicates that moisture advection toward the KH, both related to and independent of these events, is an important component of regional precipitation. Moving forward, analysis of variability in WD generated KH precipitation

should account for large-scale processes including tropical/extra-tropical interactions, which affect the amount of precipitable water over the Indian sub-continent, and undergo significant modification by global modes of atmospheric variability.

1.9 Conclusions

The objective of this research was to investigate Winter Westerly Disturbances (WD) within a framework that facilitated both the observation of individual events and the creation of a large database with information specific to each recorded event. Using Climate Forecast System Reanalysis (CFSR), we created a WD tracking method based on the presence of upper-level troughs, which are characteristic features of these events. This enabled both the recording of attributes of the disturbances as they moved and evolved, and the simultaneous recording of variables related to precipitation in the western Himalaya/Karakoram (KH). The benefit of our wave-tracking methodology over existing cyclone-tracking techniques is specific to regions of high topography and, in our analysis of WD, gave a unique perspective of the relationship between transient systems and precipitation within our region of interest. Though we do not perform a comprehensive comparative analysis between our methodology and existing extratropical cyclone tracking techniques, such as those described in Neu et al. (2013), our Northern Hemisphere track densities compare well to the established work of Hoskins and Hodges (2002), which also identified mid-latitude disturbances at the 500-hPa level, and Syed et al. (2010) with a specific focus on High Mountain Asia.

Between 1979 and 2013, we observed more than 600 WD events, 209 of which occurred proximal to the KH (60-75°E, 25-40°N), in a region identified by Cannon et al. (2014) as intimately linked to KH precipitation. The relationship between the dynamics of

the identified systems and KH precipitation was investigated with the original goal of identifying multi-annual changes in WD that are indicative of long-term regional climatic variability with significant consequences for KH hydrology, There is much interest in relating variability in the region's hydrometeorology to seasonal snowpack changes (Tahir et al. 2011) and even regional glacier behavior (Kapnick et al. 2014), and better understanding the KH's primary climatic influence is one of many important components in this area of research. Though trends in WD activity were not discernable, we illustrate the complex relationships between WD, the mechanisms that drive orographic precipitation in the KH, and how these relationships transform over the course of the winter season.

A significant change from 1979 to 2013 in the number of WD events affecting the KH was indeterminable from CFSR. We observed there to be an average of 5-6 WD events in this region per year, with large interannual variability that is likely attributable to teleconnections with global modes of atmospheric variability (Barros et al 2004; Syed et al 2006; Yadav et al. 2010; Cannon et al. 2014). In this work, we observed large variability in dynamics and precipitation between individual WD according to a variety factors. The unique benefit of our tracking method over Eulerian statistics is to facilitate the investigation of precipitation exclusively associated with WD events and to specifically observe the intensity of these events as identified by upper-level trough depth. This approach allowed for the direct relation of WD intensity to the mechanisms that drive orographic precipitation in High Mountain Asia as well as to each event's respective precipitation total.

500-hPa geopotential height anomalies at the WD center, precipitable water in the KH, 500-hPa meridional wind in the KH, and precipitation in the KH were analyzed for 209 WD in our region of interest for winter seasons 1979-2013. Unsurprisingly, the depth of the

500-hPa anomaly at the center of the trough and the 500-hPa meridional wind were significantly correlated. Deeper WD manifested an intensified pressure gradient, thus enhancing the geostrophic wind. The 500-hPa meridional wind during these events was also significantly correlated to precipitation, as orographic lifting is the primary determinant of KH precipitation. On the east side of the disturbance, cyclonic winds produce southerly flow, which advects moisture from the tropics and drives it against KH topography. This relationship between the depth of WD, the strength of the wind and the amount of precipitation was observed to change over the course of the winter season. In December, January and February (DJF), when the temperature gradient across the northern Hemisphere is strongest, the subtropical jet is at a maximum and is positioned at the same latitude as the Himalaya (Krishnamurti, 1961; Holton, 2004). Consequently, WD occurring during DJF were observed to have deeper geopotential height anomalies and higher wind speeds. Upper-level divergence aids large-scale convection, and mechanical forcing of precipitation due to orographic lifting is strongest during these events. Contrastingly, during March and April (MA) the jet has shifted north of the Tibetan Plateau and geopotential-height anomalies are shallower, implying weaker winds. However, the Indian subcontinent is considerably warmer than during DJF, and atmospheric moisture content has increased due to increased saturation vapor pressure (Holton, 2004). Though WD in MA are not as dynamically intense, weaker orographic forcing is compensated by the warmer, moister and less stable conditions, in which orographic precipitation occurs more readily. This illustrated that dynamically weak WD can thereby produce heavy precipitation events through the enhancement of available moisture, which can be associated with, or independent of, the WD event, and further exemplifies the complex relationship between WD and precipitation in the KH.

In addition to seasonal changes in the relationship between WD and KH precipitation, teleconnections have a strong effect on differences in precipitation produced by WD occurring at the same time of the year. It is likely that WD associated precipitation is highly dependent on a number of factors that are often regulated by global modes of atmospheric variability, including tropical-extratropical interactions and consequent changes in available moisture. Differences between individual WD precipitation events in the High Mountain Asia are therefore modulated by the Madden Julian Oscillation (Barlow et al. 2005; Hoell et al. 2013), El Niño Southern Oscillation (Syed et al. 2006; Yadav et al. 2010) and the North Atlantic Oscillation/Arctic Oscillation (Gong et al. 2001; Wu and Wang, 2002; Yadav et al. 2009; Syed et al. 2010; Filippi et al. 2014). WD are affected by complex non-linear relationships throughout the global atmosphere, which significantly alter the dynamics that drive precipitation. Consequently, precipitation totals are dependent on much more than just the strength of the disturbance and should be analyzed accordingly, as was done in this work.

By investigating an inclusive perspective of WD, which accounts for the dynamics of the systems, how they change across seasons, and how they interact with the background atmosphere, we have improved our understanding of the factors that influence KH precipitation. Moving forward, this creates a basis by which we may better comprehend how a changing climate will affect WD and, consequently, winter precipitation in High Mountain Asia's Mountains. This undoubtedly augments our understanding of recent climatic conditions in the region and will improve our ability to project into future decades while minimizing uncertainty with respect to Asia's water resources.

1.10 Acknowledgements

This research was supported by the Climate and Large-scale Dynamics Program, from the National Science Foundation (NSF award-AGS 1116105) and by NASA Headquarters under the NASA Earth and Space Science Fellowship Program (Grant Number 13-EARTH13F-26). The CFSR data used in this research were developed by NOAA's National Centers for Environmental Prediction (NCEP) and provided by NCAR. TRMM data were acquired by an international joint project sponsored by the Japan National Space Development Agency (NASDA) and the U.S. National Aeronautics and Space Administration (NASA) Office of Earth Science. The Authors would also like to thank Dr. Bodo Bookhagen for his help throughout this project.

1.11 References

Akperov MG, Yu M, Bardin E, Volodin M, Golitsyn GS, Mokhov II (2007) Probability distributions for cyclones and anticyclones from the NCEP/NCAR reanalysis data and the INM RAS climate model. Izv Atmos Oceanic Phys 43, 705-712

Anders AM, Roe GH, Hallet B, Montgomerey DR, Finnegan NJ, Putkonen J (2006) Spatial patterns of precipitation and topography in the Himalaya. Geol Soc Am Spec Pap 398:39-53

Archer DR, Fowler HJ (2004) Spatial and temporal variations in precipitation in the Upper Indus Basin, global teleconnections and hydrological implications. Hydrol Earth Syst Sc 8:47-61

Barlow M, Wheeler M, Lyon B, Cullen H (2005) Modulation of daily precipitation over southwest Asia by the Madden-Julian oscillation. Mon Weather Rev 133:3579-3594

Barros AP, Joshi M, Putkonen J, Burbank DW (2000) A study of the 1999 monsoon rainfall in a mountainous region in central Nepal using TRMM products and rain gauge observations. Geophys Res Lett 27:3683-3686

Barros AP, Chiao S, Lang TJ, Burbank D, Putkonen J (2006) From weather to climate – Seasonal and interannual variability of storms and implications for erosion processes in the Himalaya. Geol Soc Am Spec Pap 398:17-38

Benestad RE, Chen D (2006) The use of a calculus-based cyclone identification method for generating storm statistics. Tellus 58A:473-486

Bhutiyani MR, Kale VS, Pawar NJ (2010) Climate change and the precipitation variations in the northwestern Himalaya: 1866-2006. Int J Climatol 30:535-548

Blender R, Schubert M (2000) Cyclone tracking in different spatial and temporal resolutions. Mon Wea Rev 128:377-384

Bolch T, Kulkarni A, Kaab A, Huggel C, Paul F, Cogley JG, Frey H, Kargel JS, Fujita K, Scheel M, Bajracharya S, Stoffel M (2012) The state and fate of Himalayan glaciers. Science 336:310-314

Bookhagen B, Burbank DW (2006) Topography, relief and TRMM-derived rainfall variations along the Himlaya. Geophys Res Lett 33:L08405

Bookhagen B, Burbank DW (2010) Towards a complete Himalayan hydrological budget: The spatiotemporal distribution of snow melt and rainfall and their impact on river discharge. J Geophys Res-Earth 115

Cannon F, Carvalho LMV, Jones C, Bookhagen B (2014) Multi-annual variations in winter westerly disturbance activity affecting the Himalaya. Clim Dyn doi:10.1007/s00382-014-2248-8

Carlson TN (1998) Mid-latitude weather systems. American Meteorological Society, Boston

Carvalho LMV, Jones C (2001) A satellite method to identify structural properties of mesoscale convective systems based on maximum spatial correlation tracking technique (MASCOTTE). J Appl Meteor 40:1683-1701

Carvalho LMV, Lavallee D, Jones C (2002) Multifractal properties of evolving convective systems over tropical South America. Geophys Res Lett doi:10.1029/2001gl014276

Chen QS, Bromwich DH (1999) An equivalent isobaric geopotential height and its application to synoptic analysis and a generalized omega equation in sigma coordinates. Mon Weather Rev 127:145-172

Cohen J, Barlow MA, Kushner P, Saito K (2007) Stratospher-troposphere coupling and links with Eurasian land-surface variability J.Clim 20:5335-43

Curio J, Maussion F, Scherer D (2014) A twelve-year high-resolution climatology of atmospheric water transport on the Tibetan Plateau. Earth Syst Dynam 6:109-124

Dimri AP, Dash SK (2012) Wintertime climatic trends in the western Himalayas. Climatic Change 111:775-800

Filippi L, Palazzi E, von Hardenberg J, Provenzale A (2014) Multidecadal variations in the relationship between the NAO and winter precipitation in the Hindu-Kush Karakoram. J Clim doi:10.1175/JCLI-D-14-00286.1

Gardelle J, Berthier E, Arnaud Y (2012) Slight mass gain of Karakoram glaciers in the early twenty-first century. Nat Geosci 5:322-325

Gong DY, Wang SW, Zhu JH (2001) East Asian winter monsoon and Arctic Oscillation. Geophys Res Lett 28:2073-2076

Grumm RH, Hart R (2001) Standardized anomalies applied to significant cold season weather events: Preliminary findings. J Forecasting 16:736-754

Hanley J, Caballero R (2012) Objective identification and tracking of multicentre cyclones in the ERA-Interim reanalysis data set. Quart J Roy Meteor Soc 138:612-625

Hatwar HR, Yadav BP, Rama Rao YV (2005) Prediction of western disturbances and associated weather over western Himalayas. Curr Sci India 88:913-920

Hewitt K (2005) The Karakoram anomaly? Glacier expansion and the "elevation effect", Karakoram Himalaya. Mountain Res Dev 25:332-340

Hewson TD, Titley HA (2010) Objective identification, typing and tracking of the complete life-cycles of cyclonic features at high spatial resolution. Meteor Appl 17:355-381

Hoell A, Barlow M, Saini R (2013) Intraseasonal and seasonal-to-interannual Indian Ocean convection and hemispheric teleconnections. J Clim 26:8850-8867

Hoell A, Funk C (2013) The ENSO-related west Pacific sea surface temperature gradient. J Climate 26:9545-9562

Hodges KI (1995) Feature tracking on the unit-sphere. Mon Wea Rev 123:3458-3465

Holton JR (2004) An introduction to dynamic meteorology. Elsevier, Burlington

Hoskins BJ, Ambrizzi T (1993) Rossby-wave propagation on a realistic longitudinally varying flow. J Atmos Sci 50:1661-1671

Hoskins BJ, Hodges KI (2002) New perspectives on the Northern Hemisphere winter storm tracks. J Atmos Sci 59:1041-1061

Huffman GJ et al (2007) The TRMM multisatellite precipitation analysis (TMPA): Quasi-global, multiyear, combined-sensor precipitation estimates at fine scales. J Hydrometeorol 8:38-55

Immerzeel WW, Droogers P, de Jong SM, Bierkens MFP (2009) Large-scale monitoring of snow cover and runoff simulation in Himalayan river basins using remote sensing. Remote Sens Environ 113:40-49

Inatsu M (2009) The neighbor enclosed area tracking algorithm for extratropical wintertime cyclones. Atmos Sci Lett 10:267-272

Jones C, Carvalho LMV, Higgins RW, Waliser DE, Schemm JKE (2004) Climatology of tropical intraseasonal convective anomalies. J Climate 17:2078-2095

Kaab A, Berthier E, Nuth C, Gardelle J, Arnaud Y (2012) Contrasting patterns of early twenty-first-century glacier mass change in the Himalayas. Nature 488:495-498

Kapnick SB, Delworth TL, Ashfaq M, Malyshev S, Milly PCD (2014) Snowfall less sensitive to warming in Karakoram than in Himalayas due to a unique seasonal cycle. Nature Geosci 7:834-840

Keable M, Simmonds I, Keay K (2002) Distribution and temporal variability of 500 hPa cyclone characteristics in the Southern Hemisphere. Int J Climatol 22:131-150

Kew SF, Sprenger M, Davies HC (2010) Potential vorticity anomalies of the lowermost stratosphere: A 10-yr winter climatology. Mon Wea Rev 138:1234-1249

Krishnamurti TN (1961) The subtropical jet stream of winter. J Meteorol 18:172-191

Lang TJ, Barros AP (2004): Winter storms in the central Himalayas. J Meteorol Soc Jpn 82:829-844

Lionello P, Kalan F, Elvini E (2002) Cyclones in the Mediterranean region: The present and the doubled CO_2 climate scenarios. Climate Res 22:147-159

Maussion F, Scherer D, Molg T, Collier E, Curio J, Finkelnburg R (2014) Precipitation seasonality and variability over the Tibetan Plateau as resolved by the High Asia Reanalysis. J Climate 27:1910-1927

Murray RJ, Simmonds I (1991a) A numerical scheme for tracking cyclone centers from digital data part I: development and operation of the scheme. Aust Met Mag 39:155-166

Neu U et al (2013) IMILAST a community effort to intercompare extratropical cyclone detection and tracking algorithms. B Am Meteorol Soc 94:529-547

Norris J, Carvalho LMV, Jones C, Cannon F (2014) WRF simulations of two extreme snowfall events associated with contrasting extratropical cyclones over the Himalayas. J Geophys Res doi:10.1002/2014JD022592

Palazzi E, von Hardenberg J, Provenzale A (2013) Precipitation in the Hindu-Kush Karakoram Himalaya: Observations and future scenarios. J Geophys Res-Atmos 118:85-100

Ramaswamy C (1956) On the sub-tropical jet stream and its role in the development of large-scale convection. Tellus 8:26-60

Rasmussen R, et al. (2012) How well are we measuring snow? The NOAA/FAA/NCAR winter precipitation test bed. B Am Meteorol Soc 93:811-829

Ridley J, Wiltshire A, Mathison C (2013) More frequent occurrence of westerly disturbances in Karakoram up to 2100. Sci Total Environ. http://dx.doi.org/10.1016/j.scitotenv.2013.03.074

Roe GH (2005) Orographic Precipitation. Annu Rev Earth Planet Sci 33:647-671

Rudeva I, Gulev SK (2007) Climatology of cyclone size characteristics and their changes during the cyclone life cycle. Mon Wea Rev 135:2568-2587

Saha S et al (2010) The NCEP Climate Forecast System Reanalysis. B Am Meteorol Soc 91:1015-1057

Serreze MC (1995) Climatological aspects of cyclone development and decay in the Arctic. Atmos Ocean 33:1-23

Simmonds I, Murray RJ, Leighton RM (1999) A refinement of cyclone tracking methods with data from FROST Aust Metero Mag Special Issue:35-49

Simmonds I, Keay K (2000) Mean Southern Hemisphere extratropical cyclone behavior in the 40-year NCEP/NCAR reanalysis. J Climate 13:873-885

Sinclair MR (1994) An objective cyclone climatology for the Southern Hemisphere. Mon Wea Rev 122:2239-2256

Singh P, Ramasastri KS, Kumar N (1995) Topographical influence on precipitation distribution in different ranges of western Himalayas. Nord Hydrol 26:259-284

Subbramayya I, Raju ASN (1982) A study of tropospheric wave disturbances over India in winter. Pure Appl Geophys120:437-452

Syed FS, Giorgi F, Pal JS, King MP (2006) Effect of remote forcings on the winter precipitation of central southwest Asia part 1: observations. Theor Appl Climatol 86:147-160

Syed FS, Giorgi F, Pal JS, Keay K (2010) Regional climate model simulation of winter climate over Central-Southwest Asia, with emphasis on NAO and ENSO effects. Int J Climatol 30:220-235

Tahir AA, Chevallier P, Arnaud Y, Ahmad B (2011) Snow cover dynamics and hydrological regime of the Hunza River basin, Karakoram Range, Northern Pakistan. Hydrol Earth Syst Sci 15:2275-2290

Trigo IF (2006) Climatology and interannual variability of storm-tracks in the Euro-Atlantic sector: A comparison between ERA-40 and NCEP/NCAR reanalyses. Climate Dyn 26:127-143

Wernli H, Schwierz C (2006) Surface cyclones in the ERA-40 dataset (1958-2001). Part I: Novel identification method and global climatology. J Atmos Sci 63:2486-2507

Wilks DS (2006) Statistical methods in the atmospheric sciences. Elsevier, Burlington

Wu BY, Wang J (2002) Possible impacts of winter Arctic Oscillation on Siberian high, the East Asian winter monsoon and sea-ice extent. Adv Atmos Sci 19:297-320

Wu BY, Wang J (2002) Winter Arctic Oscillation, Siberian High and East Asian winter monsoon. Geophys Res Lett 29:1-4

Wulf H, Bookhagen B, Scherler D (2010) Seasonal precipitation gradients and their impact on fluvial sediment flux in the Northwest Himalaya. Geomorphology 118:13-21

Yadav RK, Rupa Kumar K, Rajeevan M (2009) Increasing influence of ENSO and decreasing influence of AO/NAO in the recent decades over northwest India winter precipitation. J Geophys Res-Atmos 114

Yadav RK, Yoo JH, Kucharski F, Abid MA (2010) Why is ENSO influencing northwest India winter precipitation in recent decades? J Climate 23:1979-1993

II. Chapter 2: The Influence of Tropical Forcing on Extreme Winter Precipitation in the Western Himalaya

Forest Cannon[1,2], Leila M.V. Carvalho[1,2], Charles Jones[1,2], Andrew Hoell[3], Jesse Norris[2], George N. Kiladis[3], Adnan A. Tahir[4]

[1] Department of Geography, University of California, Santa Barbara, USA

[2] Earth Research Institute, University of California, Santa Barbara, USA

[3] NOAA Earth System Research Laboratory, Physical Sciences Division, Boulder, CO

[4] Department of Environmental Science, COMSATS Institute of Information Technology, Pakistan

2.1 Abstract

Within the Karakoram and western Himalaya (KH), snowfall from Winter Westerly Disturbances (WD) maintains the region's snowpack and glaciers, which melt seasonally to sustain water resources for downstream populations. WD activity and subsequent precipitation are influenced by global atmospheric variability and tropical-extratropical interactions. On interannual time-scales, El Niño related changes in tropical diabatic heating induce a Rossby wave response over southwest Asia that is linked with enhanced dynamical forcing of WD and available moisture. Consequently, extreme orographic precipitation events are more frequent during El Niño than La Niña or neutral conditions. A similar spatial pattern of tropical diabatic heating is produced by the MJO at intraseasonal scales. In comparison to El Niño, the Rossby wave response to MJO activity is less spatially uniform over southwest Asia and varies on shorter time-scales. This study finds that the MJO's

relationship with WD and KH precipitation is more complex than that of ENSO. Phases of the MJO propagation cycle that favor the dynamical enhancement of WD simultaneously suppress available moisture over southwest Asia, and vice versa. As a result, extreme precipitation events in the KH occur with similar frequency in most phases of the MJO, however, there is a transition in the relative importance of dynamical forcing and moisture in WD to orographic precipitation in the KH as the MJO evolves. These findings give insight into the dynamics and predictability of extreme precipitation events in the KH through their relationship with global atmospheric variability, and are an important consideration in evaluating Asia's water resources.

2.2 Introduction

Extratropical cyclones that affect southwest Asia from November through April are the primary climatic influence in the Karakoram and western Himalaya (KH) during non-monsoon months (Singh et al. 1995; Lang and Barros, 2004; Barlow et al. 2005; Dimri et al. 2015). In excess of 50% of the total annual precipitation in the KH is delivered by fewer than ten of these " winter westerly disturbance" (WD) events each winter season (Lang and Barros, 2004; Barlow et al. 2005; Barros et al. 2006; Bookhagen and Burbank, 2010; Cannon et al. 2014). Their associated frontal systems interact with topography to produce heavy orographic precipitation, while the lapse-rate ensures that precipitation falls as snow over the KH's high mountains. Snowfall generated by WD maintains regional snowpack and glaciers (Anders et al. 2006; Tahir et al. 2011; Bolch et al. 2012; Ridley et al. 2013; Cannon et al. 2015), and is essential to water resources for downstream populations (Immerzeel et al. 2009; Bolch et al. 2012; Hewitt, 2014).

Significant relationships exist between WD activity over southwest Asia (25-40°N; 40-80°E) and global modes of climate variability, including; the Madden-Julian Oscillation (MJO) (Barlow et al. 2005; Hoell et al. 2012), the El Niño Southern Oscillation (ENSO) (Syed et al. 2006; Yadav et al. 2010; Hoell et al. 2013), the Arctic Oscillation/North Atlantic Oscillation (NAO) (Gong et al. 2001; Wu and Wang, 2002, Yadav et al. 2009; Syed et al. 2010; Filippi et al. 2014) and the Polar Eurasia Pattern (Lang and Barros, 2004). During the boreal winter, southwest Asia, and specifically the Karakoram, are within the subtropical belt of upper-level westerlies (Krishnamurti, 1961), which serve as a baroclinic wave-guide (Wallace et al. 1988). Variability in the upper-level jet over southwest Asia, and subsequent variability in shear, maximum wind speed, and deformation, has a complex relationship with WD activity (Barlow et al. 2005). Large-scale changes in atmospheric circulation that modify the jet, such as ENSO (Rasmussen and Carpenter, 1982; 1983), the NAO (Barnston and Livezey, 1987) and the MJO (Madden and Julian, 1972; 1994), significantly modify the frequency and intensity of WD, thereby altering seasonal precipitation totals in High Asia (Yadav et al. 2009; Dimri et al. 2012; Fillippi et al. 2014). Furthermore, these modes influence low-level circulation and moisture conditions, resulting in important differences in the background atmosphere with which individual WD interact. It appears that the influence of global modes of variability on KH precipitation is more complex than previously appreciated, as both upper-level dynamics and thermodynamic conditions over southwest Asia can be modified uniquely, thus altering the development of WD and orographic precipitation in a manner that is not well-documented in the literature addressing this region's climate to date (Cannon et al. 2015).

Previous studies have typically explored how precipitation in the KH is related to global modes of climate variability at monthly or seasonal scales (e.g. Archer and Fowler, 2004; Lang and Barros, 2004; Dimri, 2012; Fillippi et al. 2014; Cannon et al. 2014). WD exist at synoptic-scales, between 2 and 7 days, therefore it is important to investigate these relationships using daily data with a specific focus on extreme events, which numerous studies attempting to quantify regional precipitation have found to contribute the vast majority of seasonal precipitation (Hewitt, 2005; Fillippi et al. 2014; Cannon et al. 2014, 2015). Cannon et al. (2015) investigated individual WD events and demonstrated significant event-to-event differences in the contribution of upper-level circulation and low-level moisture to extreme precipitation in the KH over the period 1979-2013. This work found that seasonal changes in the atmosphere regulated the relative importance of dynamic and thermodynamic components of WD systems to orographic precipitation generation, suggesting that intraseasonal and interannual variability, which also produce large-scale changes in circulation and moisture availability, may be an additionally important consideration for understanding regional precipitation. In the current manuscript we explore the role of ENSO and the MJO in modifying WD and subsequent KH precipitation through tropical forcing.

Heat, moisture and momentum exchanges relate intraseasonal and interannual variability in the atmosphere to severe weather and extreme precipitation in the extratropics, and are fundamental to understanding how the MJO and ENSO influence storm tracks (Lee and Lim, 2012; Takahashi and Shirooka, 2014), including WD. The basis of the linkage between the tropics and southwest Asia is in a forced Rossby wave response of the upper troposphere to stationary diabatic heating anomalies in the tropics (Barlow et al. 2005),

which resembles a Gill-Matsuno-like response (Matsuno 1966; Gill 1980). During enhanced convection over the eastern Indian Ocean, local upper-level divergence intensifies and forces anomalous subsidence over southwest Asia. Both ENSO and the MJO produce similar spatial patterns of anomalous diabatic heating in the tropics, but the considerable differences in time-scales and Rossby wave responses over southwest Asia produce differing relationships with the region's climate.

On interannual time-scales, the Rossby wave response to El Niño increases southwest Asia precipitation by weakening climatological subsidence over the region (Hoell et al. 2013). A Rossby wave response is also generated by the MJO on intraseasonal scales, and is responsible for increased precipitation over southwest Asia as a result of anomalous regional ascent (Barlow et al. 2005). However, in comparison to El Niño, the Rossby wave response to MJO activity is less spatially uniform over southwest Asia and exists on a much shorter time-scale. Consequently, this mode's relationship with WD and KH precipitation is more complex. Although the KH is within the larger southwest Asia domain and similarly relies on WD to deliver precipitation, we will illustrate that the response to tropical forcing at intraseasonal scales is unique relative to previous results that investigated southwest Asia as a whole (e.g. Barlow et al. 2005; Hoell et al. 2012), largely on account of the KH's extreme topography and location. Here, we perform a comprehensive study of the role of tropical forcing on winter storms in the KH.

This manuscript discusses the frequency of extreme precipitation events in the KH during different phases of ENSO and the MJO, and individual mechanisms within WD events that relate large-scale tropical forcing by the MJO and ENSO to extreme orographic precipitation in the KH. Understanding the dynamics behind the independent and combined

influences of the MJO and ENSO on WD variability and extreme precipitation in the KH is essential to understanding the region's hydrology. These weather-climate relationships will lead to better forecasting of winter storms (Schubert et al. 2002; Barlow et al. 2005) and long-term predictability of water resources over southwest Asia and the KH (Immerzeel et al. 2009; Ridley et al. 2013).

2.3 Data

a. Precipitation Datasets

Meteorological data from the sparse network of stations within topographically complex High Asia is limited. Furthermore, extant data can be of marginal quality due to sampling errors or biases (Anders et al. 2006; Bookhagen and Burbank, 2010; Maussion et al. 2014). In this research, the influence of ENSO and the MJO on large-scale winter (November to April) precipitation over High Asia and surrounding regions is investigated using satellite observations from the Tropical Rainfall Measurement Mission 3B42V7 (TRMM), interpolated station data from the Asian Precipitation Highly Resolved Observational Data Integration Towards Evaluation (APHRODITE) dataset, and reanalysis precipitation from Climate Forecast System Reanalysis (CFSR). Precipitation in the KH is additionally investigated using a set of meteorological stations maintained by the Pakistani Meteorological Department and the Water and Power Development Authority of Pakistan.

TRMM 3B42V7 is a multi-satellite data set that provides near-global 0.25° resolution precipitation estimates at three-hour intervals for the period 1998-2015 (Huffman 2007). TRMM has well known deficiencies in estimating light precipitation as well as solid-state precipitation (Barros et al. 2000, 2006; TRMM Working Group Summaries). APHRODITE

(Yatagai et al. 2009) is produced using distance-weighted interpolation between station observations, and is available at daily 0.25° resolution over Asia for the period 1951-2007. This product is included as an additional measure of robustness, but performs less than ideally over High Asia, where observations are sparse and topography is complex (Anders et al. 2006; Bookhagen and Burbank, 2006). CFSR precipitation, at 0.5° horizontal resolution, is too coarse to resolve the complexities of orographic precipitation in the KH, but along with TRMM and APHRODITE is used to evaluate the timing of extreme events. Cannon et al. (2014, 2015) have utilized these precipitation datasets for similar studies and further documented their efficacy in the study region. Additionally, Norris et al. (2015a,b) have evaluated TRMM precipitation in comparison to dynamically downscaled precipitation using the Weather Research and Forecasting model (Skamarock et al. 2008) over the study region and found their general distributions to be correlated significantly, though as Norris et al. (2015a) exhibit, there is less consistency amongst precipitation products at high elevations.

Data from 12 in-situ stations spread over northern Pakistan at altitudes between 1,260 and 4,440m are also employed in this study (similar to Palazzi et al. 2015). The principal characteristics of the stations—altitude, coordinates, temporal resolution and managing agency—are detailed in Table 1, and their locations, along with a reference map of the study region, are shown in Fig. 1. Here, we consider daily-accumulated precipitation from seven PMD stations for the period 1960-2012. Additionally, we utilize 15 years (1995-2009) of daily-accumulated precipitation from five meteorological stations in the ablation zone of the Upper Indus Basin that are maintained by the Water and Power Development Authority of Pakistan (WAPDA). WAPDA stations are used for validation of the longer PMD record during overlapping periods, and indicate good agreement amongst the timing of extreme

events (not shown here). Here, we assume that extant biases in the magnitude of station-measured precipitation in the KH (Hewitt et al. 2014) are constant in time and thus do not affect the selection of extreme events relative to all other dates in the record.

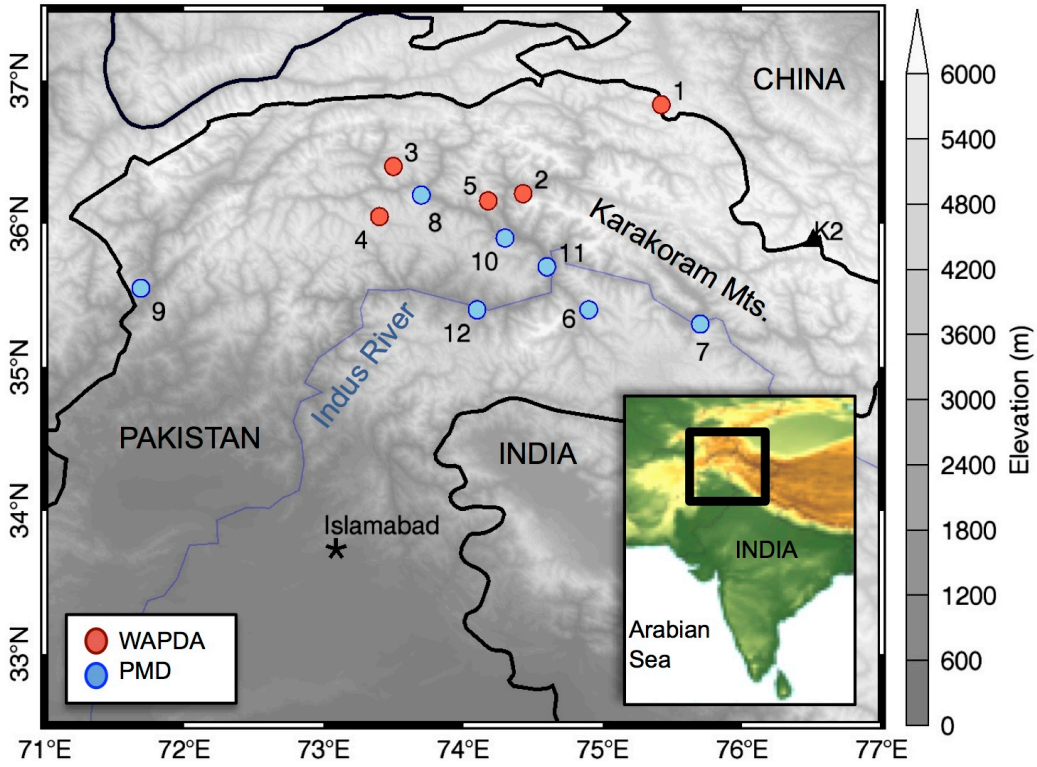

Figure 1 – Locations of meteorological stations in the western Himalaya and Karakoram from which precipitation data was acquired. Grayshade shows topography. A number of major geographical features and country names and borders are also included. The inset map shows the location of the study region (black box) over color-shaded topography.

Stations	Elev. (m)	Lat(°N)	Lon(°E)	Agency	Date Range
1. Khunjerab	4440	36.83	75.42	WAPDA	1995-2009
2. Ziarat	3020	36.21	74.43	WAPDA	1995-2009
3. Yasin	3280	36.40	73.50	WAPDA	1995-2009
4. Ushkore	3051	36.05	73.41	WAPDA	1995-2009
5. Naltar	2898	36.16	74.18	WAPDA	1995-2009
6. Astore	2168	35.33	74.90	PMD	1960-2012
7. Skardu	2317	35.30	75.68	PMD	1960-2012
8. Gupis	2156	36.16	73.40	PMD	1960-2012
9. Chitral	1498	35.85	71.83	PMD	1960-2012
10. Gilgit	1460	35.90	74.30	PMD	1960-2012
11. Bunji	1372	35.67	74.63	PMD	1960-2012
12. Chilas	1250	35.42	74.10	PMD	1960-2012

Table 1 – Index of station names, latitude, longitude, elevation, collecting agency and date range for the 12 meteorological stations shown in Fig. 1.

b. Meteorological Data from Reanalyses

CFSR data, from the National Centers for Environmental Prediction (Saha et al. 2010), are used to investigate large-scale climate and the dynamics of WD. CFSR is available at 0.5° horizontal-resolution for the period 1979-2013. CFSR was chosen on account of its spatial resolution, modern data assimilation system, and coupling of atmosphere, ocean, land and ice models in the generation of 6-hourly guess fields, from which the reanalysis is initialized (Saha et al. 2010). These advancements are unique relative to most previous reanalyses. Multi-reanalysis comparisons with observations (stations and radiosondes) over High Asia found CFSR to be among the best performing products (Bao and Zhang 2012; Wang and Zeng, 2012). Analysis of geopotential height, omega, wind, moisture, and temperature are performed at near-surface, 850, 500 and 200-hPa levels with daily temporal

resolution. Anomaly fields were derived by removing the mean seasonal cycle over the duration of the timeseries.

c. Outgoing Longwave Radiation

This study uses National Oceanic and Atmospheric Administration – Daily Climate Data Record PSD Interpolated Version outgoing longwave radiation (OLR) data (1° resolution), consisting of satellite observed mean OLR at the top of the atmosphere (Lee, 2014).

d. Intraseasonal and Interannual Indices

MJO events are identified using the methodology of Jones (2009), in which combined empirical orthogonal function (EOF) analysis of equatorially averaged (15°S-15°N) 20-200 day bandpass-filtered anomalies of outgoing longwave radiation, 200-hPa zonal wind and 850-hPa zonal wind yields first and second EOFs that are in good agreement with those of Wheeler and Hendon (2004). The phase diagram of the first two normalized principal components approximately follows the eight-phase convention of the real-time multivariate MJO index of Wheeler and Hendon (2004). The primary difference between this approach and that of Wheeler and Hendon (2004) is the use of bandpass filtered anomalies, which more accurately represent the temporal evolution of MJO events. In this study, an MJO event was defined when 1) the phase angle between the first two principal components systematically rotated anticlockwise, indicating eastward propagation at least to phase 5; 2) the amplitude was always larger than 0.35; 3) the mean amplitude during the event was larger than 0.9; and 4) the entire duration of the event lasted between 30 and 90 days. Based on

these conditions, all MJO events identified in this study started in phases 1–4, propagated eastward, and ended in phases 4–8 (i.e., isolated events) or restarted from previous MJO occurrences (i.e., successive events; phase continues from 8 to 1). Further details can be found in Jones (2009).

It is important to consider that the use of different MJO indices may lead to disparate conclusions concerning MJO timing and strength (Kiladis et al. 2014). Thus, the analyses presented in this study were additionally performed using the real-time multivariate MJO index of Wheeler and Hendon (2004), which is also circulation based, as well as an OLR-only version of the Jones (2009) index and the OLR MJO Index (OMI, Kiladis et al. 2014). Although the general features of circulation and OLR for MJO composites (discussed in section 2.5) are similar regardless of index, diversity in the amplitude and phase of individual MJO events according to the index used does produce moderately dissimilar distributions of extreme KH precipitation events across the eight phases of the MJO (section 2.4). Despite the sensitivity of event distributions to the choice of MJO index on account of the relatively small number of total extreme events (< 10 per phase of the MJO in ENSO neutral conditions), the composites of circulation and moisture during these events (section 2.6) are extremely similar across indices, as the majority of dates considered for the composites do not change. Furthermore, dates that do not correspond between indices still exhibit similar OLR anomalies in the tropics (the temporal evolution of the various MJO indices are similar), and their effect on large-scale circulation remains consistent. Consequently, the discussion of the mechanisms that link KH precipitation to MJO variability presented here is not especially sensitive to the choice of MJO index. The Jones (2009) index was ultimately selected for this study based on the advantage of filtering out day-to-day variability that is

included in the real-time multivariate MJO index, as well as the inclusion of large-scale circulation, which is not considered in OLR-only indices.

ENSO variability was defined based on the Oceanic Niño index, which is calculated by averaging sea surface temperature for the Niño 3.4 region and applying a 3-month running mean (Trenberth, 1997). Data were retrieved from the National Oceanic and Atmospheric Administration's Climate Prediction Center website. ENSO conditions were classified based on monthly ONI values greater than 0.5 (El Niño), less than -0.5 (La Niña), and between -0.5 and 0.5 (neutral).

2.4 Extreme Precipitation Events

a. Extreme Precipitation Event Definition

Throughout this manuscript, analyses of individual events are performed based on the identification of extreme precipitation using a combination of CFSR and PMD station data. Principal component analysis of the PMD station data for Nov.-Apr. was performed using a covariance matrix to reduce the number of variables by identifying a leading orthogonal pattern of variability that represents heavy precipitation dates at all seven stations from 1960 to 2012 (Wilks, 2006). The first principal component explained 53% of the variability amongst stations, and high values were observed to correspond to high-magnitude precipitation at multiple PMD stations, with heavy precipitation that was widely distributed over the KH in CFSR. Independent 90^{th} percentile dates (only the highest magnitude day of all consecutive 90^{th} percentile days is retained) from the station-based first principal component timeseries and independent 90^{th} percentile dates from aggregated CFSR precipitation in the KH (73-78°E, 34-37°N) produced a collection of extreme precipitation

events that overlapped or occurred within a 1-day lag period in 205 cases, or approximately 67% of the time, (PMD had 295 independent events and CFSR had 308) during Nov.-Apr., 1979-2012. These 205 overlapping extreme events are used throughout the manuscript to investigate how tropical forcing relates to WD and KH precipitation during the few days that account for the majority of regional precipitation. The approximately 33% of events that did not correspond between datasets were generally associated with precipitation totals slightly below the extreme event threshold in both datasets or above the threshold for only one of the datasets. These events were discarded from further evaluation. However, analyses that did include these events were not inconsistent with the results presented here.

b. Contribution of Extreme Events to Seasonal and Annual Precipitation

Table 2 shows the distribution of precipitation at individual stations, their relationship with the first principal component that represents the combined variance of all stations, and the percent contribution of the 205 identified extreme events to total precipitation. Total precipitation for 3-day periods centered on the 205 events, which accounts for less than 10% of all winter days, comprised 67% of total PMD averaged precipitation for Nov.-Apr., 1979-2012 and 36% of precipitation for all dates from 1979-2012. The 205 winter events contributed between 52 and 76% of total winter precipitation and between 30 and 43% of total annual precipitation at individual PMD stations over the 34-year study period. The considerable contributions to annual precipitation exhibited here are likely too low, as the magnitude of precipitation in winter is severely underestimated on account of difficulties in measuring snowfall in the KH (Palazzi et al. 2015; Norris et al. 2015b). Additionally, each individual station's precipitation correlates significantly (greater than 0.7) to the first

principal component that represents their combined variability, and alpha values below 1.0 indicate gamma distributions that are skewed to the right (Wilks, 2006) and are representative of infrequent moderate-heavy precipitation, which accounts for a comparatively large amount of the seasonal total (Jones et al. 2004). With respect to average annual precipitation reported in Table 2, it is important to note that these stations are located in valleys, which receive three to five times less precipitation than is observed on surrounding mountains during winter storms (Hewitt, 2005; 2014). The precipitation statistics reported here illustrate the importance of the extreme events investigated throughout this manuscript to KH climate and regional water resources.

Stations	**Correlation**	**Gamma (α)**	**Total/Year (mm)**	**% Wint.**	**% Event Wint.**	**% Event Tot.**
Astore	0.84	0.83	477	61	60	37
Skardu	0.71	0.90	230	68	63	43
Gupis	0.55	0.79	210	46	69	31
Chitral	0.47	0.82	450	77	52	40
Gilgit	0.79	0.68	149	40	73	30
Bunji	0.83	0.93	168	40	76	31
Chilas	0.80	0.75	180	56	76	43
Average	0.71	0.81	266	64	67	36

Table 2 – Statistics of station precipitation include: Correlation between station precipitation and the all-station first principal component for winter months, alpha values (shape) of the gamma distribution for winter precipitation, the average annual precipitation, the percent of the annual precipitation that falls in winter (Nov. – Apr.), the percent of winter precipitation that is attributed to the extreme events investigated here, and the percent of the total annual precipitation that is attributed to extreme events.

c. Intraseasonal and Interannual Variability in the Distribution of Events

The differences in the number of events according to MJO and ENSO conditions are presented here as motivation to better understand the relationships between tropical forcing,

WD and KH precipitation. The number of extreme precipitation events in the KH per winter season is shown in Fig. 2, which additionally identifies seasons with predominantly El Niño, Neutral or La Niña conditions. A significant long-term trend in the number of events per season is not readily identified, though the most noticeable feature in the timeseries is the near decade-long period of below average values immediately following the 1997-98 El Niño. This period included three weak El Niño seasons and four La Niña seasons. Though ENSO is not the only influence on extreme events, the Niño 3.4 index is significantly correlated ($p < 0.05$ via a Monte Carlo Simulation) to the number of extreme events per season, with a Pearson moment correlation of 0.41 (removing the 1997/98 El Nino reduces this correlation to 0.31, which is still significant, but highlights that a few strongly correlated seasons contribute considerably to the relationship). The average number of extreme events per season during El Niño conditions (9 seasons) is 6.8, while during La Niña conditions (9 seasons), this value drops significantly (t-test; $p<0.05$) to 5.4. The number of events in Neutral conditions (15 seasons) averages to 5.9. Additionally, the maximum number of events observed in a single year (10) was recorded during the 1997-98 El Niño, while the minimum number (2) was recorded during the 2000-01 La Niña.

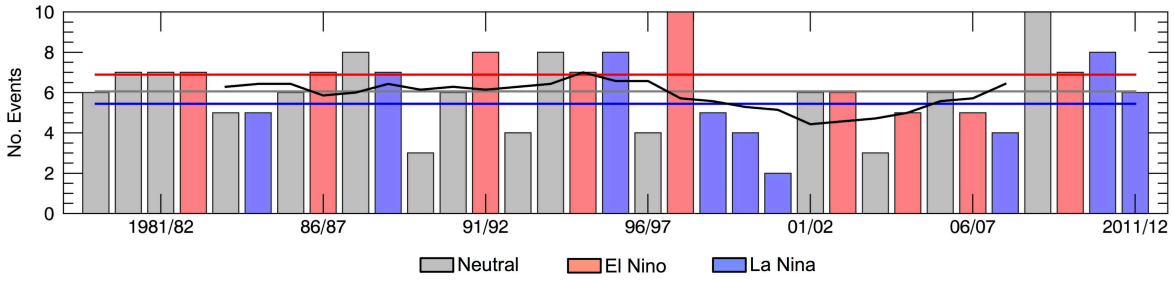

Figure 2 – Number of extreme precipitation events per winter season (Nov. – Apr.) and categorization based on ENSO conditions. Red line indicates mean number of events during 9 El Niño seasons. Blue line indicates mean for 9 La Niña seasons. Gray line indicates mean for 15 ENSO neutral seasons. Black line identifies a 7-year running mean.

Figure 3 displays the percentage of days within each phase of MJO activity that recorded an extreme precipitation event in the KH during winter seasons, 1979-2012. These statistics are additionally categorized according to ENSO conditions. We note that the distribution of events across phases is somewhat sensitive to the choice of MJO index, but that the overall conclusions presented here are consistent across the four indices tested (see Section 2.3). According to the Jones (2009) MJO index, phases 6, 7 and 8, experience proportionally more events than non-active MJO conditions, indicated here as phase 0. The frequency of events in MJO phases 1-4 are close to the proportions of non-active MJO, while the only phase that produces appreciably fewer extreme events is phase 5. The differences between the number of events per phase are not statistically significant. The relatively consistent distribution of extreme precipitation events in the KH across phases is interesting given that previous research has defined significant relationships between phases of the MJO and stormtracks (Lee and Lim, 2012; Penny et al. 2012) and has also found precipitation over southwest Asia as a whole to vary according to MJO phase (Barlow et al. 2005; Hoell et al. 2014). Spatial differences in total winter precipitation across southwest Asia, including the KH, according to ENSO and MJO conditions are discussed in the following section. Differences in KH precipitation between El Niño and La Niña, and similarities between phases of the MJO are in agreement with the extreme precipitation event distributions observed here (Figs. 2 & 3).

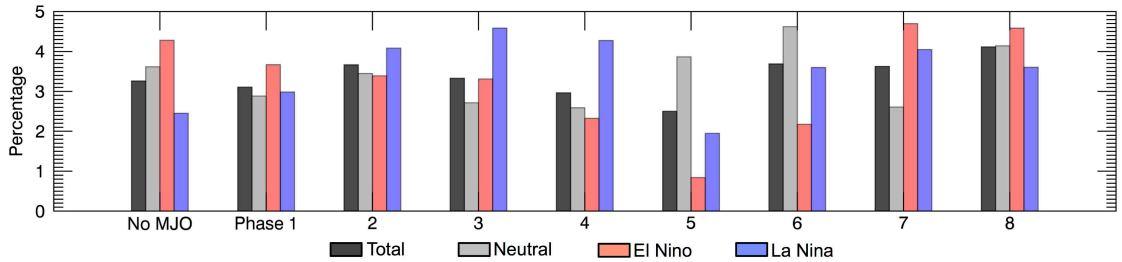

Figure 3 – Percentage of extreme precipitation events in each phase of MJO activity with

specified ENSO conditions (Nov-Apr, 1979-2012). The percentage is calculated by dividing the number of events in each phase by the total number of days.

Previous research has linked significant reductions in winter precipitation over southwest Asia to phases of the MJO that enhance convection in the eastern Indian Ocean and maritime continent (Barlow et al. 2005; Hoell et al. 2012). Contrastingly, phases that diminish convection in that tropical region enhance precipitation over southwest Asia. Based on those findings, this research originally investigated MJO influence on KH precipitation with the hypothesis that phases 3 and 4 would reduce precipitation in the KH, and that phases 7 and 8 would enhance it. While composites of precipitation conditioned on each phase of the MJO did display a large-scale precipitation signal over much of southwest Asia, precipitation differences in the KH were generally weak and spatially inhomogeneous. Furthermore, it was apparent that the MJO did not have a discernible effect on the number of extreme precipitation events in the KH in any phase (Shown in Fig. 3). Interestingly, insignificant differences in KH precipitation between phases is not due to a lack of influence of the MJO, but rather appears to be attributable to competing signals between the MJO's influence on moisture availability and dynamical forcing during WD (discussed in sections 2.5 and 2.6). MJO analyses presented in the following sections focus on combined phases 3 and 4, and combined phases 7 and 8, which represent the opposite ends of this relationship.

Additionally, the added influence of ENSO during MJO activity has an interesting effect on extreme precipitation event frequency. Inactive MJO periods experience proportionally more extreme precipitation events in the KH than all active phases during El Niño, with the exception of phases 1 and 7. In contrast, all MJO active phases experience more events than non-active periods during La Niña. Given the fact the MJO was generally

less active during La Niña (68% of winter days during El Nino conditions had an active MJO, compared to 60% in La Nina), it is especially interesting that a higher proportion of La Nina condition extreme events occurred when the MJO was also active (64% of La Nina extreme precipitation events occurred during MJO active periods compared to 58% of events during El Nino conditions). The observed event frequencies under the independent and combined influences of ENSO and the MJO motivate our discussion of the influence of tropical forcing on large-scale dynamics and moisture availability, and its importance to KH precipitation.

2.5 MJO and ENSO Influences

The relationship between WD and extreme precipitation events in the KH depends on a number of factors that are influenced by both tropical and extratropical forcing. WD are infrequent, synoptic occurrences throughout the winter season that are fundamentally related to KH precipitation by orographic processes; however, the magnitude of orographic precipitation varies as a function of the moisture content of the flow, atmospheric stability, and cross-barrier wind speed (Roe et al. 2005). Both the WD, and the state of the background atmosphere are important in determining moisture flux, and their combined influence determines the spatial distribution and intensity of precipitation in the mountains. Cannon et al. (2015) showed that extreme precipitation in the KH can be generated by either strong cross-barrier winds, related to the position or intensity of a trough, abundant moisture, which may be related to a warm, moist airmass ahead of the front, seasonal changes in temperature, or a combination of influences. Although these mechanisms are not entirely independent, each WD in this analysis exhibited varying balances of influence between these components

according to the prevailing large-scale circulation. This section discusses the influence of tropical forcing at intraseasonal and interannual scales on southwest Asia climate using composites of variables related to orographic precipitation during different phases of ENSO and the MJO. The influence of these modes on individual WD at the event-scale is discussed in Section 2.6.

a. Vertical Structure of Geopotential Height Anomalies

Figure 4 shows the vertical structure of geopotential height anomalies related to ENSO and MJO activity using CFSR data for the months of November through April, 1979-2013. In this analysis we investigate MJO by combining phases 3 and 4, as well as a combination of phases 7 and 8. These phases were selected as the concomitant dynamical-forcing and moisture-availability responses over southwest Asia are at opposite extremes between them, while phases 1, 2, 5 and 6 are transition phases. Only significant anomalies (above the 95th confidence interval, as determined by a z-test) are displayed. Significant OLR anomalies are also displayed to identify anomalous tropical convection. The composites in Fig. 4, and for all further analysis, include only dates for the respective phase during which the other mode was neutral (e.g. La Niña conditions with no MJO activity). There were 491 El Niño dates with neutral MJO, 980 La Niña dates with neutral MJO, 399 dates in MJO phases 7 and 8 with neutral ENSO, and 414 dates in MJO phases 3 and 4 with neutral ENSO. The discrepancy between non-MJO dates during El Niño and La Niña reflects both comparatively more La Niña dates in the record, and decreased MJO activity during La Niña in the period investigated.

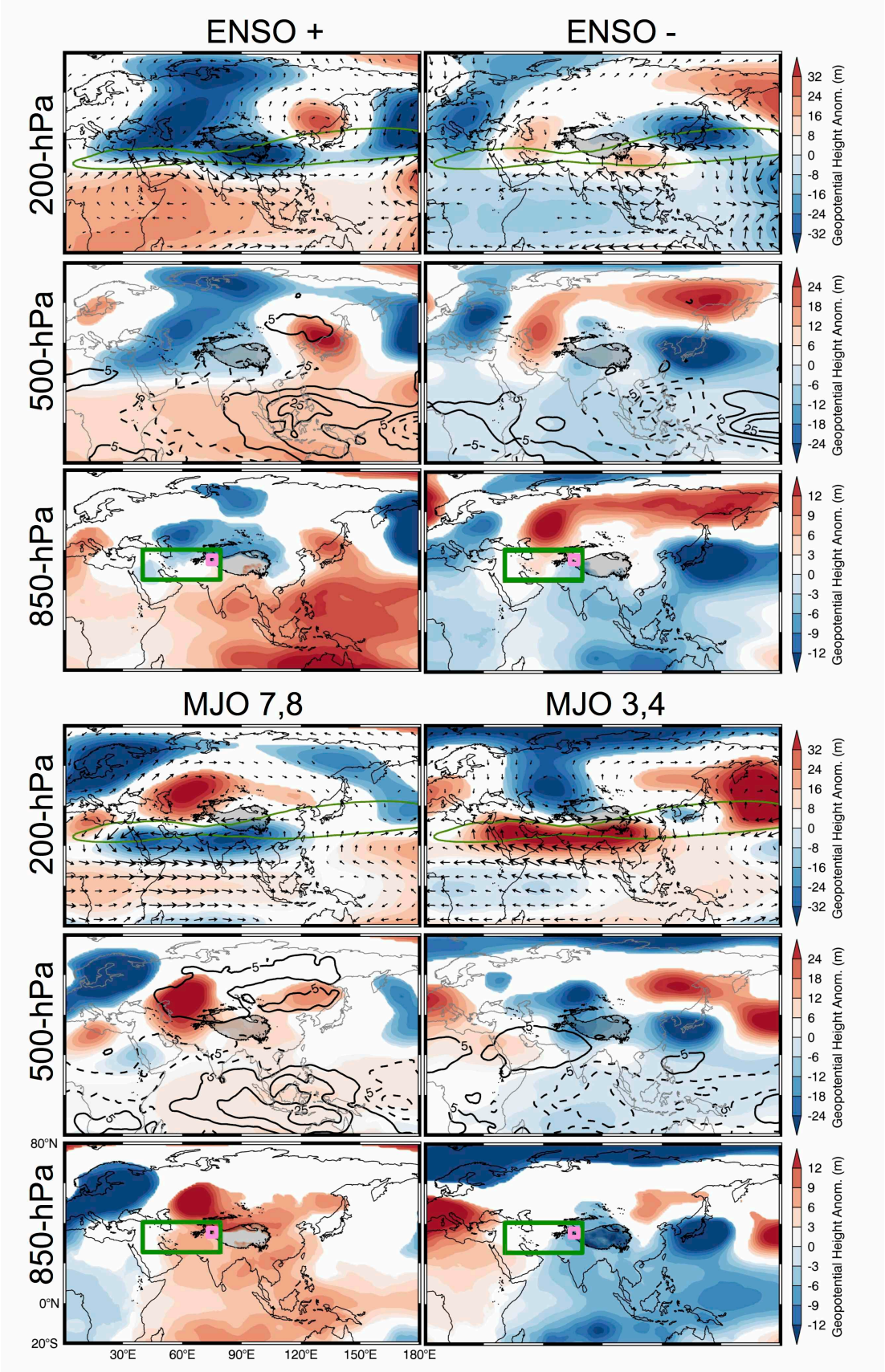
ENSO +
ENSO -
MJO 7,8
MJO 3,4
200-hPa
500-hPa
850-hPa
Geopotential Height Anom. (m)
80°N
0°N
20°S
30°E
60°E
90°E
120°E
150°E
180°E

Figure 4 – Composites of geopotential height anomalies at 200, 500 and 850-hPa (bottom row) for El Nino, La Nina, MJO phases 7 and 8 and MJO phases 3 and 4. Composites include all dates of a given index in its respective phase during which the other index was not active. The top row for ENSO and MJO panels include 200-hPa wind anomaly vectors, and the green line indicates the mean position of the core of the subtropical jet (> 40m/s) during Nov to Apr. The 3000m elevation contour of the Tibetan Plateau is illustrated by a thick black line in all panels. OLR anomalies (contours; negative values are dashed) are included in the 500-hPa panels to indicate the approximate location of enhanced tropical convection related to ENSO and MJO. Only significant values are displayed (z-test $p<0.05$). The green box in 850-hPa panels indicates southwest Asia and the pink box indicates the Karakoram.

During El Niño (La Niña) OLR anomalies over the Maritime Continent (Fig. 4; overlaid on the 500-hPa panels) are associated with diabatic cooling (heating) and a tropically forced Rossby wave response in geopotential height anomalies over continental Asia, including southwest Asia (25-40°N; 40-80°E) (Fig. 4; 850-hPa panels). Barotropic geopotential height anomalies greater than 30gpm over southwest Asia indicate a stationary anticyclone during La Niña conditions, and the weakening of the subtropical jet (Fig. 4; 200-hPa panels), while also enhancing regional stability. Both mechanisms are unfavorable for the development or intensification of WD and extreme precipitation. Contrastingly, El Niño conditions exhibit negative geopotential height anomalies below -30gpm with barotropic structure over nearly all of continental Asia. This favors large-scale ascent and also intensifies the subtropical jet, while shifting it slightly southward. In positive ENSO conditions, large-scale circulation favors precipitation across southwest Asia and the KH, and is consistent with previously documented relationships between El Niño and ample southwest Asia precipitation (Yadav et al. 2010, Hoell et al. 2012). Interestingly, MJO activity does not have a comparable relationship with total precipitation in the KH (Fig. 10),due to differences in mid-to-upper tropospheric circulation responses to spatially similar

OLR anomalies across the Indian Ocean and Maritime Continent (implying similar diabatic heating changes) at intraseasonal scales.

In MJO phases 3 and 4 during ENSO neutral conditions, significant OLR anomalies below -20W m^{-2} indicate enhanced convection and diabatic heating in the eastern Indian Ocean (Fig. 4). Positive 200-hPa and negative 500-hPa geopotential height anomalies over southwest Asia indicate that the Rossby wave response to anomalous tropical forcing exhibits a baroclinic structure over the region of interest (Fig. 4). It can also be seen that the 200-hPa Rossby wave generated anticyclone is found only over southern southwest Asia, while significant barotropic negative anomalies are observed to the north. Opposing signs of geopotential height anomalies straddling the climatological position of the subtropical jet serve to intensify the storm track in MJO phases 3 and 4. Atmospheric conditions over southwest Asia favor increased stability in the region of 200-hPa subsidence; however, the intensified jet on the northern boundary of this region, at the approximate latitude of the KH (Fig. 4; top row), actually favors more precipitation on account of stronger dynamical forcing aloft and at the mountain front. These conditions, which are reversed in MJO phases 7 and 8, are explored in more detail using 500-hPa omega, wave tracks, moisture availability and precipitation distributions.

b. Vertical Velocity

Figure 5 displays 500-hPa omega for the different phases of ENSO and MJO considered previously. The figure is illustrative of the differences between vertical velocity responses over southwest Asia to MJO and ENSO tropical forcing. During MJO influence, the 200-hPa dipole in geopotential height anomalies that straddles the subtropical jet (Fig. 4)

produces opposing signs of 500-hPa omega between southwest Asia and the KH (Fig. 5). Significant omega below -2.5 x 10^{-3} Pa s^{-1} is observed over southwest Asia, where the Rossby wave response induces ascent, in MJO phase 7/8 (Fig. 5; top left). Simultaneously, the weakened jet to the north of the anticyclone generates anomalous descent at the KH orographic barrier, where dynamical forcing is reduced. While large-scale ascent augments precipitation over southwest Asia, the concomitant weakening of orographic forcing in the KH is unfavorable for precipitation in the mountains. The relationship is reversed during MJO phase 3/4, which inhibits precipitation over southwest Asia through increased subsidence, but favors dynamically forced ascent and precipitation at the KH orographic barrier (Fig. 5; top right). The vertical velocity signal is more uniform between regions under ENSO conditions, with broad-scale ascent during El Niño and subsidence during La Niña (Fig. 5; bottom left and right, respectively). These differences have important ramifications with respect to WD activity and thermodynamic balance in the region.

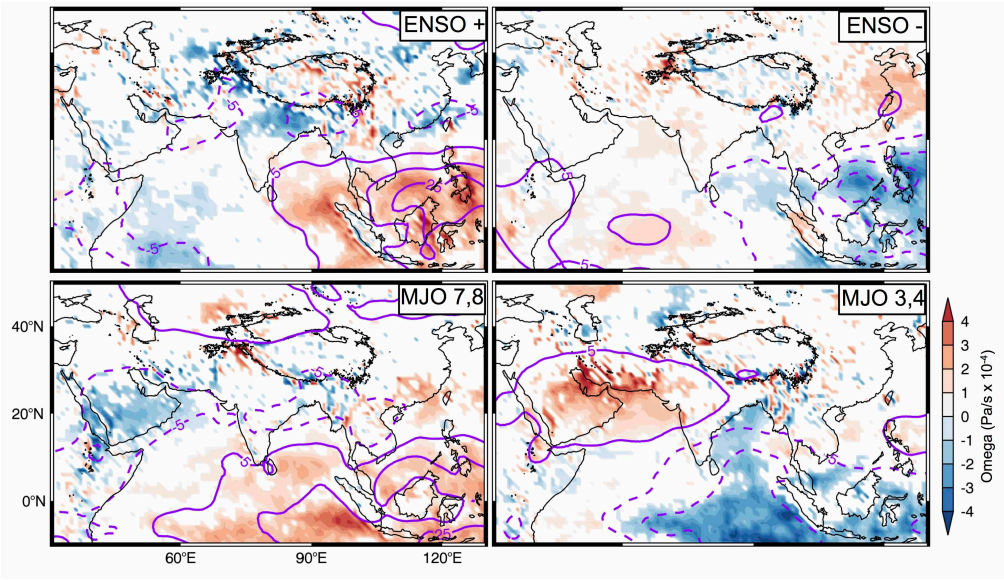

Figure 5 – Composites of significant (z-test; $p < 0.05$) 500-hPa omega anomalies during El Niño (bottom left), La Niña (bottom right), MJO phases 7 and 8 (top left) and MJO phases 3 and 4 (top right). Composites include all dates of a given index in its respective phase during which the other index was not active (Nov. – Apr. 1979-2013). The 3000m-elevation contour

of the Tibetan Plateau is illustrated by a thick black line. OLR anomalies (purple contours; negative values are dashed) indicate the approximate location of enhanced tropical convection related to ENSO and MJO. Only significant values are displayed.

c. Wave Tracks

Lagrangian approaches to investigating the effect of the MJO on winter storm tracks over the Northern Hemisphere (e.g. Penny et al. 2012) have been performed previously, but an analysis specific to southwest Asia has not yet been undertaken. The frequency of 500-hPa wave tracks in each phase of ENSO and the MJO, which indicates the propagation of WD over southwest Asia (Cannon et al. 2015), is shown in Figs. 6 and 7, respectively. The tracking technique employed here is that of Cannon et al. (2015), which uses the 500-hPa signature of WD in standardized geopotential height anomalies to differentiate individual disturbances (troughs) from the background flow, and to track their propagation in the Northern Hemisphere using the day-to-day spatial correlation of cyclonic features. The advantage of this particular technique is specific to WD, which propagate along relatively low latitudes, encounter highly variable topography, exhibit strong tropical influences and are spatially complex. This method is proven to accurately identify the primary atmospheric circulation pattern that produces KH precipitation events and has been used for additional analysis of regional climate (see Cannon et al. 2015 for additional details).

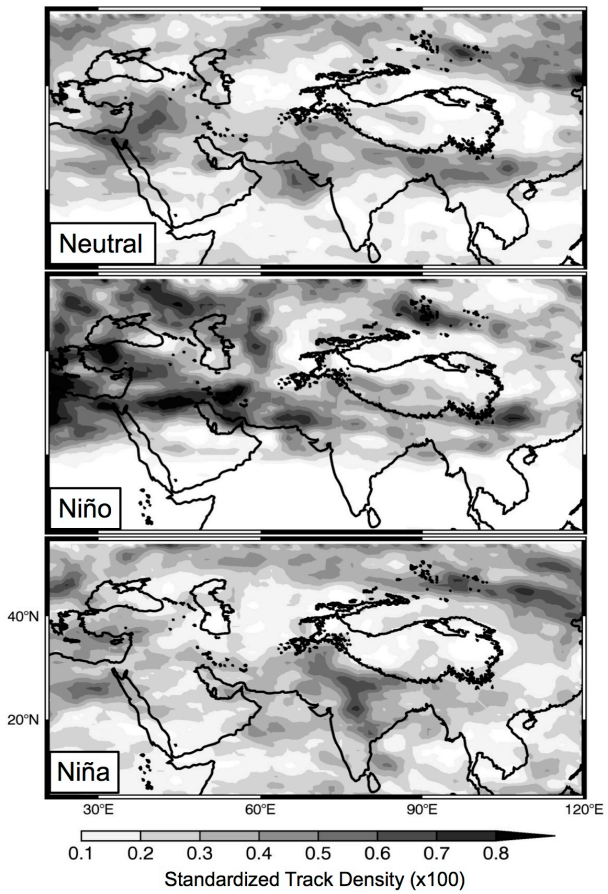

Figure 6 – 500-hPa wave track density (number of tracks recorded divided by the number of days in the given ENSO phase when MJO was inactive) map indicating trajectories of centers of disturbances recorded during Neutral (top), El Niño (middle) and La Niña (bottom) ENSO conditions, Nov. to Apr. 1979-2013. The 3000m-elevation contour of the Tibetan Plateau is identified by a thick black line.

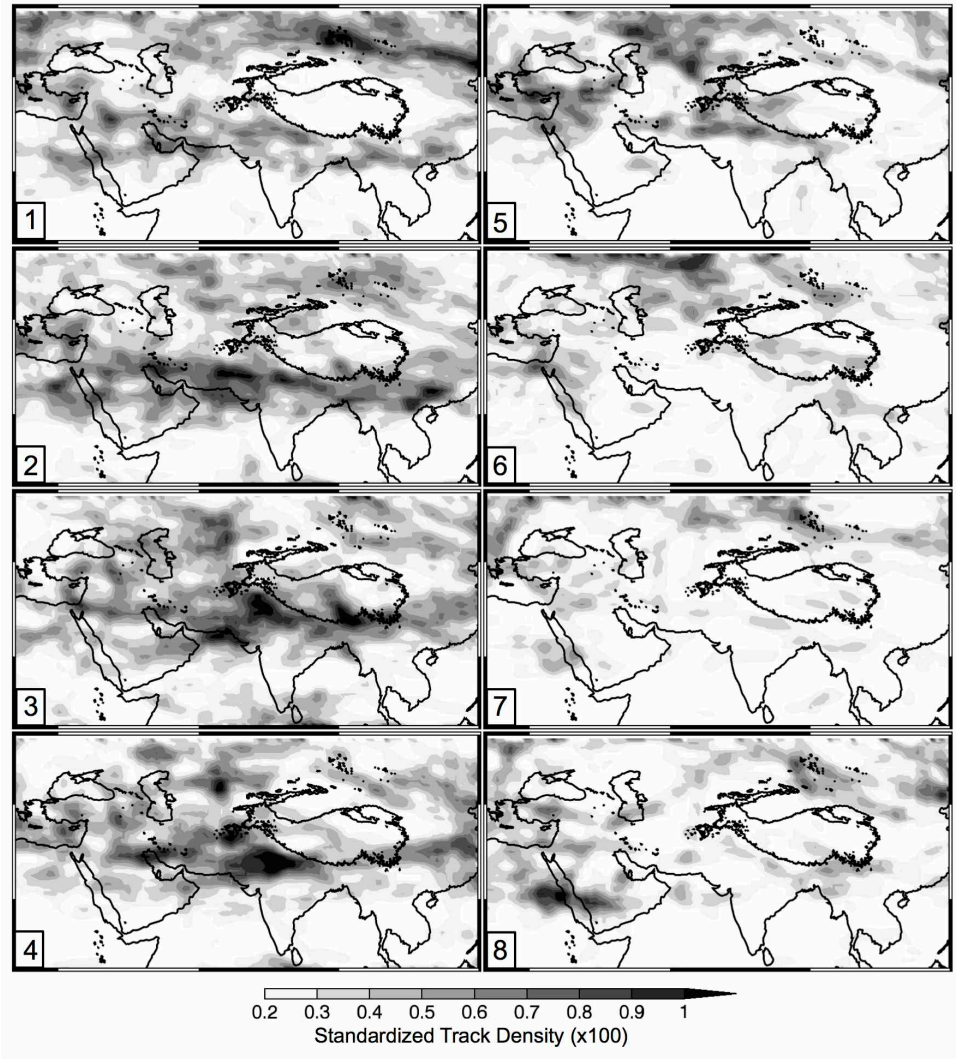

Figure 7 – 500-hPa wave track density (number of tracks recorded divided by the number of days in the given MJO phase when ENSO was neutral) map indicating trajectories of centers of disturbances recorded during MJO phases 1-8, Nov. to Apr. 1979-2013. The 3000m-elevation contour of the Tibetan Plateau is identified by a thick black line.

Figure 6 illustrates increased WD track activity over southwest Asia during ENSO warm phases relative to neutral and cool phases, when the MJO was inactive. This corresponds with an increase in the strength of the subtropical jet (Cannon et al. 2014) and barotropic negative geopotential height anomalies over the region (Fig. 4). Contrastingly, track frequency during MJO phases without ENSO influence (Fig. 7) is increased during

phases in which tropical forcing favors subsidence over southwest Asia (Phases 2-4). The discussion above indicated important differences in the vertical structure of Rossby wave responses to tropical forcing from either ENSO or the MJO (Fig. 4). The baroclinic response observed during MJO activity in the eastern Indian Ocean (phases 2-4) results in enhanced track activity, likely related to the intensification of the subtropical jet to the north of the anomalous region of subsidence, while the barotropic response during the cool phase of ENSO reduces WD activity. Takashi and Shirooka (2014) similarly show increased vertically integrated eddy kinetic energy over southwest Asia during El Niño and the negative phase of the MJO, confirming the positive influence on the region's storm track observed here using a Lagrangian approach.

d. Moisture Availability

In addition to dynamical forcing by WD impinging on topography, moisture availability is essential to orographic precipitation generation (Roe et al. 2005). Despite dissimilarities in mid-level circulation and WD activity, similar reductions in precipitation over southwest Asia between MJO phases 3/4 and La Niña (Hoell et al. 2012) may be attributable to decreased moisture flux toward the region in both cases. Figure 8 shows precipitable water and vertically integrated moisture flux anomalies for MJO phases 3/4 and 7/8, and ENSO in positive and negative phases. The reduction in available moisture during MJO phases 3/4, as indicated by significant precipitable water anomalies below -2kg m^{-2} over all of southwest Asia, greatly reduces the efficiency of orographic precipitation and cloud generation for mountainous regions of southwest Asia, despite abundant track activity (Fig. 7). Interestingly though, these generalizations for southwest Asia do not hold true for the

Karakoram, where extreme topography adjacent to the climatologically moist Gangetic Plain complicates the relationship between tropical forcing by the MJO and WD precipitation. It is also important to note that the spatial distribution of vertically integrated moisture flux anomalies is nearly identical between MJO 3/4 and La Niña, as well as between MJO 7/8 and El Niño. Strong anomalous flow from southwest Asia toward the region of enhanced convection over the eastern Indian Ocean is observed in the MJO 3/4 and La Niña, and opposite flow in the MJO 7/8 and El Niño.

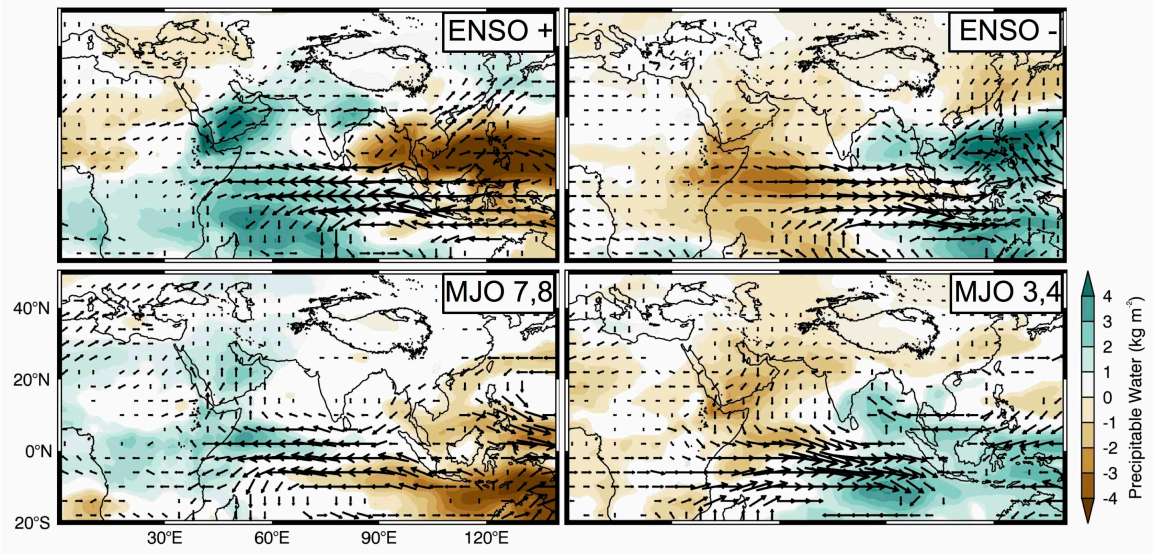

Figure 8 – Significant precipitable water and vertically integrated moisture flux anomalies for ENSO and MJO activity, as indexed in Fig. 3.

Despite the similarities in moisture conditions amongst phases of the MJO and ENSO, the observed temperature anomalies are not consistent (Fig. 9). El Niño, which produces anomalous moisture exceeding 2kg m^{-2} over the Indian Subcontinent, exhibits significantly negative temperature anomalies over all of southwest Asia. The more than 2°C drop in average temperature during El Niño conditions is attributable to cold air protruding further south than climatologically expected on account of the significant barotropic negative

geopotential height anomalies over southwest Asia. Similar moisture conditions are observed during MJO 7/8, but temperature anomalies are of the opposite sign, as significant warming is generated by warm-air advection that balances anomalous regional ascent within the baroclinic environment (Fig. 5; top left). It is also worth emphasizing that the two modes exist on very different time scales. Interannual dry or wet periods related to ENSO likely produce significant changes in temperature and moisture via land-atmosphere feedbacks over southwest Asia that are not as well established over the relatively short duration of an MJO event.

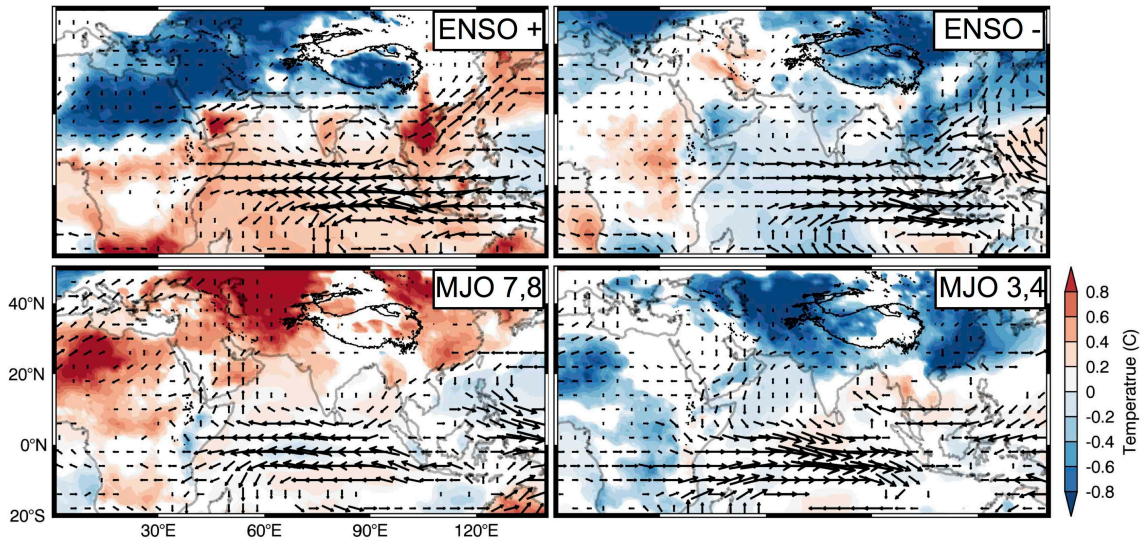

Figure 9 – Significant 2m temperature and vertically integrated moisture flux anomalies for ENSO and MJO activity, as indexed in Fig. 3.

e. Contributions of Dynamical Forcing and Moisture Availability to Precipitation

During El Niño periods without MJO activity, increased available moisture and dynamical forcing (Figs. 6 & 8) greatly enhance precipitation across southwest Asia and in the KH relative to La Niña conditions, which simultaneously limit these contributions to WD-driven precipitation (Fig. 10). Similar precipitation teleconnections are documented in

previous studies (e.g. Mariotti, 2007; Yadav et al. 2010; Cannon et al. 2014). However, tropical forcing related to the MJO has a more complex relationship with the KH as dynamical forcing and moisture influences that enhance precipitation are not observed in the same phases across all of southwest Asia. For example, in MJO phases 3/4 during ENSO neutral conditions, the spatial patterns of moisture flux and precipitable water anomalies are similar to La Niña; however, large-scale descent is observed over southwest Asia (Fig. 5), which remains dry, while an intensified subtropical jet to the north, at the approximate latitude of the KH, dynamically enhances ascent at the orographic barrier (Fig. 4). In the KH, orographic forcing is thus intensified and reduced available moisture does not translate to reduced precipitation relative to phases 7/8 (Fig. 10; bottom). Compared to the rest of southwest Asia, which demonstrates significant precipitation differences amongst MJO phases (Barlow et al. 2005), orographic precipitation in the KH benefits from more moisture, which is garnered from the Arabian Sea and recycled from the Gangetic Plain (Curio et al. 2015), and higher topography, which increases the effectiveness of dynamical forcing in generating precipitation.

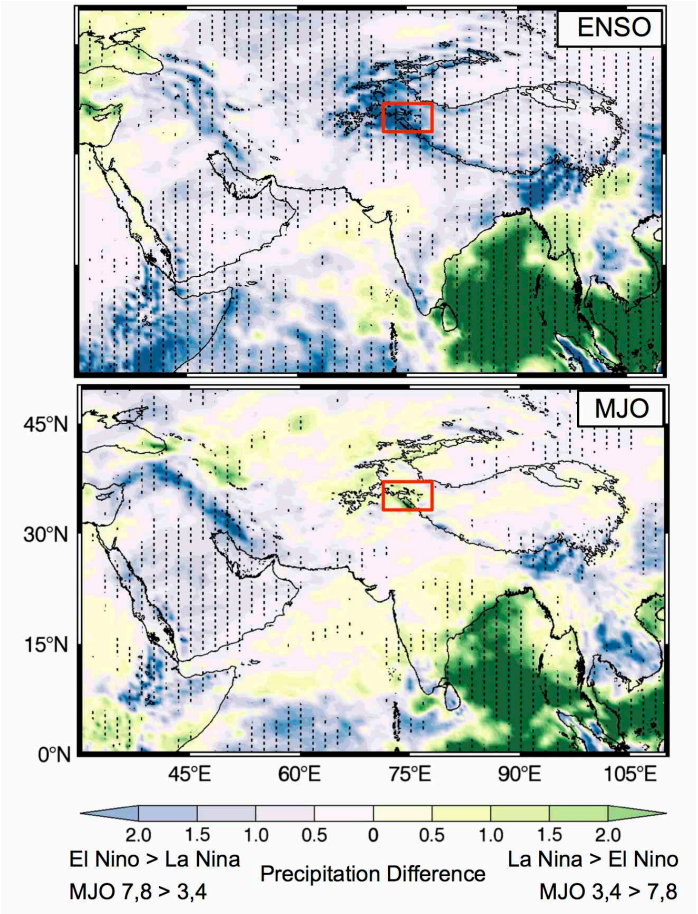

Figure 10 – Differences in CFSR precipitation between El Niño and La Niña (top) and MJO phases 7, 8 and 3, 4 (bottom). Values that exceed the 95th percentile confidence interval (based on a t-test) are stippled. Blue shading indicates comparatively higher precipitation accumulations in El Niño (top) and MJO 7,8 (bottom), while green shading indicates higher accumulations in La Niña (top) and MJO 3,4 (bottom). The red box indicates the location of the KH region.

f. Spatial and Temporal Patterns of Precipitation

Given the difficulties associated with modeling or measuring precipitation within the study area's heterogeneous topography (Lang and Barros, 2004; Bookhagen and Burbank, 2010; Norris et al. 2015a,b), this section evaluates the consistency of precipitation patterns related to the MJO and ENSO across data sets. Figure 11 demonstrates differences in precipitation between MJO phases 3/4 and 7/8 during ENSO neutral, and between El Niño

and La Niña without MJO activity, for CFSR, APHRODITE (land only) and TRMM. Large-scale precipitation patterns associated with ENSO and the MJO are consistent amongst all three data sets. Precipitation over the eastern Indian Ocean is significantly enhanced in MJO 3/4 and La Niña, on account of the location of related tropical convection in the eastern Indian Ocean and Maritime Continent (note that Aphrodite does not cover oceanic areas). Additionally, all three datasets are consistent in indicating increased precipitation over southwest Asia in MJO 7/8 and El Niño. These similarities lend confidence to the robustness of the large-scale pattern of precipitation associated with the observed changes in dynamics and moisture related to tropical forcing (Fig. 10).

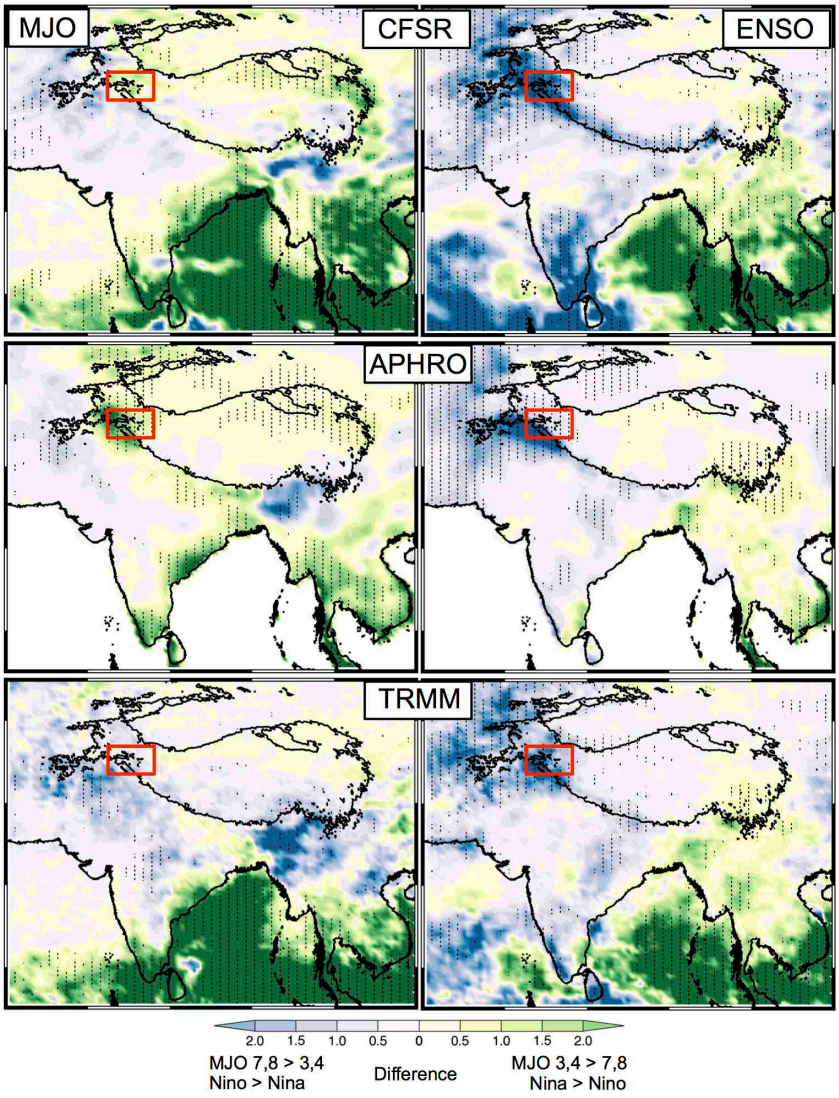

Figure 11 – Differences in CFSR (top), APHRODITE (middle) and TRMM (bottom) precipitation between MJO phases 7, 8 and 3, 4 (left column) and between El Niño and La Niña (right column) Nov-Apr, 1998-2007. Values that exceed the 95th percentile confidence interval (based on a t-test) are stippled. Blue shading indicates comparatively higher precipitation accumulations in MJO 7, 8 or La Niña, while green shading indicates higher accumulations in MJO 3, 4 or El Niño. The red square identifies the KH.

On a regional scale, orographic precipitation is less consistent amongst datasets. Though TRMM, APHRO and CFSR record significantly more precipitation throughout the majority, if not all, of the KH during El Niño than La Niña, large discrepancies exist between MJO phases. APHRODITE estimates significantly more precipitation in the KH during MJO

3/4, while CFSR and TRMM do not indicate a significant difference between phases. This discrepancy accentuates that the magnitude and distribution of precipitation in the KH is not consistent amongst datasets due to persistent biases in each product. The better-established differences at interannual scales (ENSO) mask this issue, while intraseasonal differences (MJO) are less defined and more prone to discrepancies. Comparisons between these precipitation dataset's climatologies have been performed previously (Palazzi et al. 2013; Cannon et al. 2014, 2015). TRMM particularly struggles with estimating solid-state precipitation at high elevations of the KH (Barros et al. 2000, 2006), and one reason for the strong bias toward increased precipitation in MJO phase 7/8 may be that increased temperatures in this phase produce proportionally more liquid precipitation at low elevations of the KH, which is better detected relative to heavy precipitation in phase 3/4. Unfortunately, APHRODITE has considerable issues in estimating precipitation in the KH that are related to the dearth of stations and their interpolation, while CFSR is too coarse to adequately resolve orographic precipitation processes and is also subject to deficiencies in model physics and parameterizations of meteorological processes. Thus, it is not possible to definitively state that any single data source is better than the others.

In order to avoid difficulties related to precipitation estimates across datasets, the emphasis of this research is on extreme precipitation events, the timing of which are more consistent amongst datasets given that the largest magnitude events are typically the most widespread and well-recorded across all platforms (Cannon et al. 2014; 2015). Thus, the relationship between tropical forcing and WD events is consistent and robust, irrespective of the precipitation dataset used, because the days for which meteorological variables are investigated are consistent. Throughout the remainder of the manuscript only mechanisms

that control orographic precipitation are considered, while the magnitude and spatial distribution of precipitation is not further investigated.

2.6 Individual Event Dynamics

Typically, 4-6 WD contribute more than half of the total seasonal precipitation (Table 2), though the exact number varies annually (Cannon et al. 2015). Beyond the few days during which these events affect the region, the relationships between global modes of atmospheric variability and KH climate are of minor consequence for observed precipitation (though temperature and cloud cover changes, which are not discussed here, may remain important for overall hydrology). Therefore, this section is dedicated to investigating differences in dynamical forcing and moisture availability within the region's atmosphere, on account of tropical forcing, on the day of WD-related extreme precipitation. Composites of individual extreme events in each phase of MJO and ENSO activity are used to identify key differences in WD attributes that alter their relationship with orographic precipitation in the KH. As in Section 2.5, ENSO influences are considered for dates when the MJO was inactive and MJO activity is investigated only during ENSO neutral conditions. We observe WD to account for extreme precipitation events across all phases of MJO and ENSO (Fig. 3), though extreme precipitation is achieved by unique contributions of dynamical forcing, moisture availability, and stability to orographic forcing.

Figure 12 shows composites of 500-hPa geopotential height and precipitable water anomalies for 21 extreme precipitation events in the KH occurring in El Niño conditions without MJO activity (top left), 24 events in La Niña conditions without MJO activity (top right), 13 events in the positive phase of MJO (phase 7/8) during ENSO neutral (bottom left)

and 11 events in the negative phase of MJO (phase 3/4) during ENSO neutral (bottom right) in winter seasons (Nov–Apr, 1979-2012).

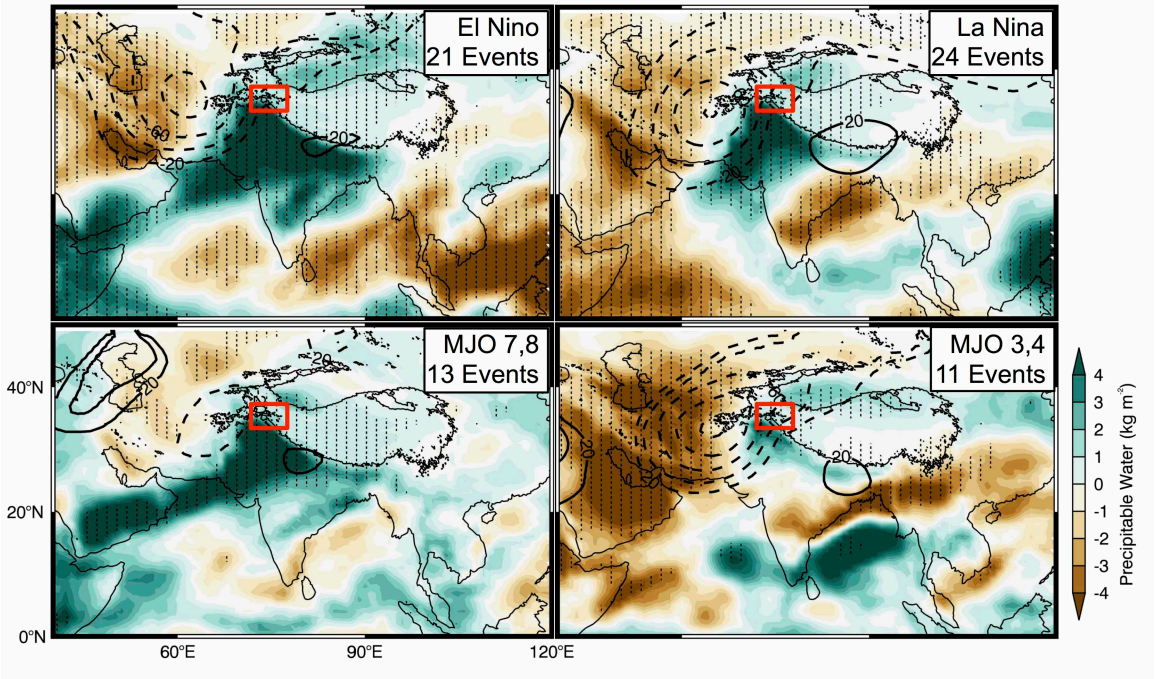

Figure 12 – Composites of precipitable water anomalies (color) and significant 500-hPa geopotential height anomalies (contour; negative values are dashed) during extreme precipitation events in the Karakoram in El Niño (top left), and La Niña (top right), as well as MJO phases 7 and 8 (bottom left) and 3 and 4 (bottom right). Only events occurring when only one mode is active are shown. The red box marks the approximate location of the Karakoram. Stippling indicates significance of precipitable water anomalies above the 95th percentile confidence interval (z-test).

a. ENSO

The signature of WD in mid-troposphere geopotential height is observed during extreme precipitation in both phases of ENSO, with deep depressions to the west of the KH. The observed trough generates cyclonic flow that is perpendicular to topography in the KH (Lang and Barros, 2004; Cannon et al. 2014). Differences in the geopotential height and precipitable water fields can be understood by superimposing average WD conditions onto the background conditions associated with positive or negative ENSO phases (Section 2.5).

El Niño conditions, associated with barotropic negative geopotential height anomalies over central Asia (Fig. 4) and an intensification of the sub-tropical jet (Yadav et al. 2010; Cannon et al. 2014), favor deeper negative anomalies that expand over a larger area during WD events. Contrastingly, an extratropical cyclone propagating across positive anomalies generated by La Niña conditions (Fig. 4) exhibits less zonal structure and more of a shortwave pattern. Shallow anomalies (-82gpm minimum compared to -95gpm minimum in El Niño) in this case are indicative of weakened cyclonic flow and diminished dynamical forcing of precipitation over topography. Precipitation differences elicited by circulation are exacerbated by additional differences in moisture availability.

ENSO related changes in surface pressure over the Maritime Continent and eastern Indian Ocean drive anomalous wind and moisture flux. Reduced convection over the Maritime Continent during El Niño relaxes equatorial Indian Ocean westerlies and reduces offshore winds from southwest Asia (Fig. 8). Precipitable water anomalies in the western Indian Ocean are significantly positive and extend northward over southwest Asia due to the weakening of the mean northeasterly moisture flux over the Arabian Sea, which curves eastward near the equator. The combination of enhanced dynamical forcing and ample moisture over southwest Asia in El Niño conditions favors high-magnitude KH precipitation during extratropical cyclones. Moisture along the cyclone's warm front is supported by the entrainment of anomalously large quantities of precipitable water over the Arabian Sea, while stronger dynamical forcing aloft enhances the intensity of orographic forcing of the moist flow. Both dynamical forcing and moisture conditions support an enhancement of orographic precipitation during WD in El Niño conditions compared to La Niña. This is presumably the reason for the observed precipitation differences at seasonal scales over

southwest Asia as well as the KH (Fig. 10) (Syed et al. 2006; Yadav et al. 2010; Dimri et al. 2012; Cannon et al. 2014). Though the 1997/98 El Nino does account for 7 of 21 events in the El Nino analysis, a composite of the remaining 14 events from El Nino conditions in other years is not appreciably different from the results shown in Fig. 12. Both the magnitude and spatial distribution of anomalies are nearly identical to that of the full set of El Nino condition events (not shown).

b. MJO

In contrast to the conditions observed during ENSO activity, phases of the MJO propagation cycle that favor the dynamical enhancement of WD simultaneously suppress available moisture over southwest Asia, and vice versa. The bottom panel of Fig. 12 shows composites of significant 500-hPa geopotential height and precipitable water anomalies during extreme precipitation events in the KH, categorized by MJO phase when ENSO was neutral. It is also important to note that each composite is comprised of only 11 and 13 events, so any single event carries considerable weight. Incipient WD in MJO 3/4 propagate in conditions that favor an intensified westerly jet upstream of the KH. Negative geopotential height anomalies at 500-hPa and below (Fig. 4) favor deeper WD troughs over southwest Asia, while available moisture is at a comparative minimum. Extreme precipitation is achieved through strong dynamical forcing at the mountain front, which efficiently extracts moisture at the orographic barrier. The average geopotential height anomaly at the WD center is lower than -100gpm during negative MJO compared to -40gpm in MJO phases 7/8, and maximum precipitable water in the KH is halved from phases 7/8 to phases 3/4. During MJO 7/8, extreme precipitation events are more strongly related to abundant moisture over

the western Indian Ocean, southwest Asia, and India, which is advected to the KH by comparatively weak cyclonic flow. Negative precipitable water anomalies over southwest Asia are found only in the trough, where cold air advection exists for the duration of the event. The high temperature and moisture content of the flow impinging on topography enables heavy precipitation (Krishbaum and Smith, 2008), both at the first orographic barrier as well as at subsequent peaks in the interior of the range, in the absence of strong cross-barrier winds (e.g. Norris et al. 2015a). Extreme precipitation is generated by enormous amounts of available moisture (significant anomalies in excess of 6kg m^{-2} upstream of the KH) and reduced stability, which compensate for diminished dynamical forcing in positive phases of the MJO.

2.7 Conclusions

Climate in the Karakoram and western Himalaya (KH) is influenced by global modes of variability at interannual and intraseasonal scales. In this work we focus on investigating how Westerly Disturbances (WD), which are the primary source of KH precipitation, are influenced by the El Niño Southern Oscillation (ENSO) and the Madden Julian Oscillation (MJO). These modes are known to modify circulation over southwest Asia by a forced Rossby wave response to changes in convection and diabatic heating over the eastern Indian Ocean/Maritime Continent. Though it is understood that no single extreme precipitation event's occurrence can be attributed to MJO activity or ENSO conditions, it is apparent that ENSO variability at interannual scales and MJO variability at intraseasonal scales have important influences on both dynamical forcing and moisture availability within westerly disturbances (WD) and thus modify the distribution of orographic precipitation in the KH.

Both ENSO and the MJO produce spatially similar patterns of OLR anomalies (a proxy for diabatic heating changes) over the Maritime Continent and eastern Indian Ocean, though tropical forcing associated with each mode uniquely influences WD activity and KH precipitation. Individual extreme precipitation events in the KH were investigated to highlight each mode's relationship with regional hydrology through the systems that dominate winter climate, which is essential to understanding the current state and future fate of High Asia's water resources.

During El Niño, atmospheric conditions that support increased precipitation over southwest Asia and the KH, including the intensification and southward displacement of the subtropical jet and abundant available moisture over southwest Asia, combine to drastically increase the frequency of observed extreme precipitation events relative to La Niña or neutral conditions. In La Niña conditions WD have minimal available moisture and exist in an environment that opposes dynamical enhancement, and thus extreme precipitation events in the KH are proportionally less frequent. The period of reduced extreme event frequency at the start of the 21st century that is defined by a strong and persistent La Niña is consistent with a well-documented catastrophic drought over southwest Asia (Argawala et al. 2001). However, it is important to note that even in the La Niña years, when large-scale dynamics inhibit the development of strong WD with abundant moisture, extreme precipitation events still occur with only one-to-two fewer events observed per season relative to the climatology. This is attributable to the influence of tropical forcing associated with the MJO, as discussed in this manuscript, and to extratropical influences on the strength and moisture content of WD, which are not discussed here.

Based on the Jones (2009) MJO index, the distribution of extreme events across phases of the MJO is relatively uniform, with the exception of phase 5, in which dynamic and thermodynamic conditions that are unfavorable for the development of orographic precipitation persist over southwest Asia. This is the transition period between moisture limited WD in phases 3/4 of the MJO and dynamical forcing limited WD in phases 7/8. A reduction of available moisture over southwest Asia similar to La Niña conditions is observed in MJO phases 3/4, but dynamical forcing of WD is intensified, as reflected by deeper troughs in event composites, likely related to intensification of the subtropical jet north of the upper-level anticyclone. The occurrence of extreme precipitation in such conditions is contingent on dynamically intense WD as prevailing moisture and stability conditions oppose extreme precipitation. In phases of MJO variability that favor enhanced available moisture over southwest Asia (phases 7/8), the intensity of WD and related cross-barrier winds in the KH are reduced. Extreme precipitation events in the mountains in phases 7/8 are largely driven by warm, moist unstable flow in absence of strong dynamical forcing. Competing contributions from dynamical and thermodynamic mechanisms exist across all phases of the MJO, and have a significant influence on the processes that produce regional extreme precipitation.

It is apparent that the MJO does not favor extreme precipitation in any one phase, but rather that the influence of dynamic and thermodynamic mechanisms that drive extreme precipitation during WD evolves as the MJO propagates. This is extremely important in understanding the influence of competing modes of variability on the relationship between WD and KH precipitation. Given the fact the MJO was generally less active during La Niña compared to El Niño, it is especially interesting that a higher proportion of this ENSO

phase's extreme events occurred when the MJO was also active.. Extreme events occurring during La Niña are comparatively more dependent on the influence of the MJO to generate the necessary dynamic and thermodynamic conditions to achieve heavy orographic precipitation in the KH. This is due to the persistence of unfavorable large-scale conditions for the development and enhancement of extreme-precipitation WD in La Niña conditions. It is also noteworthy that, of 205 extreme events in the KH, 34 occurred in ENSO neutral seasons when the MJO was inactive, which emphasizes that there are influences on WD and KH precipitation beyond those related to tropical forcing. Teleconnections other than the MJO and ENSO, and extratropical forcing, are outside the scope of this paper, but remain relevant to understanding KH hydrology.

The unique relationships between global variability and KH precipitation discussed here are a consequence of the region's unique geographical setting and climate, which juxtaposes a warm ocean with the world's highest mountains, in the path of the subtropical jet. Similar relationships would not be expected in many other regions around the globe. This research has demonstrated that extreme precipitation events in the KH are related to different contributions of dynamical forcing and moisture availability within WD, according to tropical forcing at intraseasonal and interannual scales. Independent and joint variability in tropical forcing by ENSO and MJO-driven diabatic heating must become major considerations of long-term evaluations of KH hydrology. Deconstructing the relationship between regional precipitation and global modes of variability allows for the evaluation of the individual components, which may not behave consistently under future climate conditions. For example, it is essential to understand the role of moisture, independent of circulation, because in a warming climate moisture availability will change exponentially

with temperature (Held and Soden, 2006; Hartmann et al. 2013). Additionally, extratropical circulation, including the position and intensity of midlatitude jets, will undergo significant changes (Fu and Lin, 2011) as 21st century warming manifests changes in global temperature gradients (Lemke et al. 2007; Hartmann et al. 2013), which the IPCC has only begun to address (Christensen et al. 2013). Consequently, hypotheses of WD behavior under ENSO or MJO influence that do not account for individual contributing components will be drastically different between current and future climate conditions. These weather-climate relationships will lead to improved forecasting of WD precipitation (Schubert et al. 2002; Barlow et al. 2005), and long-term predictability of water resources over southwest Asia and the KH (Immerzeel et al. 2009; Palazzi et al. 2013; Ridley et al. 2013; Kapnick et al. 2014).

Continued research should additionally utilize regional climate models to investigate how changes in temperature, humidity, and wind at the orographic barrier, which are related to global modes of variability, modify mesoscale spatial and temporal distributions of snowfall in the KH during WD events. The influence of dynamic and thermodynamic contributions to orographic precipitation are likely increasingly complex at these scales, and will be necessary to understand in order to evaluate regional hydrology in future climate scenarios. Continued progress toward identifying the effect of global climate on Karakoram and western Himalaya hydrology will ultimately benefit hundreds of millions of people that are dependent on the region's water resources.

2.8 Acknowledgements

This research was supported by the Climate and Large-Scale Dynamics Program, from the National Science Foundation (NSF award-AGS 1116105) and by NASA

Headquarters under the NASA Earth and Space Science Fellowship Program (Grant Number 13-EARTH13F-26). The CFSR data used in this research were developed by NOAA's National Centers for Environmental Prediction (NCEP) and provided by NCAR. NCEP/NCAR R1 and NOAA OLR data was provided by the NOAA/OAR/ESRL PSD, Boulder, Colorado, from their website (http://www.esrl.noaa.gov/psd/). APHRODITE data were provided by the Environment Research & Technology Development Fund of the Ministry of the Environment, Japan. TRMM data were provided by an international joint project sponsored by the Japan National Space Development Agency (NASDA) and the U.S. National Aeronautics and Space Administration (NASA) Office of Earth Science. Station data was provided by the Water and Power Development Authority of Pakistan (WAPDA) and the Pakistan Meteorological Department (PMD). The authors would also like to thank Dr. Elisa Palazzi and Dr. Mathew Barlow for their help on this manuscript.

2.9 References

Anders AM, Roe GH, Hallet B, Montgomerey DR, Finnegan NJ, Putkonen J (2006) Spatial patterns of precipitation and topography in the Himalaya. Geol Soc Am Spec Pap 398:39-53

Archer DR, Fowler HJ (2004) Spatial and temporal variations in precipitation in the Upper Indus Basin, global teleconnections and hydrological implications. Hydrol Earth Syst Sc 8:47-61

Argawala S, Barlow M, Cullen H (2001) The drought and humanitarian crisis in central and southwest Asia: A climate perspective. IRI Special Report 01-11,24pp

Bao X, Zhang F (2012) Evaluation of NCEP-CFSR, NCEP-NCAR, ERA-Interim, and ERA-40 reanalysis datasets against independent sounding observations over the Tibetan Plateau. J Clim 26:206-214

Barlow M, Wheeler M, Lyon B, Cullen H (2005) Modulation of daily precipitation over southwest Asia by the Madden-Julian oscillation. Mon Weather Rev 133:3579-3594

Barnston AG, Livezey RE (1987) Classification, seasonality and persistence of low-frequency atmospheric circulation patterns. Mon Wea Rev 115:1083-1126

Barros AP, Joshi M, Putkonen J, Burbank DW (2000) A study of the 1999 monsoon rainfall in a mountainous region in central Nepal using TRMM products and rain gauge observations. Geophys Res Lett 27:3683-3686

Barros AP, Chiao S, Lang TJ, Burbank D, Putkonen J (2006) From weather to climate – Seasonal and interannual variability of storms and implications for erosion processes in the Himalaya. Geol Soc Am Spec Pap 398:17-38

Bolch T, Kulkarni A, Kaab A, Huggel C, Paul F, Cogley JG, Frey H, Kargel JS, Fujita K, Scheel M, Bajracharya S, Stoffel M (2012) The state and fate of Himalayan glaciers. Science 336:310-314

Bookhagen B, Burbank DW (2006) Topography, relief and TRMM-derived rainfall variations along the Himlaya. Geophys Res Lett 33:L08405

Bookhagen B, Burbank DW (2010) Towards a complete Himalayan hydrological budget: The spatiotemporal distribution of snow melt and rainfall and their impact on river discharge. J Geophys Res-Earth 115

Cannon F, Carvalho LMV, Jones C, Bookhagen B (2014) Multi-annual variations in winter westerly disturbance activity affecting the Himalaya. Clim Dyn 44:441-455

Cannon F, Carvalho LMV, Jones C, Norris J (2015) Winter westerly disturbance dynamics and precipitation in the western Himalaya and Karakoram: a wave-tracking approach. Theor Appl Climatol doi:10.1007/s00704-015-1489-8

Christensen JH, Krishna Kumar K, Aldrian E, An SI, Cavalcanti IFA, de Castro M, Dong W, Goswami P, Hall A, Kanyanga JK, Kitoh A, Kossin J, Lau NC, Renwick J, Stephenson DB, Xie SP, Zhou T (2013) Climate Phenomena and their Relevance for Future Regional Climate Change. In: Climate Change 2013: The Physical Science Basis. Contribution of Working Group I to the Fifth Assessment Report of the Intergovernmental Panel on Climate Change [Stocker, T.F., D. Qin, G.-K. Plattner, M. Tignor, S.K. Allen, J. Boschung, A. Nauels, Y. Xia, V. Bex and P.M. Midgley (eds.)]. Cambridge University Press, Cambridge, United Kingdom and New York, NY, USA.

Curio J, Maussion F, Scherer D (2014) A twelve-year high-resolution climatology of atmospheric water transport on the Tibetan Plateau. Earth Syst Dynam 6:109-124

Dimri AP, Dash SK (2012) Wintertime climatic trends in the western Himalayas. Climatic Change 111:775-800

Dimri AP, Niyogi D, Barros AP, Ridley J, Mohanty UC, Yasunari T, Sikka DR (2015) Western disturbances: a review. Rev Geophys 53:225-246

Filippi L, Palazzi E, von Hardenberg J, Provenzale A (2014) Multidecadal variations in the relationship between the NAO and winter precipitation in the Hindu-Kush Karakoram. J Clim doi:10.1175/JCLI-D-14-00286.1

Fu Q, Lin P (2011) Poleward shift of subtropical jets inferred from satellite-observed lower-stratospheric temperatures. J Clim 24:5597-5603

Gill AE (1980) Some simple solutions for heat-induced tropical circulation. Quart J Roy Meteor Soc 106:447-462

Gong DY, Wang SW, Zhu JH (2001) East Asian winter monsoon and Arctic Oscillation. Geophys Res Lett 28:2073-2076

Hartmann DL, Klein Tank AMG, Rustucci M, Alexander LV, Bronnimann S, Charabi Y, Dentener FJ, Dlugokencky EJ, Easterling DR, Kaplan A, Soden BJ, Thorne PW, Wild M, Zhai PM (2013) Observations: Atmosphere and Surface in: Climate Change 2013: The Physical Science Basis. Contribution of Working Group I to the Fifth Assessment Report of the Intergovernmental Panel on Climate Change [Stocker TF, Qin D, Plattner GK, Tignor M, Allen SK, Boschung J, Nauels A, Xia Y, Bex V, Midgley PM (eds.)] Cambridge University Press, Cambridge, United Kingdom and New York, NY, USA.

Held IM, Soden BJ (2006) Robust responses of the hydrological cycle to global warming. J Climate 19:5686-5699

Hewitt K (2005) The Karakoram anomaly? Glacier expansion and the "elevation effect", Karakoram Himalaya. Mountain Res Dev 25:332-340

Hewitt K (2014) Glaciers of the Karakoram Himalaya: Glacial environments, processes, hazards and resources. Springer, Dordrecht, Netherlands

Hoell A, Barlow M, Saini R (2012) The leading pattern of intraseasonal and interannual Indian Ocean precipitation variability and its relationship with Asian circulation during the Boreal cold season. J Climate 25:7509-7526

Hoell A, Barlow M, Saini R (2013) Intraseasonal and seasonal-to-interannual Indian Ocean convection and hemispheric teleconnections. J Clim 26:8850-8867

Hoell A, Barlow M, Wheeler MC, Funk C (2014) Disruption of El Niño-Southern Oscillation teleconnections by the Madden Julian Oscillation. Geophys Res Lett 41:998-1004

Huffman GJ et al (2007) The TRMM multisatellite precipitation analysis (TMPA): Quasi-global, multiyear, combined-sensor precipitation estimates at fine scales. J Hydrometeorol 8:38-55

Immerzeel WW, Droogers P, de Jong SM, Bierkens MFP (2009) Large-scale monitoring of snow cover and runoff simulation in Himalayan river basins using remote sensing. Remote Sens Environ 113:40-49

Jones C, Waliser DE, Lau KM, Stern W (2004) Global occurrences of extreme precipitation and the Madden-Julian Oscillation: Observations and predictability. J Climate 17:4575-4589

Jones C (2009) A homogeneous stochastic model of the Madden-Julian Oscillation. J Climate 22:3270-3288

Kapnick SB, Delworth TL, Ashfaq M, Malyshev S, Milly PCD (2014) Snowfall less sensitive to warming in Karakoram than in Himalayas due to a unique seasonal cycle. Nature Geosci 7:834-840

Kiladis GN, Dias J, Straub KH, Wheeler MC, Tulich SN, Kikuchi K, Weickmann KM, Ventrice MJ (2014) A comparison of OLR and circulation-based indices for tracking the MJO. Mon Wea Rev 142:1697-1715

Krishbaum DJ, Smith RB (2008) Temperature and moist-stability effects on midlatitude orographic precipitation. QJR Meteorol Soc 134:1183-1199

Krishnamurti TN (1961) The subtropical jet stream of winter. J Meteorol 18:172-191

Lang TJ, Barros AP (2004): Winter storms in the central Himalayas. J Meteorol Soc Jpn 82:829-844

Lee HT (2014) Climate algorithm theoretical basis document (C-ATBD): Outgoing longwave radiation (OLR) – Daily. NOAA's Climate Data Record (CDR) Program. CDRP-ATBD-0526, 46pp

Lee YY, Lim GY (2012) Dependency of the North Pacific winter storm tracks on the zonal distribution of MJO convection. J Geophys Res 117:1-12

Lemke, P, Ren J, Alley RB, Allison I, Carrasco J, Flato G, Fujii Y, Kaser G, Mote P, Thomas RH, Zhang T (2007) Observations: Changes in snow, ice and frozen ground. In Climate Change 2007: The Physical Science Basis. Contribution of Working Group 1 to the Fourth Assessment Report of the Intergovernmental Panel on Climate Change [Solomon S, Qin D, Manning M, Chen Z, Marquis M, Averyt KB, Tignor M, Miller HL (eds.)]. Cambridge University Press, Cambridge, United Kingdom and New York, NY USA.

Mariotti A (2007) How ENSO impacts precipitation in southwest central Asia. Geophys Res Lett 34:1-5

Matsuno T (1966) Quasi-geostrophic motions in the equatorial area. J Meteor Soc Japan 44:25-42

Maussion F, Scherer D, Molg T, Collier E, Curio J, Finkelnburg R (2014) Precipitation seasonality and variability over the Tibetan Plateau as resolved by the High Asia Reanalysis. J Climate 27:1910-1927

Norris J, Carvalho LMV, Jones C, Cannon F (2015) WRF simulations of two extreme snowfall events associated with contrasting extratropical cyclones over the Himalayas. J Geophys Res doi:10.1002/2014JD022592

Norris J, Carvalho LMV, Jones C, Cannon F, Bookhagen B (2015) The spatiotemporal variability of precipitation in the Himalaya: Validation of a one-year WRF model simulation. Clim Dyn (*submitted)*

Palazzi E, von Hardenberg J, Provenzale A (2013) Precipitation in the Hindu-Kush Karakoram Himalaya: Observations and future scenarios. J Geophys Res-Atmos 118:85-100

Palazzi E, Tahir AA, Cristofanelli P, Vuillermoz E, Provenzale A (2015) Climatic characterization of Baltoro Glacier (Karakoram) and northern Pakistan from in-situ stations. *Engineering Geology for Society and Territory*. Springer, Switzerland

Penny SM, Battisti DS, Roe GH (2012) Examining mechanisms of variability within the Pacific storm track: Upstream seeding and jet-core strength. J Climate 26:5242-5259

Rasmusson EM, Carpenter TH (1982) Variations in tropical sea surface temperature and wind fields associated with the southern oscillation/El Nino. Mon Wea Rev 111:517-528

Ridley J, Wiltshire A, Mathison C (2013) More frequent occurrence of westerly disturbances in Karakoram up to 2100. Sci Total Environ 468-469:S31-S35

Roe GH (2005) Orographic Precipitation. Annu Rev Earth Planet Sci 33:647-671

Saha S et al (2010) The NCEP Climate Forecast System Reanalysis. B Am Meteorol Soc 91:1015-1057

Schubert S, Dole R, Van den Dool H, Suarez M, Waliser D (2002) Proceedings from a workshop on prospects for improved forecasts of weather and short-term climate variability on subseasonal (2 week to 2 month) time scales. Vol. 23 NASA Tech. Memo. 2002-104606, 171pp

Singh P, Ramasastri KS, Kumar N (1995) Topographical influence on precipitation distribution in different ranges of western Himalayas. Nord Hydrol 26:259-284

Skamarock WC, Klemp BJ, Dudhia J, Gill DO, Barker DM, Duda MG, Huang XY, Wang W, Powers JG (2008) A description of the Advanced Research WRF Version 3. NCAR Technical Note – 4751STR

Syed FS, Giorgi F, Pal JS, King MP (2006) Effect of remote forcings on the winter precipitation of central southwest Asia part 1: observations. Theor Appl Climatol 86:147-160

Syed FS, Giorgi F, Pal JS, Keay K (2010) Regional climate model simulation of winter climate over Central-Southwest Asia, with emphasis on NAO and ENSO effects. Int J Climatol 30:220-235

Tahir AA, Chevallier P, Arnaud Y, Ahmad B (2011) Snow cover dynamics and hydrological regime of the Hunza River basin, Karakoram Range, Northern Pakistan. Hydrol Earth Syst Sci 15:2275-2290

Takahashi C, Shirooka R (2014) Storm track activity over the North Pacific associated with the Madden-Julian Oscillation under ENSO conditions during boreal winter. J Geophys Res Atmos 119:10663-10683

Trenberth KE (1997) The definition of El Niño. Bull Amer Met Soc 78:2771-2777

Wang A, Zeng X (2012) Evaluation of multireanalysis products with in situ observations over the Tibetan Plateau. J Geophys Res 117:1-12

Wallace J, Lim GH, Blackmon M (1988) Relationship between cyclone tracks, anticyclone tracks and baroclinic waveguides. J Atmos Sci 45:439-462

Wheeler MC, Hendon HH (2004) An all-season real-time multivariate MJO index: Development of an index for monitoring and precipitation. Mon Wea Rev 132:1917-1932

Wilks DS (2006) Statistical methods in the atmospheric sciences. Elsevier, Burlington

Wu BY, Wang J (2002) Winter Arctic Oscillation, Siberian High and East Asian winter monsoon. Geophys Res Lett 29:1-4

Yadav RK, Rupa Kumar K, Rajeevan M (2009) Increasing influence of ENSO and decreasing influence of AO/NAO in the recent decades over northwest India winter precipitation. J Geophys Res-Atmos 114

Yadav RK, Yoo JH, Kucharski F, Abid MA (2010) Why is ENSO influencing northwest India winter precipitation in recent decades? J Climate 23:1979-1993

III. Chapter 3: Preface

Dynamical downscaling of reanalysis for extreme precipitation event case studies benefits the investigation of High Mountain Asia hydroclimate by more realistically representing regional orographic precipitation processes and meteorological forcing than is possible with coarse grid-scale reanalyses, which do not resolve the region's topographic complexity (Maussion et al. 2014; Norris et al. 2015). Well-tuned Weather Research and Forecasting (WRF) model configurations at high spatiotemporal resolution have proven capable of simulating WD dynamics and precipitation in mountainous regions of Asia (Maussion et al. 2014; Norris et al. 2015). Norris et al. (2015; 2016) built upon work by Maussion et al. (2011; 2014) to develop a WRF configuration that was tuned to simulate mesoscale precipitation patterns in High Asia by evaluating WRF against available in-situ observations and remotely sensed data. Results from mesoscale modeling studies have enabled investigations of High Asia climate and regional hydrology that would not have otherwise been possible (e.g. Collier et al. 2013; Norris et al. 2015; Curio and Scherer, 2016). In the third chapter of this dissertation, the optimal model configuration from Norris et al. (2015; 2016) is utilized to perform a set of modified topography experiments to test the effect of smoothed topography, such as that resolved by a global circulation model, on extreme precipitation event simulation over High Mountain Asia.

III. Chapter 3: Effects of Topographic Smoothing on the Simulation of Winter Precipitation in High Asia

Forest Cannon[1,2], Leila M.V Carvalho[1,2], Charles Jones[1,2],

Jesse Norris[1,2], Bodo Bookhagen[3], and George N. Kiladis[4]

[1] Department of Geography, University of California Santa Barbara, Santa Barbara, CA

[2] Earth Research Institute, University of California Santa Barbara, Santa Barbara, CA

[3] Institute of Earth and Environmental Science, University of Potsdam, Potsdam, Germany

[4] NOAA Earth System Research Laboratory, Physical Sciences Division, Boulder, CO

3.1 Abstract

Efficient water-resource management in High Mountain Asia is essential to sustain populations across a large portion of Asia. Numerous studies have projected future changes in the region's hydrology based on temperature and precipitation from global circulation models (GCM) under future climate scenarios. Although the potential benefit of such studies is immense, coarse grid-scale GCMs are unable to resolve High Mountain Asia's complex topography and thus have a biased representation of regional weather and climate. We investigate biases in the simulation of physical mechanisms that generate snowfall and contribute to snowpack in High Mountain Asia in coarse topography experiments using the Weather Research and Forecasting model. Regional snowpack is event driven, thus 33 extreme winter orographic precipitation events are simulated at fine atmospheric resolution with 6.67km-resolution topography and smoothed 1.85°x1.25°-GCM topography. As with many modified topography experiments performed in other regions, the distribution of

precipitation is highly dependent on first-order orographic effects, which dominate regional meteorology. However, we demonstrate that topographic smoothing enhances circulation in simulated extratropical cyclones, with significant impacts on orographic precipitation. Despite precipitation reductions of 28% over the highest ranges, due to reduced ascent on windward slopes, total precipitation over the study domain increased by an average of 9% in smoothed topography experiments on account of intensified extratropical cyclone dynamics and cross-barrier moisture flux. These findings identify an important source of bias in coarse-resolution simulated precipitation in High Mountain Asia, with important implications for the application of GCMs toward projecting future hydroclimate in the region.

3.2 Introduction

Developing future water management and planning strategies requires the estimation of current and future precipitation magnitudes and variability (Wehner, 2013). In recent years, a large number of studies have employed global circulation models (GCM) to estimate future precipitation in High Mountain Asia (e.g. Lutz et al. 2013; Kapnick et al. 2014; Palazzi et al. 2013, 2014; Shea et al. 2015). The work of Palazzi et al. (2014) analyzed the properties of precipitation in western High Mountain Asia as simulated by 32 state-of-the-art GCMs participating in the Coupled Model Intercomparison Project phase 5 (CMIP5; World Climate Research Program, 2011). They found that the multi-model ensemble mean, and most individual models, exhibit a wet bias with respect to observations in western High Mountain Asia for all seasons, and that the models differ considerably in their representation of seasonal climatologies. In general, no single model (or group of models) consistently outperformed all others for all the statistics considered, and the large spread in the behavior of individual models warrants caution in evaluating multi-model ensemble means over high topography (Palazzi et al. 2014). Despite model uncertainty, a number of studies have utilized ensemble mean precipitation and temperature from GCMs to drive hydrologic models under future climate conditions and project changes in High Mountain Asia's water resources (e.g. Lutz et al. 2013; Shea et al. 2015; Soncini et al. 2015; Su et al. 2016). Miller et al. (2012) provides a synthesis of previous studies projecting hydroclimate changes in High Mountain Asia. Though uncertainty in GCM-simulated precipitation is not well understood, a pertinent concern for High Mountain Asia, which our study addresses, is the effect of topographic resolution on the simulation of orographic forcing in the region's complex topography.

GCMs typically have resolutions on the order of hundreds of kilometers and, consequently, have coarse topography and an unrealistic representation of topographic forcing of weather and climate (Yorgun and Rood, 2014). The current study investigates how topographic smoothing affects the simulation of the primary drivers of precipitation in western High Mountain Asia. Extratropical cyclones are the primary climatic influence in High Mountain Asia during non-monsoon months (Singh et al. 1995; Lang and Barros, 2004; Barlow et al. 2005; Dimri et al. 2015), delivering in excess of 50% of the total annual precipitation (Lang and Barros, 2004; Barlow et al. 2005; Barros et al. 2006; Bookhagen and Burbank, 2010; Cannon et al. 2014; Wulf et al. 2016). These events, termed "Westerly Disturbances" (WD), generate heavy orographic precipitation when moisture flux along the cyclone's front encounters High Mountain Asia topography. The majority of WD-generated precipitation falls as snow over the Karakoram and western Himalaya's high mountains, thus augmenting the region's snowpack and glaciers (Anders et al. 2006; Tahir et al. 2011; Ridley et al. 2013; Cannon et al. 2015).

Amongst extreme events, there is considerable variability in the dynamic and thermodynamic influences on precipitation, as available moisture, atmospheric stability and the strength and orientation of cross-barrier winds that drive orographic uplift, all vary on an event-by-event basis (Cannon et al. 2015, 2016). This manuscript details the effects of topographic smoothing on simulated relationships between dynamical forcing, moisture availability and orographic precipitation in High Mountain Asia, and quantifies bias in the representation of precipitation in coarse-topography simulation. In reference to previous studies that have identified significant influences of topographic resolution over meteorological simulation (e.g. Mass et al. 2002; Colle et al. 2008; Gutmann et al. 2012), the

modified experiments presented here are unique in their focus on real WD events and their control of horizontal resolution.

Here, The Weather Research and Forecasting model is used to investigate the influence of topographic smoothing on model bias by simulating 33 WD events using both 6.67km-resolution topography and smoothed 1.85°x1.25°-GCM topography. Differences in the generation of orographic precipitation are quantified across experiment types by evaluating the absolute magnitude and percentage change of dynamic and thermodynamic mechanisms. Identifying bias improves understanding of uncertainty in GCM representation of regional climate, and is essential for the prudent application of GCM output toward projecting water resources availability in High Mountain Asia, as well as other mountainous regions.

3.3 Data

a. In-Situ Data

Data from 7 in-situ stations located at low elevations of the Karakoram aid in the selection of extreme precipitation events for WRF simulation. A reference map of the study region and station locations is shown in Fig. 1. Here, we consider daily-accumulated precipitation from 7 Pakistani Meteorological Department (PMD) stations for the period 1960-2012. We assume that extant biases in the magnitude of station-measured precipitation in the Karakoram and western Himalaya (Hewitt et al. 2014) are constant in time and thus do not affect the selection of extreme events relative to all other dates in the record (Cannon et al. 2016).

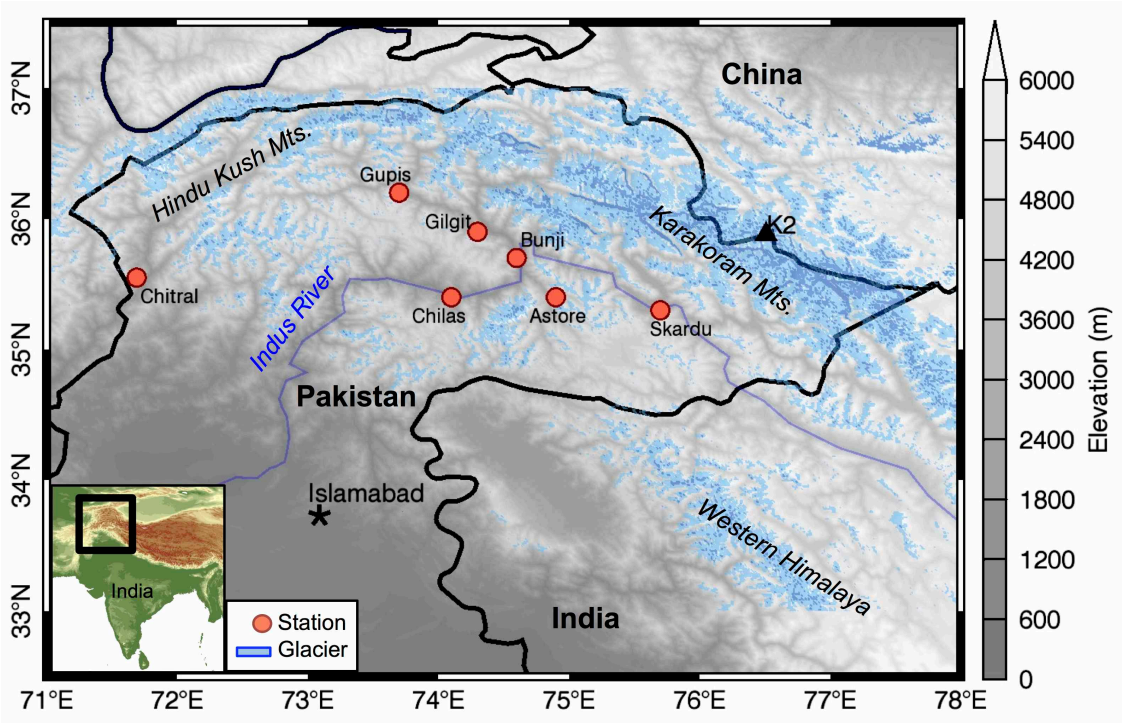

Figure 1 – Topography map of the study area and station data locations (red circles). International borders are outlined in black. Blue shading indicates glacier coverage. The inset map shows the location of the study region (black box) over color-shaded topography.

b. Meteorological Data from Reanalyses

Climate Forecast System Reanalysis (CFSR) data, from the National Centers for Environmental Prediction (Saha et al. 2010), are used to investigate large-scale climate and the dynamics of WD, as well as to initialize WRF simulations. CFSR is available at 0.5° horizontal-resolution for the period 1979-2013. CFSR was chosen on account of its spatial resolution and modern data assimilation system (Saha et al. 2010).

c. Extreme Precipitation Event Definition

Analyses of individual events are performed based on the identification of extreme precipitation using a combination of CFSR and PMD station data (Cannon et al. 2016). First, principal component analysis of the data from PMD stations for Nov.-Apr. was performed

using a covariance matrix to reduce the number of variables by identifying a leading orthogonal pattern of precipitation variability across all 7 stations from 1979 to 2012 (Wilks, 2006). The first principal component explained 53% of the variability amongst stations, and high values were observed to correspond to high-magnitude precipitation at multiple PMD stations. CFSR, which was not included in the PCA analysis, also exhibited heavy precipitation over the western Himalaya and Karakoram during peaks in the first principal component. Independent 90^{th} percentile dates (only the highest magnitude day of all consecutive 90^{th} percentile days is retained) from the station-based first principal component timeseries and independent 90^{th} percentile dates from aggregated CFSR precipitation in the western Himalaya and Karakoram (73-77°E, 34-37°N) produced a collection of extreme precipitation events that overlapped in 205 cases, or approximately 67% of the time, (PMD had 295 independent events and CFSR had 308) during Nov.-Apr., 1979-2012. For this work we dynamically downscale only 33 of the 205 extreme events on account of limited computing resources. Details on the event selection process are given in Section 3.5.

3.4 Model Configuration

Each one-day extreme precipitation event was simulated using version 3.7 of the Advanced Research Weather and Forecasting (ARW-WRF, hereafter WRF) model (Skamarock et al. 2008). For each selected date, 36-hour simulations were initialized at 12UTC the day preceding the event, with the first 12 hours of simulation being discarded as "spin-up" (Maussion et al. 2014). Simulations were performed with two domains using one-way interaction, with an outer domain horizontal resolution of 20km and an inner domain resolution of 6.67km (3:1 ratio) on a Mercator projection (similar to Norris et al. 2015a,b).

An adaptive time step with an upper limit of 120s for the outer domain and 45s for the inner domain was used. Initial and lateral boundary conditions were garnered from CFSR. The parameterization schemes employed are listed in Table 1. Norris et al. (2015) performed thorough testing of this particular configuration. They concluded that although no single configuration is ideal across all conditions, this particular set-up demonstrated the most realistic results for WD simulations in High Mountain Asia. WRF uses a terrain following vertical coordinate (50 levels in these simulations), but output has been interpolated to pressure levels for this discussion.

Microphysics	Thompson (Thompson et al. 2008)
Surface Layer	MM5 Monin-Obukhov (Monin and Obukhov, 1955)
Land Surface	Noah (Niu et al. 2011)
Longwave Radiation	Rapid Radiative Transfer Model (RRTM, Mlawer et al. 1997)
Shortwave Radiation	Dudhia (Dudhia, 1989)
Boundary Layer	Yonsei University (Hong et al. 2006)
Cumulus	Kain – Fritsch (Kain, 2004) - outer domain only

Table 1 – Parameterizations employed in WRF experiments.

We additionally performed simulations of the 33 extreme events using coarse resolution topography to test how regional meteorology and orographic precipitation are modified when simulated over GCM-type topography, which is considerably smoother. Modified topography experiments were performed using topography from the Hadley Center global circulation model (HadGEM2-ES; Martin et al. 2011) (1.875°x1.25° horizontal resolution) that was resized to 6.67km resolution, smoothed using cubic convolution

interpolation to remove steep transitions across grid cells (Park and Schowengerdt, 1983), and then resampled onto WRF's grid. The mean elevations of the two topography experiments' domains are within 10m. A 90m DEM from the Shuttle Radar Topography Mission (Farr et al. 2007), the original 6.67km topography and modified topography for the High Mountain Asia study region are shown in Fig. 2. The spatial extent of the topography figures corresponds to the spatial extent of WRF's inner domain for this study. The WRF configuration for original and modified topography experiments is identical except for changes to the input topography characteristics in the geographic information (geogrid) file. Land surface variables that may be related to elevation, such as land use and land cover, were not altered because the 36-hour simulation of winter events was found to be insensitive to these in previous testing (not shown). Simulations of 48-hours (24-hour spin-up) and 72 hours (48-hour spin-up) were tested for several events without significant differences from the 36-hour simulations with 12 hours of spin-up presented here. The computation time required for each simulation restricted sensitivity tests of different topographic smoothing techniques and horizontal resolutions. However, while the smoothing technique applied may alter the magnitude of the statistics presented, the processes that underlie the key findings of this research are robust. This research emphasizes the physical effect of smooth topography on the simulation of precipitation mechanisms, rather than focusing on statistical differences alone.

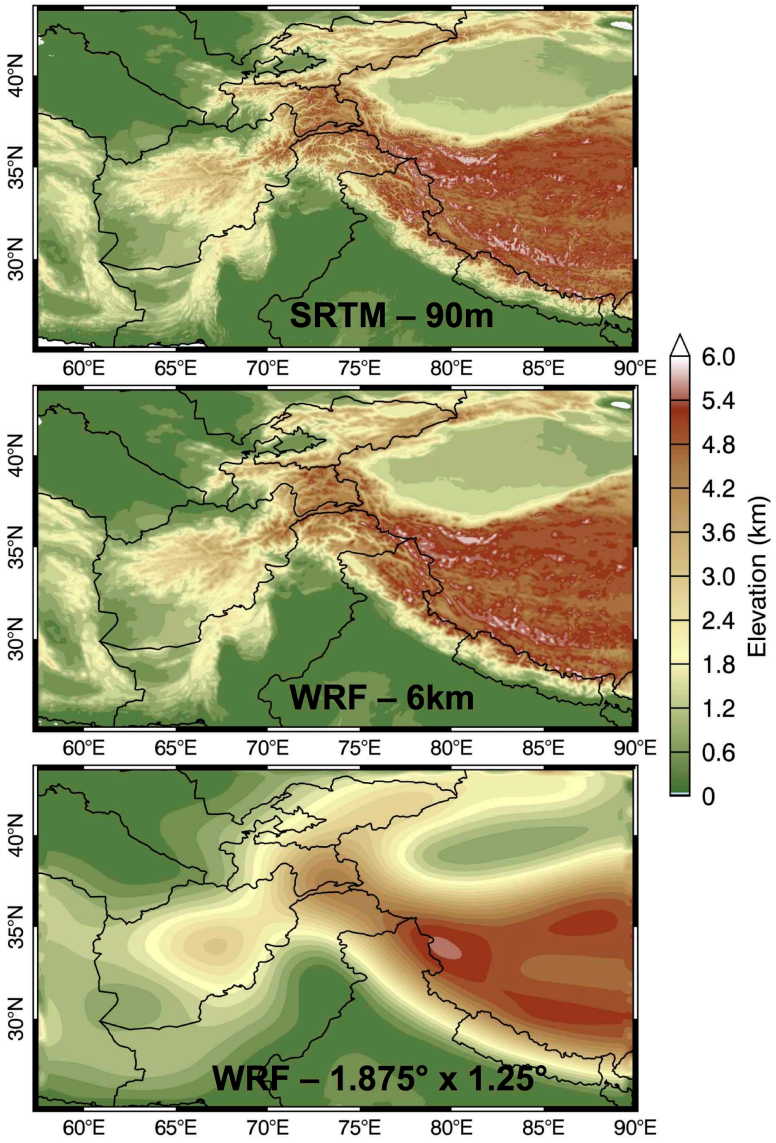

Figure 2 – Shuttle Radar Topographic Mission 90m resolution topography (top), WRF original topography (6.67x6.67km; middle), and WRF smoothed topography (~175x140km; bottom). International borders are outlined in black.

3.5 Extreme Event Categories

Cannon et al. (2015) found extreme winter precipitation events in western High Mountain Asia to be driven by two primary mechanisms: 1) dynamical forcing, related primarily to the strength of cross-barrier winds that force moisture against topography, and 2)

thermodynamic forcing, related to moisture availability and instability, which enhances orographic precipitation in the cross-barrier flow.

Here, events are categorized based upon the findings of Cannon et al. (2016), which indicated that intraseasonal variability associated with the Madden Julian Oscillation (MJO; Madden and Julian, 1972) significantly influences dynamic and thermodynamic drivers of precipitation during WD events in High Mountain Asia (Barlow et al. 2005; Hoell et al. 2014; Cannon et al. 2016). Using the MJO index of Jones (2009), phases of the MJO propagation cycle that favor the dynamical enhancement of WD through an extratropical Rossby wave response (phases 3 and 4; when enhanced convection is positioned over the eastern Indian Ocean and Maritime Continent) simultaneously suppress available moisture over southwest Asia (Cannon et al. 2016). In these phases strong dynamic forcing compensates for relatively little available moisture to produce extreme precipitation during WD events. As the MJO propagates the primary driver of precipitation in WD transitions so that in phases 7 and 8 (suppressed convection over the eastern Indian Ocean and Maritime Continent) WD exhibit relatively weak dynamics, while precipitation generation is attributable to large quantities of moisture exported from the tropics. In addition, the 205 extreme precipitation events identified in Section 3.3c were categorized by MJO influence during neutral periods of the El Nino Southern Oscillation (ENSO). 33 events from the following three MJO categories, representing differing contributions of dynamical and thermodynamic forcing to orographic precipitation, were selected for simulation:

1) The 13 events that occurred during MJO phases 7 and 8 with ENSO neutral.
2) The 10 events that occurred during MJO phases 3 and 4 with ENSO neutral.
3) The 10 largest-magnitude precipitation events during neutral MJO and ENSO.

Figure 3 shows average significant (t-test; $p < 0.05$) precipitable water and 500-hPa geopotential height anomalies (annual cycle removed) from CFSR for extreme events that occurred in MJO phases 7 and 8 (top), phases 3 and 4 (middle), and neutral phases (Jones, 2009). The neutral condition group exhibits a well-developed trough, with minimum geopotential height of -90gpm, west of High Mountain Asia. Cyclonic winds along the leading edge of the system draw upon a considerable moisture supply extending from the tropics, around the Horn of Africa. These precipitation events are driven by strong contributions from both dynamical forcing and available moisture. In comparison, events in MJO phases 3/4 exhibit slightly deeper geopotential height anomalies (minimum of -105gpm), leading to strong dynamical forcing, while enhanced available moisture is observed only over the Gangetic Plain. Events in MJO phases 7/8 exhibit a relatively shallow trough (~-30gpm), but a significant moisture plume that extends from equatorial Africa (significant anomalies in excess of 8kg m^{-2} upstream of High Mountain Asia) compensates for reduced dynamical forcing of precipitation. These composites illustrate the influence of tropical forcing on regional extreme events (Cannon et al. 2016), but more importantly identify the influence of strong orographic forcing by well-developed cyclones and available moisture contributions to extreme precipitation, which are essential to examine individually in order to explain bias in coarse-resolution topography simulation.

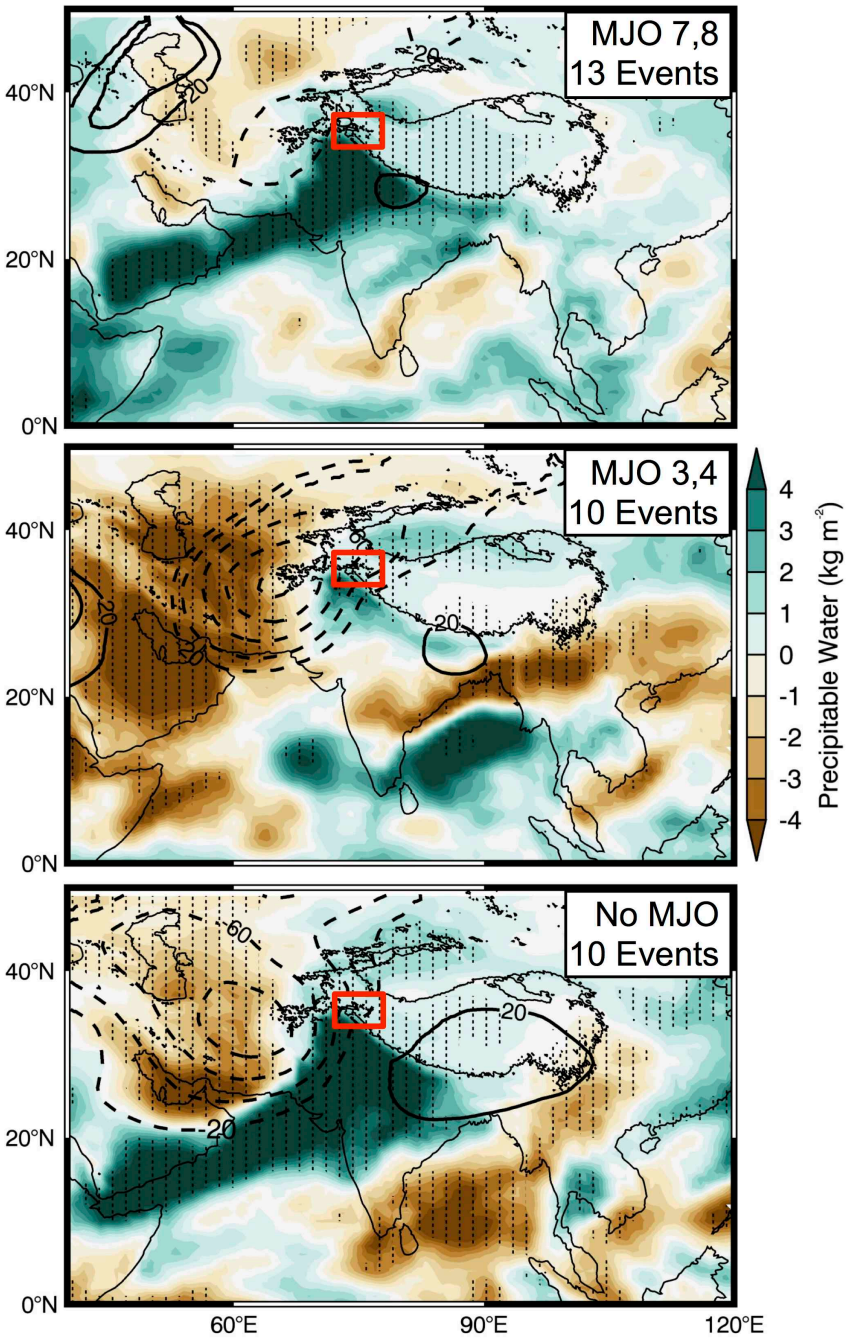

Figure 3 – Composites of precipitable water anomalies (color) and 500-hPa geopotential height anomalies (contour; negative values are dashed) during extreme precipitation events in the Karakoram in MJO phases 7 and 8 with ENSO neutral conditions (top), MJO phase 3/4 with ENSO neutral (middle), and neutral MJO and ENSO conditions (bottom). The red box identifies the precipitation-indexing region. Stippling indicates significance of precipitable water anomalies above the 95th percentile confidence interval.

3.6 WRF Experiment Results

a. Precipitation Distributions: Control vs. Modified Topography Experiments

Previous studies have identified the importance of model resolution in simulating the spatial distribution of precipitation (e.g. Mass et al. 2002; Gao et al. 2006, Guttman et al. 2011). This study is unique in its focus on topographic effects, which is made possible by maintaining consistent convection-resolving resolution (6.67km) for both experiment groups. Controlling for horizontal resolution, which may generate model sensitivity as an artifact of possibly erroneous or inconsistent assumptions in the parameterizations schemes at different resolutions (Giorgi and Marinucci, 1996), allows for a more direct investigation of the role of topographic forcing on the simulated events.

Figure 4 demonstrates that the large-scale spatial distributions of both rainfall and snowfall are similar for all event categories and across experiment types, though coarse-topography experiments exhibit considerable smoothing. Despite similar spatial patterns, which are driven by the interaction of the WD with topography, it is notable that, locally, precipitation magnitudes are much greater in 6.67km topography experiments for the western Himalaya and Karakoram ranges (the two bands of enhanced snowfall). Mass et al. (2002) identified similar orographic enhancement from 12km to 4km resolution simulations in the Cascades. Here, the differences between simulations are also primarily attributable to topographic smoothing. However, Fig. 4 identifies that precipitation covers a larger area in modified topography experiments, and quantitative analyses presented in the following sections demonstrate that total precipitation over High Mountain Asia increased in modified topography experiments.

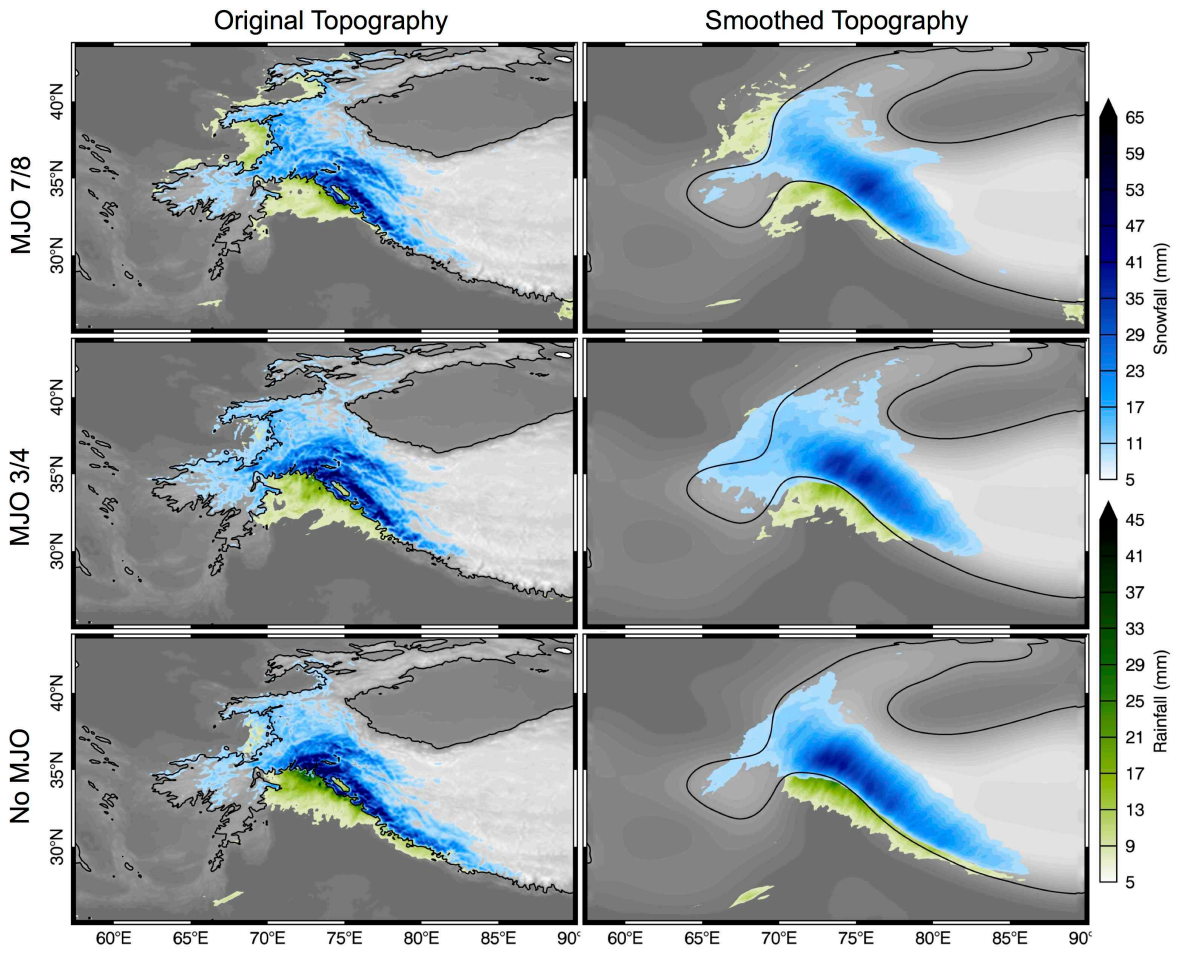

Figure 4 – Composite rainfall (green) and snowfall (blue) during extreme precipitation events in the Karakoram in MJO phases 7 and 8 with ENSO neutral conditions (top), MJO phase 3/4 with ENSO neutral (middle), and neutral MJO and ENSO conditions (bottom). The 2000m topography contour is outlined in black and topography is shown as grayshade. Original topography experiments occupy the left column and modified topography experiments appear in the right column.

b. Transects

i. Control Experiments

High-resolution WRF simulations of extreme events enable the investigation of thermodynamic and dynamic processes in the vertical and along individual slopes. Figure 5 shows composite cross-sections of meridional wind for a transect across the western

Himalaya and Karakoram at 73.5E. Only one transect is shown, though the differences observed between experiment types and event categories are consistent throughout the study region. The maximum value of southerly wind in the MJO 7/8 composite is 16ms^{-1}, while in MJO 3/4 southerly wind exceeds 25ms^{-1}, resulting in stronger topographically forced vertical motions (not shown).

Based on the snowfall distribution shown in Figs. 4 and 5 it is clear that windward facing slopes receive the majority of snowfall and that further downwind, accumulation decreases at each subsequent orographic feature. The downwind decrease in snowfall can be explained by differences in the mixing ratio, which is considerably higher for extreme events in MJO phase 7/8. The snowfall distributions are similar across event categories, despite considerable differences in dynamic and thermodynamic contributions to generating orographic precipitation, and are largely defined by first-order orographic effects (Roe, 2005). In MJO phase 7/8 events, extreme precipitation is achieved despite relatively weak dynamical forcing, largely on account of increased available moisture and reduced stability at the orographic barrier, as observed through theta-e profiles (discussed below in subsection 3.6f). Extreme precipitation is generated in phase 3/4 events by comparatively strong vertical ascent on windward slopes (not shown), which effectively forces precipitation despite reduced moisture. Neutral-case events benefit from enhancements of both available moisture and cross-barrier wind speed, with mixing ratios exceeding 6.5g kg^{-1} and southerly winds in excess 25ms^{-1} along the transect.

ii. Modified Experiments

The general patterns of moisture availability and cross-barrier wind in modified topography experiments (Fig. 5; right column) are similar across event types. However,

differences in the strength of cross-barrier winds, the amount of available moisture, and the distribution of snowfall between original and modified topography experiments are evident. In all modified topography simulations, southerly wind is intensified and moisture propagates further north than in original topography simulations on account of topographic smoothing. The area of $25ms^{-1}$ ($20ms^{-1}$) southerly wind aloft increases in size in the neutral and MJO 3/4 (7/8) composites. The elevation profile in the coarse-topography experiments exhibits a single large hill, with precipitation peaking upstream of the crest and gradually tapering-off northward. The precipitation distribution of the 6.67km topography experiment exhibits multiple peaks co-located with windward ridges, while valleys in the interior receive relatively little precipitation due to gravity wave induced descent and evaporation (Colle, 2008). The secondary maximum in precipitation in the original topography experiments, at the latitude of the Karakoram, benefits from moisture transported through the Indus river valley. In the smooth topography case, precipitation at the approximate latitude of the Karakoram is in the lee of the single maximum that appears at approximately 3500m elevation.

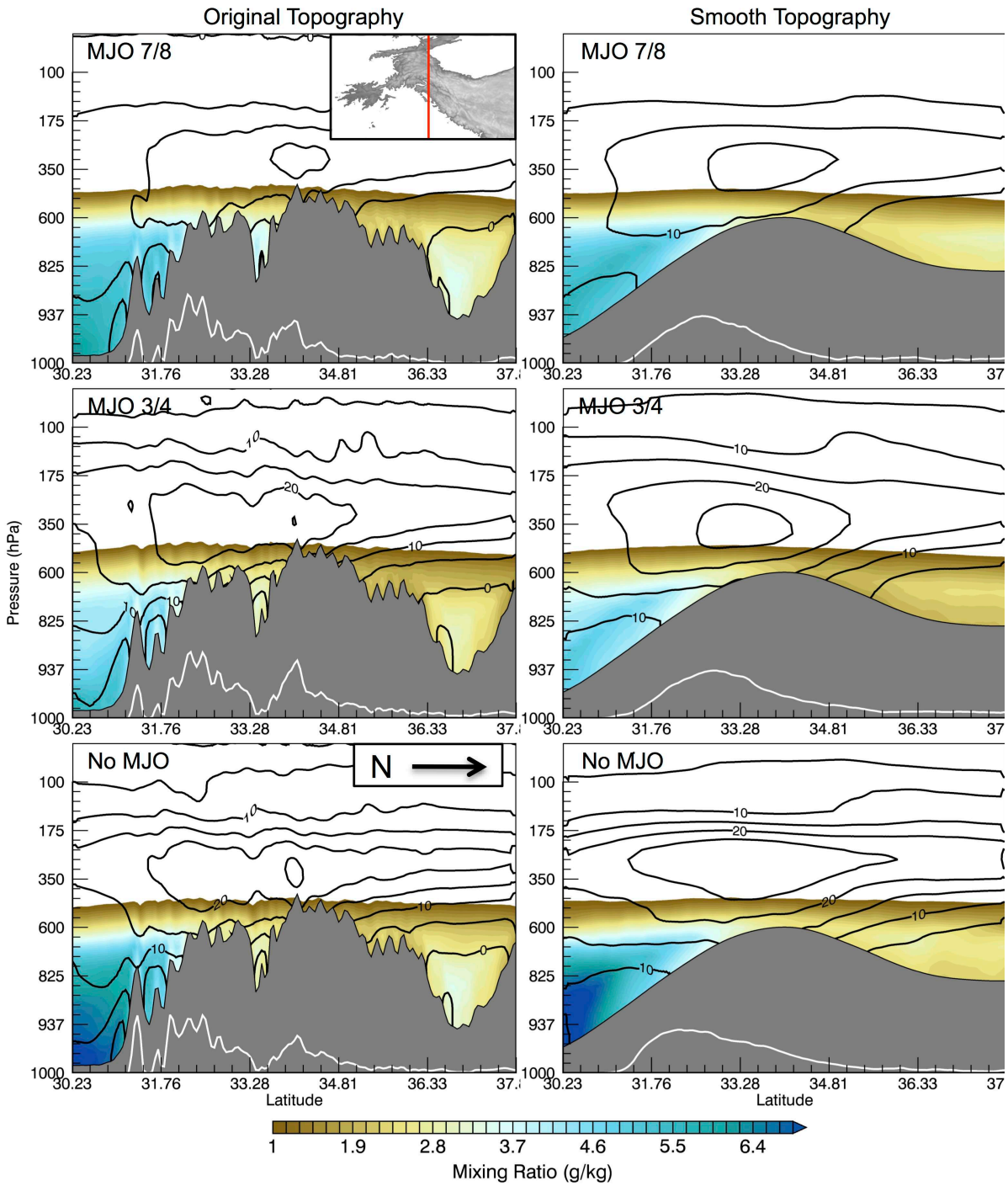

Figure 5 – Vertical transect composites of mixing ratio (color) and southerly 500-hPa wind (contour) during extreme precipitation events in the Karakoram in MJO phases 7 and 8 with ENSO neutral conditions (top), MJO phase 3/4 with ENSO neutral (middle), and neutral MJO and ENSO conditions (bottom). Topography is shaded gray, and the white line indicates the location of snowfall accumulation (standardized to show spatial distribution). Original topography experiments occupy the left column and modified topography experiments are shown on the right.

c. 500-hPa Geopotential Height: Control vs. Modified Topography Experiments

The changes in cross-barrier windspeeds across experiment types shown in Fig. 5 are explained by differences in the simulated development of WD. The influence of topographic smoothing on 500-hPa geopotential height anomalies associated with WD for each event category is shown in Fig. 6. In smoothed topography simulations WD are dynamically stronger, as evidenced by deeper geopotential height anomalies. MJO 3/4 experiments with smoothed topography exhibited a deepening of the composite WD trough by more than 30gpm. The center of each WD in all event categories recorded a lower 500-hPa geopotential height in the modified topography simulation than its original-topography counterpart. The mean of the differences between trough depths in original and modified topography experiments, which were uniformly negative, were found to be significantly different from a hypothetical unbiased set of events (mean difference of zero) based on a t-test ($p < 0.05$).

It is also important to note that the ridge ahead of the trough was significantly amplified in the modified topography simulations. The deeper troughs and more pronounced ridges of the modified topography experiments are evident in the enhanced dipole structure shown in Fig. 6 (right column), which infers enhanced development of WD, an intensified geopotential height gradient, and intensified southerly cross-barrier winds over western High Mountain Asia (as observed in Fig. 5). Topographic smoothing has a significant effect on WD dynamics here, and has previously been shown to degrade the skill of mesoscale models in simulating extratropical cyclones near topography (Weyngandt and Seaman 1994). We hypothesize that the observed bias is attributable to either reduced mountain drag (Carlson, 1998), or the effect of differences in mountain height on vorticity generation, as explained in

quasi-geostrophic theory (Holton and Hakim, 2014), or a combination of factors, though this is not tested. Here we demonstrate that the modification of the intensity of cross-barrier winds is an important factor in determining the spatial and temporal distribution of precipitation.

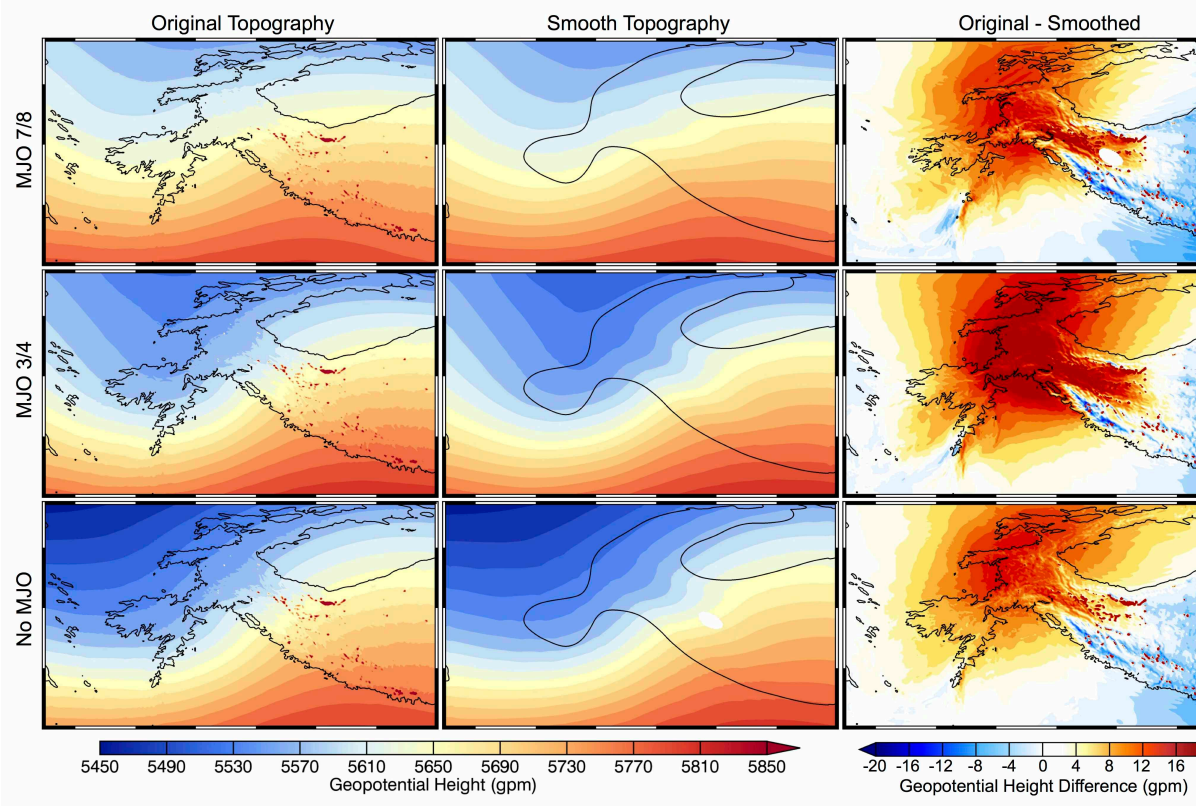

Figure 6 – Composites of 500-hPa geopotential height during extreme precipitation events in the Karakoram in MJO phases 7 and 8 with ENSO neutral conditions (top), MJO phase 3/4 with ENSO neutral (middle), and neutral MJO and ENSO conditions (bottom). The 2000m topography contour is outlined in black. Original topography experiments occupy the left column and modified topography experiments are shown on the middle column. The difference between the two experiment types is shown in the right column for each event category.

d. Differences in Modified Topography Simulation

Prior work identified that moisture availability and cross-barrier winds are the primary determinants of the magnitude of orographic precipitation during WD (Cannon et al.

2015). Figure 7 shows the spatial distribution and magnitude of differences between modified topography simulations and control experiments for 2m specific humidity, 500-hPa meridional winds and snowfall, for all 33 events, irrespective of category. The mean of the differences between original and modified topography experiments is shown only for gridpoints that exhibited statistically significant difference (t-test; 5% significance level).

Topographic smoothing in modified topography experiments resulted in increased 2m specific humidity over much of High Mountain Asia, primarily due to higher temperatures and saturation vapor pressure at lower altitudes. The entire Himalayan front exhibits a 2-3g/kg increase in 2m specific humidity in modified topography simulations, primarily because topography is lower and air-temperature is higher, thus the air holds more moisture (Clausius-Clapeyron relationship). Similarly, low-elevation areas adjacent High Mountain Asia and valleys in the interior of topography exhibit a decrease in humidity associated with increased surface elevation resulting from the smoothing/redistribution of High Mountain Asia's mountains. In addition to direct elevation changes, topographic smoothing results in less efficient blocking of moist flow, allowing moisture to advect further into the interior, while the smoothing of valley systems, such as the Indus River Valley, reduces moisture transport to the interior through these conduits (Curio et al. 2014). Moisture transport is discussed in detail in Section 3.6f.

Section 3.6c identified that topographic smoothing also alters WD strength. The intensified 500-hPa geopotential height gradient (Fig. 6) in modified topography experiments is shown to enhance cross-barrier winds (Fig. 7). The average magnitude of 500-hPa winds over the entire domain increased 7% in modified topography experiments (Table 2; discussed in detail Section 3.6e). Although topographic smoothing enhances WD dynamics and

moisture availability, Fig. 7 indicates that the maximum precipitation magnitudes are not enhanced in modified-topography simulation. Rather, precipitation is redistributed according to changes in topography and thus, orographic forcing. Generally, the steep slopes of the western Himalaya and Karakoram exhibit significant reductions in snowfall, while lower elevations experience significant increases, according to the redistribution of slopes that force orographic motions in the modified topography experiments. While the redistribution is not surprising, and could have been inferred by simply looking at the difference between topography, the following section demonstrates that changes in orographic forcing, WD dynamics, available moisture and stability have significant influences over total accumulated precipitation in High Mountain Asia.

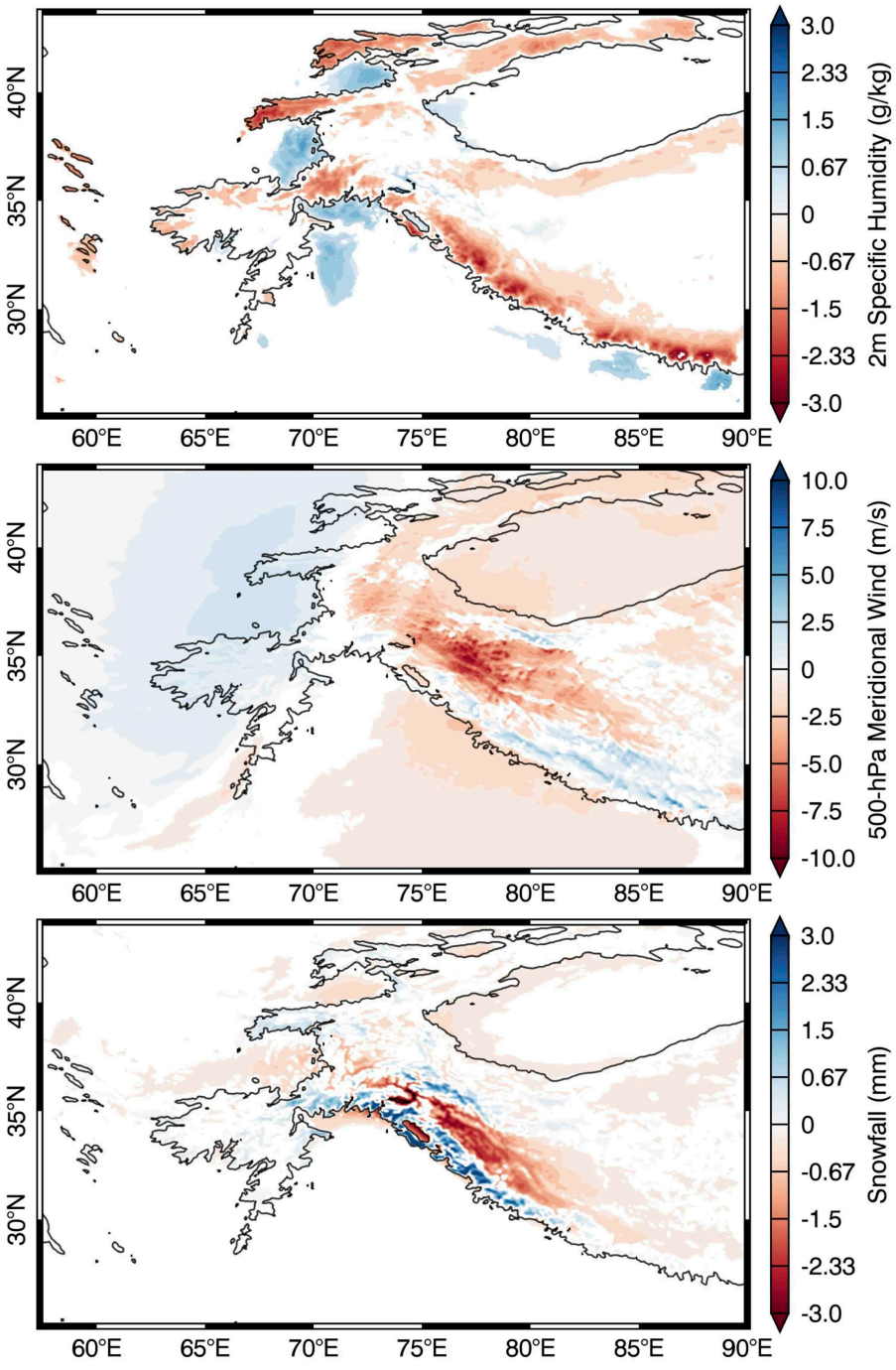

Figure 7 – Statistically significant differences in 2m specific humidity (top), 500-hPa meridional wind (middle) and snowfall (bottom) between original topography and modified topography simulations (all 33 events are included). Red values indicate a positive bias in modified topography experiments relative to original topography experiments.

e. Effects of Simulation Differences on Orographic Forcing and Precipitation

Scatterplots of each event's averages of 2m specific humidity, 500-hPa meridional wind, snowfall, and vertical wind speed, measured over the Karakoram region (limited to grid cells with fractional glacier cover (Fig. 1; Randolph Glacier Inventory V5.0; Arendt et al. 2015) for original and modified topography simulations, are shown in Fig. 8. Additionally, their statistics are displayed in Table 2. For glaciated areas of the Karakoram, located in the interior of topography and at high elevation, specific humidity differences between phases of the MJO are not as apparent as when the large-scale is considered (Fig. 3) because of more efficient drying of the moist flow over the first orographic barriers of the Himalaya via precipitation, and considerable blocking of low-level flow. Gridpoints corresponding to the Karakoram have higher surface humidity amounts in smooth topography simulations than in the original simulations across all event categories, despite the fact that the Indus River Valley has been smoothed and does not serve as a moisture conduit. The average 2m specific humidity increase in this region is approximately 13% (Table 2). Additionally, average 500-hPa southerly wind speeds for the same group of gridpoints are approximately 34% stronger in modified topography simulations, as noted earlier in this section based on composites. MJO 3/4 events, which had an average wind-speed of 18.25ms^{-1}, increased by 38%, while MJO 7/8 events, with an average wind-speed of 10.31ms^{-1}, increased 32%.

Despite positive differences in both moisture availability and dynamical forcing in smooth-topography experiments, vertical motions over the Karakoram in modified topography simulations are a fraction of the intensity exhibited in the original simulations. The average percentage decrease in the magnitude of vertical velocity was nearly 90% across

all event categories. Given diminished vertical forcing, precipitation uniformly decreases in the modified topography simulations (average decrease of 28% across all event categories). Furthermore, because events in MJO phase 7/8 were already associated with relatively weak dynamical forcing, the reduction in orographic ascent velocities exacerbates the difference in accumulated snowfall in comparison to MJO phase 3/4 events, which see a slightly smaller reduction in snowfall on account of generally increased available moisture over lower and smoother topography (35% reduction in MJO 7/8 compared to 26% in MJO 3/4 and 19% in neutral cases).

In contrast to the high-topography of the glaciated Karakoram, specific humidity over the entire domain exhibits a negligible difference between experiment types (Fig. 8, Table 2) because elevation, which is the primary moisture control, has been redistributed so that the mean is roughly the same. The spatial redistribution of moisture is discussed in detail in the following section. Additionally, the intensification of WD in modified topography experiments results in a uniform increase in the mean magnitude of 500-hPa winds in the domain, with an average increase of 7% (Table 2), though the mean magnitude of vertical velocity was reduced by 67%. Despite reduced vertical velocities on account of topographic smoothing, snowfall increased by an average of 9% across the entire domain (rainfall increases by 6%; not shown). This result is explained through differences in vapor transport and stability in the two experiment types in the following section.

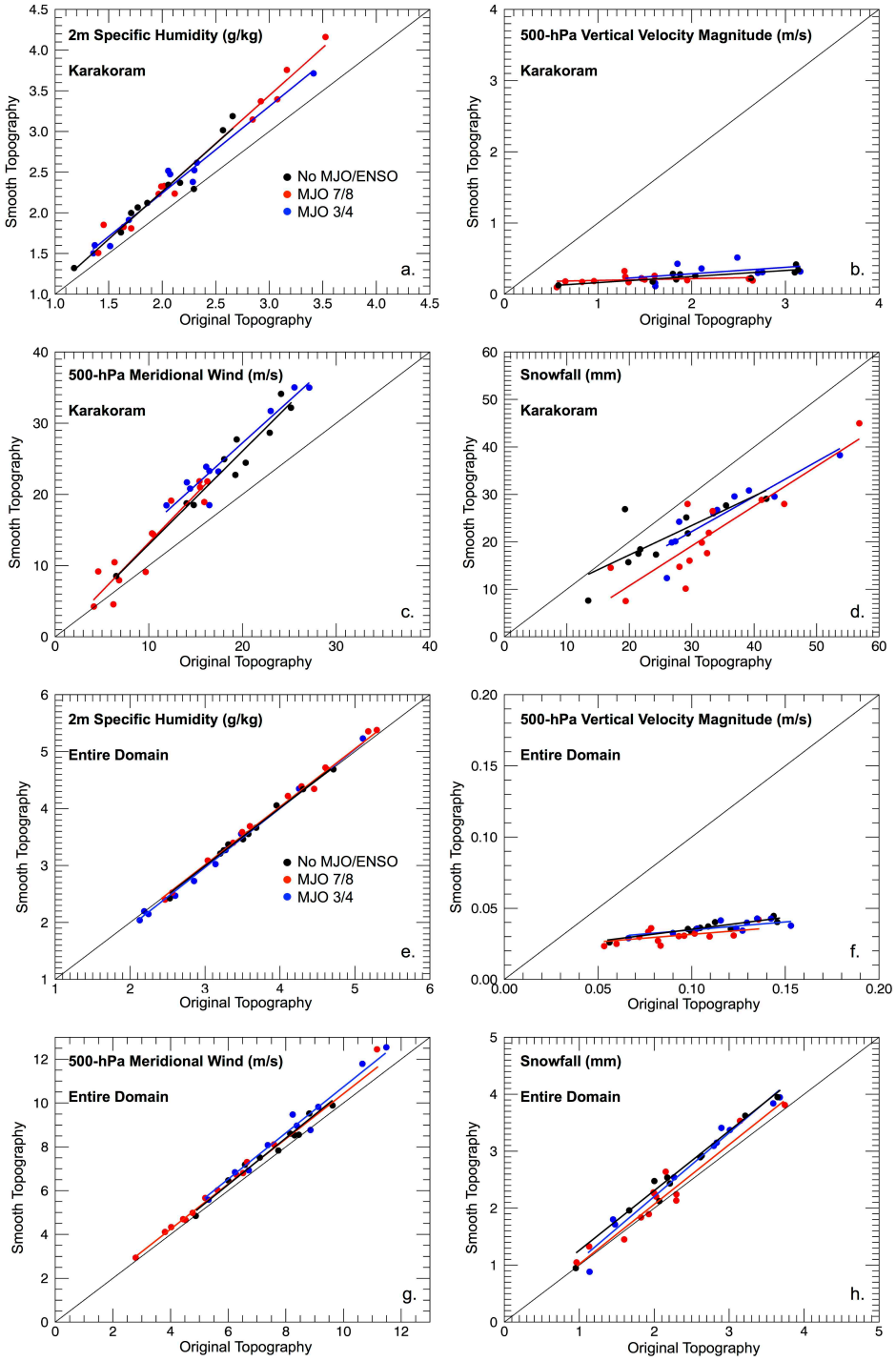

Figure 8 – Scatterplots indicate original topography (x-axis) and smoothed topography (y-axis) simulated values of area-averaged 2m specific humidity (a, e), 500-hPa meridional wind (c, g), 500-hPa vertical velocity magnitudes (absolute value; b, f) and snowfall (d, h) within the Karakoram (a-d) and the entire domain (e-h) for extreme precipitation events. Events are color-coded according to MJO activity (a), and a best-fit line is drawn for each category.

		Karakoram						WRF Inner Domain			
		3/4	**7/8**	**NEUT**	**ALL**			**3/4**	**7/8**	**NEUT**	**ALL**
Specific Humidity (g/kg)	**Orig.**	2.04	2.29	1.98	2.12	Specific Humidity (g/kg)	**Orig.**	3.12	3.93	3.6	3.59
	Coarse	2.28	2.61	2.24	2.4		**Coarse**	3.1	3.98	3.6	3.6
	Diff	0.24	0.32	0.26	0.28*		**Diff**	-0.02	0.05	0	0.01
	% Diff	12%	14%	13%	13%*		**% Diff**	-1%	1%	0%	0%
Meridional Wind (m/s)	**Orig.**	18.25	10.31	18.45	15.18	Meridional Wind (m/s)	**Orig.**	8.23	5.64	7.56	7
	Coarse	25.15	13.62	24.05	20.28		**Coarse**	8.87	6.06	7.9	7.47
	Diff	6.9*	3.31	5.6*	5.1*		**Diff**	0.64	0.42	0.34	0.47
	% Diff	38%*	32%	30%*	34%*		**% Diff**	8%	7%	4%	7%
Vertical Velocity (m/s)	**Orig.**	0.72	0.47	0.72	0.62	Vertical Velocity (m/s)	**Orig.**	0.12	0.09	0.11	0.1
	Coarse	0.07	0.06	0.07	0.06		**Coarse**	0.037	0.03	0.036	0.034
	Diff	-0.65*	-0.41*	-0.65*	-0.56*		**Diff**	-0.03*	-0.06*	-0.07*	-0.06*
	% Diff	-90%*	-87%*	-90%*	-89%*		**% Diff**	-69%*	-67%*	-67%*	-66%*
Snowfall (mm)	**Orig.**	34.87	32.73	25.6	31.22	Snowfall (mm)	**Orig.**	2.51	2.08	2.31	2.28
	Coarse	25.75	21.43	20.71	22.52		**Coarse**	2.77	2.2	2.58	2.49
	Diff	-9.12*	-11.3*	-4.89	-8.7*		**Diff**	0.26	0.12	0.27	0.21
	% Diff	-26%*	-35%*	-19%	-28%*		**% Diff**	10%	6%	12%	9%

Table 2 – Statistics of mean 2m specific humidity, 500-hPa meridional wind, 500-hPa vertical wind and snowfall for the greater Karakoram study region (left) and the glaciated, high-elevation regions of the Karakoram (right). A "*" indicates significance based on a t-test comparing the means of the two samples.

f. Vapor Transport and Stability

The average integrated vapor transport of all 33 extreme events is shown in Fig. 9 for the original and modified topography experiments. The difference between these composites illustrates that reduced blocking in the modified topography experiments allows for the transport of moisture further into topography, with the largest differences observed at and downstream of the Himalaya. The right column of Fig. 9 shows the up-slope component of vapor transport, which was calculated by projecting vapor transport into the cross-barrier direction for slopes greater than 2% and with an aspect less than 90° different than the

direction of vapor transport. This allows us to isolate the magnitude of vapor transport that is mechanically lifted by topography. The difference between original and modified topography experiments shows that the amount of vapor transport impinging on topography and being forced to rise is considerably larger in the modified topography simulations. While orographic forcing over smooth topography is considerably reduced, and precipitation rates are smaller, the total vapor transport over the entire domain is enhanced by 8% in smooth topography simulations, largely due to intensified WD dynamics, while the cross-barrier vapor transport is increased by 19%, and the cross-barrier vapor transport above 2000m elevation is increased by 14%.

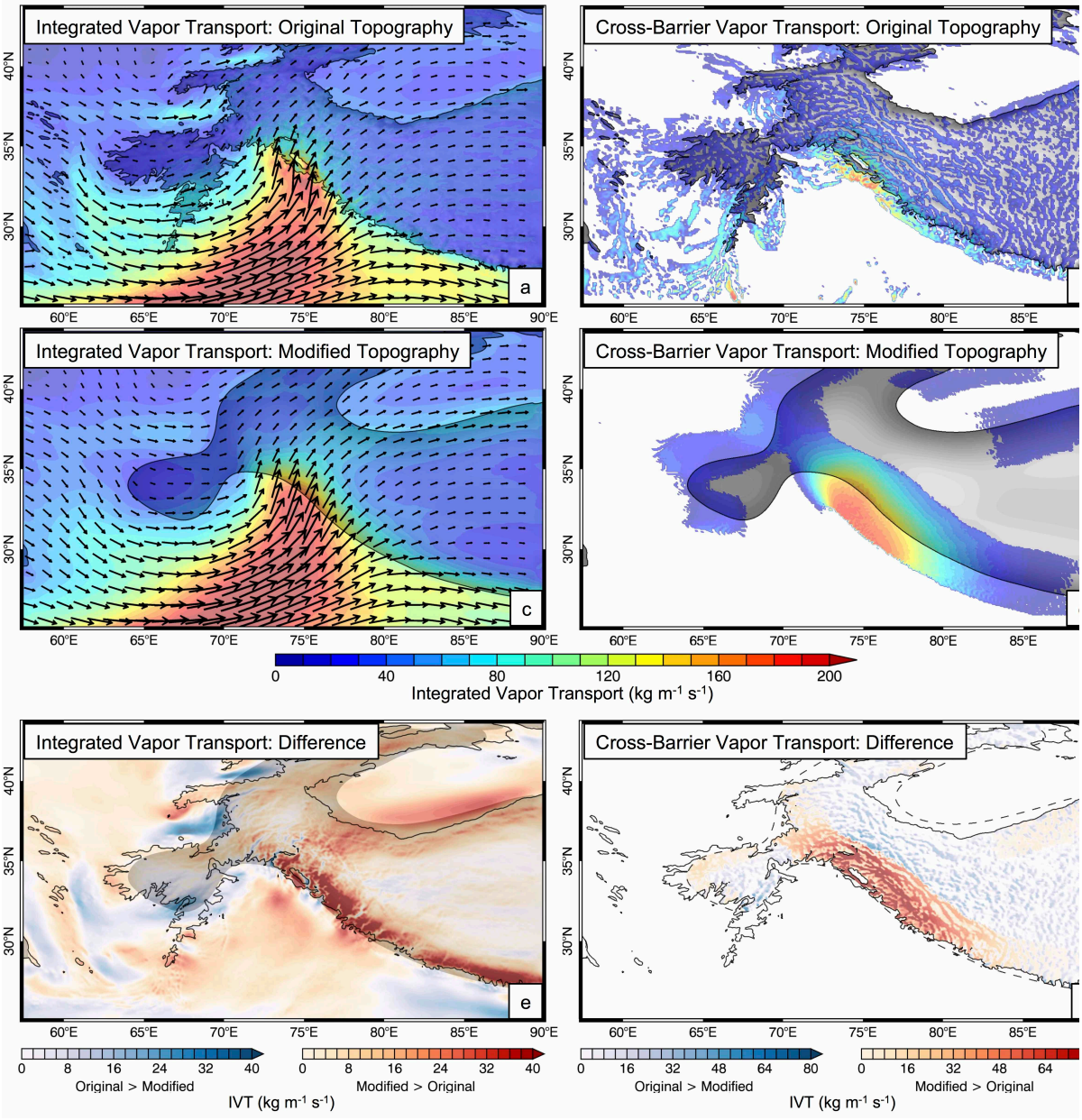

Figure 9 – Average vertically integrated moisture flux magnitude and direction for 33 extreme events across all event categories (a, c). Average cross-barrier component of moisture flux (b, d). Original topography experiment results appear in the top row and modified topography results in the middle row. The bottom row shows the difference in moisture flux magnitude between original and modified topography experiments (e), and the difference in the cross-barrier component of moisture flux above 2000m between experiment types (f). The 2000m elevation contour is shaded and outlined for each figures respective topography.

Increased near-surface heat and moisture content at high elevations in the modified topography experiments also impacts atmospheric stability. Figure 10 shows convectively available potential energy (CAPE) composites of extreme events in MJO phases 7/8 and 3/4, for both original and modified topography simulations. While CAPE values in the composites are generally low, values for foothill regions of High Asia were observed in excess of 2000J/kg at 1-hour temporal resolution during individual MJO 7/8 events (not shown). CAPE is included to illustrate spatial differences of atmospheric stability as a vertical integral. The difference between experiment types indicates that the enhanced transport of warm and moist air to high elevations in the smooth topography simulations (Fig. 9) creates conditions over the southern portion of High Mountain Asia that are comparatively less stable. Vertical transects of equivalent potential temperature across the western Himalaya and Karakoram (Fig. 11) identify increased near-surface values in smooth topography experiments relative to original topography simulations in both MJO 7/8 and 3/4 composites. The color scale is stretched to emphasize gradients over the southern slope of High Mountain Asia. In the MJO 3/4 smooth-topography composites the advection of warm moist air upslope is seen to reduce the vertical gradient of θ_e between 900 and 500-hPa above the south facing slope. Additionally, the deepening of the upper-level trough in smooth-topography simulations (subsection 3.6c) decreases temperature aloft in both MJO 7/8 and 3/4 composites, thus further reducing the vertical gradient of equivalent potential temperature and enhancing instability. The difference in CAPE between experiment types is most dramatic for the MJO 7/8 events (Fig. 10), which contain comparatively more heat and moisture than MJO 3/4 events.

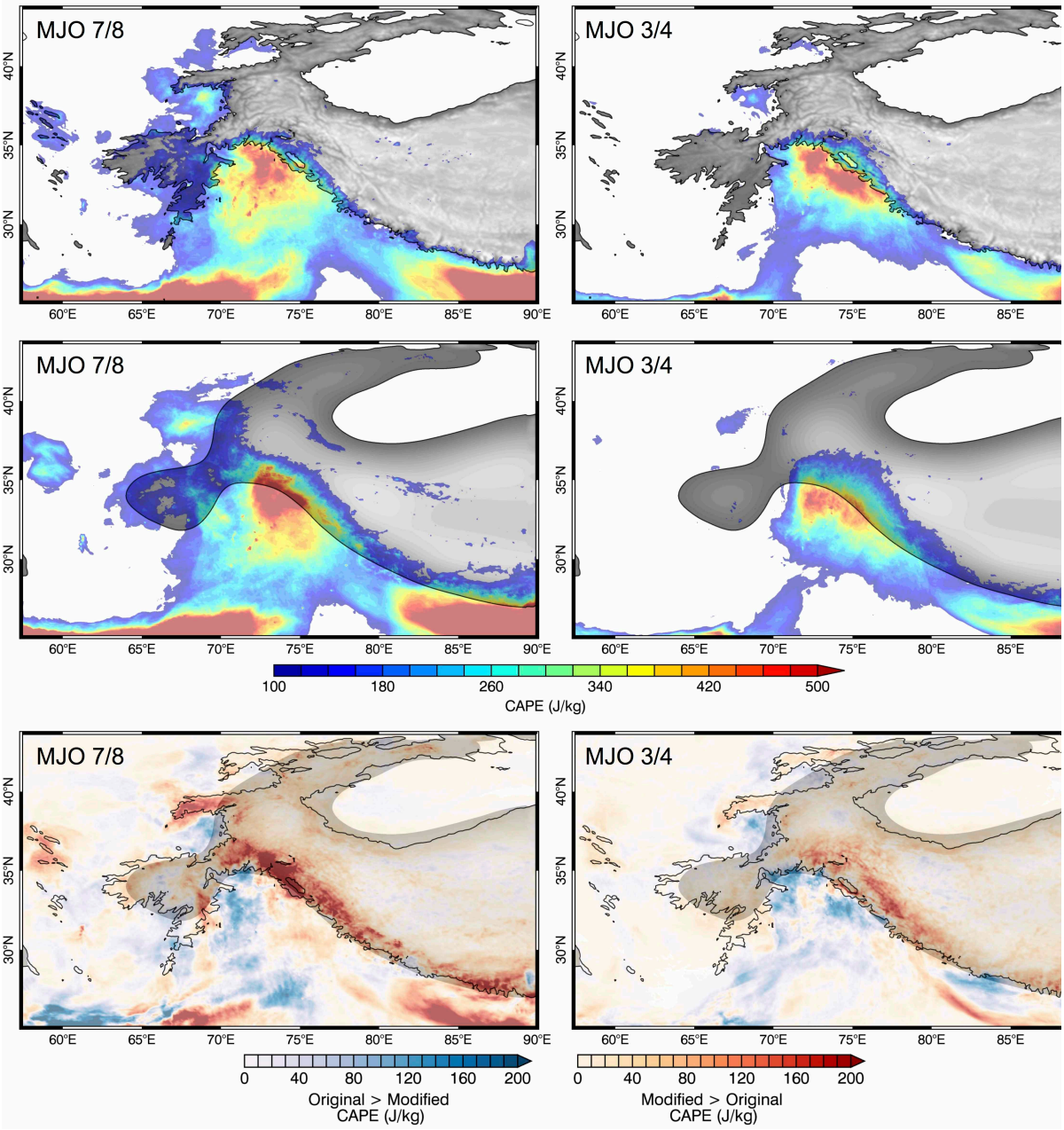

Figure 10 – CAPE values for extreme events in MJO phases 7/8 (left column) and 3/4 (right column) under original (top row) and modified (middle row) topography conditions. Differences between experiment types are shown in the bottom row. The 2000m-elevation contour for experiment types is shaded and outlined.

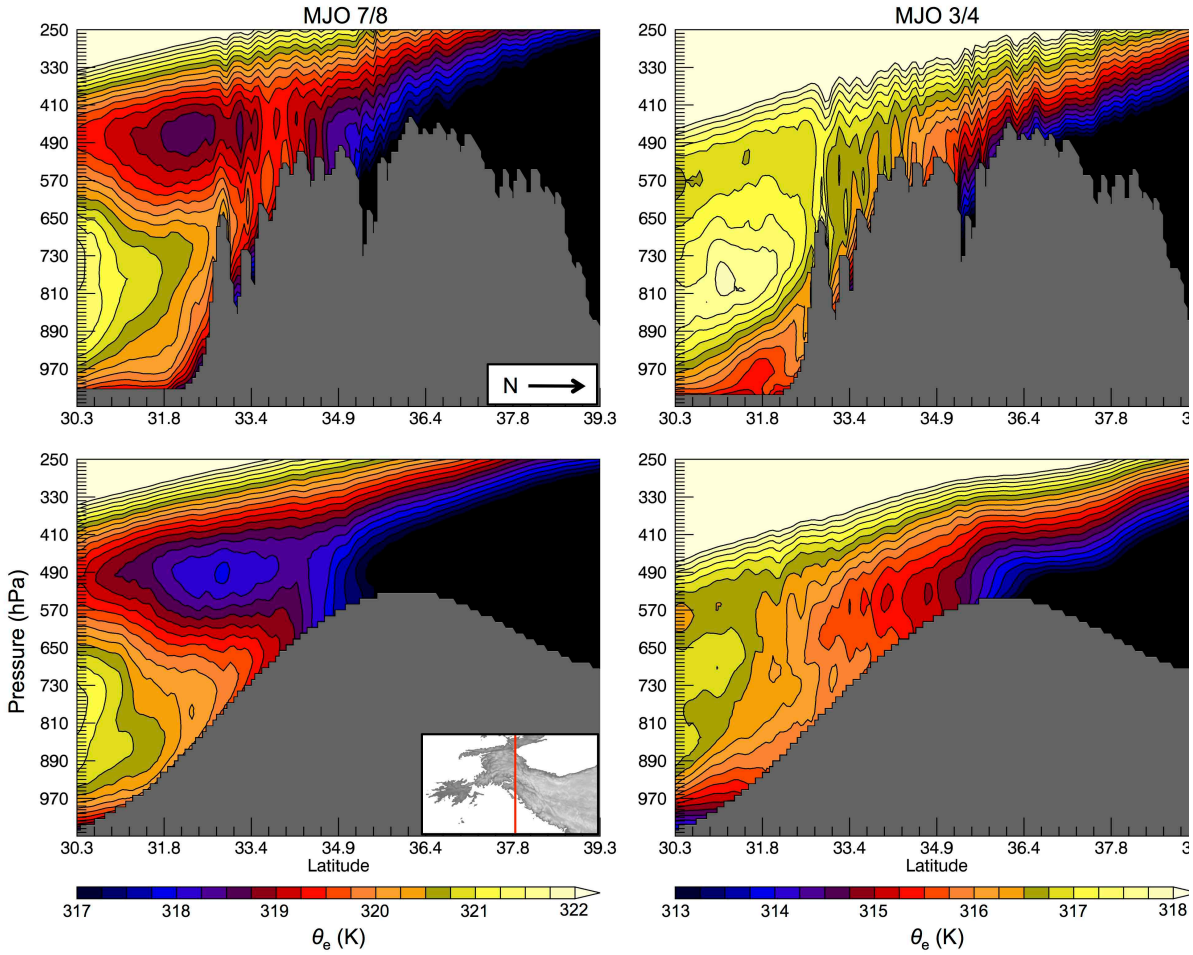

Figure 11 – Vertical transect of equivalent potential temperature (θ_e) for events in MJO phases 7/8 (left column) and 3/4 (right column) under original (top row) and modified (middle row) topography conditions. Topography is shaded gray.

In these simulations, the effect of reduced vertical forcing on precipitation that results from smooth topography is partially cancelled by the bias toward enhanced thermodynamic mechanisms. This is especially evident in MJO phases 7 and 8. Based on the 9% increase in precipitation over the entire study domain in modified topography simulation (Table 2), it appears that the effect of increased cross-barrier moisture flux and instability over smooth topography exceeds that of reduced orographic uplift on precipitation totals. While precipitation rates in smooth topography simulations do not rival those of original

topography simulations over the western Himalaya and Karakoram's steep slopes, the aggregated effect of enhanced vapor transport on precipitation over High Asia results in a positive bias, and more importantly, illustrates differences in precipitation mechanisms according to topographic resolution.

3.7 Caveats

The results of this study are not directly comparable with many idealized experiment studies, which typically evaluate the influence of changes in dynamical forcing or moisture availability independently from changes in topography, in order to isolate their effects across experiment types (e.g. Colle, 2008). The present study is unique in that the mechanisms that drive precipitation are significantly biased in modified topography experiments. Furthermore, total precipitation over High Mountain Asia is sensitive to a large number of mesoscale phenomena and microphysical processes (e.g. Medina and Houze et al. 2003). It is beyond the scope of this paper to isolate the individual influences of each of these, though overall, the moderate positive precipitation bias over High Mountain Asia in modified topography experiments is most likely a result of enhanced wind speeds and horizontal moisture flux, which outweigh the orographic lifting and microphysical processes that enhance precipitation in the original topography experiments. While computational costs limited the number of experiments that could be performed, it is clear that topographic smoothing significantly alters the simulation of WD dynamics and biases the representation of physical mechanisms that drive orographic precipitation in High Mountain Asia, based on changes in large-scale circulation, mesoscale orographic forcing, and thermodynamic influences.

3.8 Conclusions

This manuscript investigates the importance of topographic resolution in simulating the physical mechanisms that generate extreme winter precipitation events in High Mountain Asia using the Weather Research and Forecasting model (WRF). A set of experiments was performed comparing WRF simulation of extreme precipitation events with varying model topography. 33 extreme events were simulated in two experiment groups using 1) native model-resolution topography (6.67km), and 2) smoothed topography from a global circulation model (GCM; 1.875°x1.25°). WRF was configured to control for the effects of horizontal resolution by maintaining 6.67km grid spacing for both original and modified topography experiments. The 33 simulated Westerly Disturbance (WD) events were selected from 205 independent 90th percentile extreme events in the period 1979-2012 based on three unique categories of dynamical and thermodynamic contributions to precipitation.

Our investigation resulted in the following key findings on the influence of topographic smoothing on meteorological simulation:

1) Smooth topography allows for the intensification of atmospheric circulation associated with WD and generates stronger cross-barrier winds.
2) Intensified cross-barrier winds in WD and reduced topographic blocking enable enhanced vapor transport to high elevations of High Mountain Asia. This, in turn, increases available moisture and reduces stability during extreme precipitation events.
3) Smooth topography generates only a fraction of the orographic ascent observed in original topography simulations of WD, thus reducing maximum precipitation rates and total precipitation over steep topography. An approximately 28% reduction in precipitation was observed across all event categories in the Karakoram.

4) Total precipitation over the study domain is 9% greater in smoothed topography experiments, indicating that the effects of enhanced moisture transport and thermodynamics over a broad and moderate slope outweigh the negative effect of reduced orographic lift on precipitation, where steep windward slopes were smoothed.

While the magnitude of the statistics presented may be sensitive to the chosen smoothing technique and resolution in the modified topography experiments, the dynamical and thermodynamic processes that underlie the relationship between topographic smoothing and High Mountain Asia meteorology during WD events are likely robust. This research emphasizes a physical basis to investigate the effect of topographic smoothing on the simulation of precipitation, rather than focusing on statistical differences alone. In summary, simulations with smoothed topography exhibit significant biases in their representations of WD dynamics, enhanced large-scale thermodynamic precipitation mechanisms, and unrealistic precipitation in High Mountain Asia.

These findings challenge the ability of coarse-resolution GCMs to resolve orographic precipitation processes in High Mountain Asia, and the observed intensification of WD dynamics, moisture transport to high elevations and instability in smooth topography experiments pose a possible explanation for their positive regional precipitation bias (Palazzi et al. 2014). It is also likely that the effect of topographic smoothing on cyclone dynamics manifests downstream of the mountains, thus influencing the simulation of global storm tracks. It appears that the suite of GCMs that have been used to produce ensemble-mean climate projections for water resource applications in High Mountain Asia (reviewed in Miller et al. 2012) do not realistically simulate extreme winter precipitation events. These

results also show that biases in precipitation simulation are unique according to the prevailing atmospheric conditions. The influences of tropical forcing and seasonality on WD dynamics and moisture availability are thus a considerable source of uncertainty in defining GCM bias. Furthermore, future changes in moisture availability (Held and Soden, 2006) or storm tracks (Hartmann et al. 2013) affecting High Mountain Asia may produce unrealistic changes in precipitation based on the poor representation of the relationships between moisture availability, dynamical forcing and orographic precipitation in smooth topography experiments. The identification of model bias is essential to effectively utilizing GCMs to study the future fate of water resources in High Mountain Asia and beyond.

3.9 Acknowledgements

This research was supported by the Climate and Large-Scale Dynamics Program, from the National Science Foundation (NSF award-AGS 1116105) and by NASA Headquarters under the NASA Earth and Space Science Fellowship Program (Grant Number 13-EARTH13F-26). The CFSR data used in this research were developed by NOAA's National Centers for Environmental Prediction (NCEP) and provided by NCAR.

3.10 References

Arendt A, et al. (2015) Randolph Glacier Inventory – A dataset of global glacier outlines: Version 5.0. Global Land Ice Measurements from Space, Boulder Colorado, USA. Digital Media

Anders AM, Roe GH, Hallet B, Montgomerey DR, Finnegan NJ, Putkonen J (2006) Spatial patterns of precipitation and topography in the Himalaya. Geol Soc Am Spec Pap 398:39-53

Barlow M, Wheeler M, Lyon B, Cullen H (2005) Modulation of daily precipitation over southwest Asia by the Madden-Julian oscillation. Mon Weather Rev 133:3579-3594

Barros AP, Chiao S, Lang TJ, Burbank D, Putkonen J (2006) From weather to climate – Seasonal and interannual variability of storms and implications for erosion processes in the Himalaya. Geol Soc Am Spec Pap 398:17-38

Bookhagen B, Burbank DW (2010) Towards a complete Himalayan hydrological budget: The spatiotemporal distribution of snow melt and rainfall and their impact on river discharge. J Geophys Res-Earth 115

Cannon F, Carvalho LMV, Jones C, Bookhagen B (2014) Multi-annual variations in winter westerly disturbance activity affecting the Himalaya. Clim Dyn 44:441-455

Cannon F, Carvalho LMV, Jones C, Norris J (2015) Winter westerly disturbance dynamics and precipitation in the western Himalaya and Karakoram: a wave-tracking approach. Theor Appl Climatol doi:10.1007/s00704-015-1489-8

Cannon F, Carvalho LMV, Jones C, Hoell A, Norris J, Kiladis G, Tahir AA (2016) The influence of tropical forcing on extreme winter precipitation in the western Himalaya. Clim Dyn doi:10.1007/s00382-016-3137-0

Colle BA (2008) Two-dimensional idealized simulations of the impact of multiple windward ridges on orographic precipitation. J Atmos Sci 65:509-523

Curio J, Maussion F, Scherer D (2014) A twelve-year high-resolution climatology of atmospheric water transport on the Tibetan Plateau. Earth Syst Dynam 6:109-124

Dimri AP, Niyogi D, Barros AP, Ridley J, Mohanty UC, Yasunari T, Sikka DR (2015) Western disturbances: a review. Rev Geophys 53:225-246

Dudhia J (1989) Numerical study of convection observed during the Winter Monsoon Experiment using a mesoscale two-dimensional model. J Atmos Sci 46:3077-3107

Farr TG, et al. (2007) The Shuttle Radar Topography Mission. Rev Geophys, 45:1-33

Gao X, Xu Y, Zhao Z, Pal JS, Giorgi F (2006) On the role of resolution and topography in the simulation of East Asia precipitation. Theor Appl Climatol 86:173-185

Giorgi F, Marinucci MR (1996) Investigation of the sensitivity of simulated precipitation to model resolution and its implications for climate studies. Mon Wea Rev 124:148-166

Gutmann ED, Rasmussen RM, Liu C, Ikeda K, Gochis D, Clark MP, Dudhia J, Thompson G (2011) A comparison of statistical and dynamical downscaling of winter precipitation over complex terrain. J Climate 25:262-281

Hartmann DL, Klein Tank AMG, Rustucci M, Alexander LV, Bronnimann S, Charabi Y, Dentener FJ, Dlugokencky EJ, Easterling DR, Kaplan A, Soden BJ, Thorne PW, Wild M, Zhai PM (2013) Observations: Atmosphere and Surface in: Climate Change 2013: The Physical Science Basis. Contribution of Working Group I to the Fifth Assessment Report of the Intergovernmental Panel on Climate Change [Stocker TF, Qin D, Plattner GK, Tignor M, Allen SK, Boschung J, Nauels A, Xia Y, Bex V, Midgley PM (eds.)] Cambridge University Press, Cambridge, United Kingdom and New York, NY, USA.

Held IM, Soden BJ (2006) Robust responses of the hydrological cycle to global warming. J Climate 19:5686-5699

Hewitt K (2014) Glaciers of the Karakoram Himalaya: Glacial environments, processes, hazards and resources. Springer, Dordrecht, Netherlands

Hong SY, Noh Y, Dudhia J (2006) A new vertical diffusion package with an explicit treatment of entrainment processes. Mon Wea Rev 134:2318-2341

Huffman GJ et al (2007) The TRMM multisatellite precipitation analysis (TMPA): Quasi-global, multiyear, combined-sensor precipitation estimates at fine scales. J Hydrometeorol 8:38-55

Jones C (2009) A homogeneous stochastic model of the Madden-Julian Oscillation. J Clim 22:3270-3288

Kain JS (2004) The Kain-Fritsch convective parameterization: An update. J Appl Meteorol 43:170-181

Kapnick SB, Delworth TL, Ashfaq M, Malyshev S, Milly PCD (2014) Snowfall less sensitive to warming in Karakoram than in Himalayas due to unique seasonal cycle. Nat Geosci 7:834-840

Lang TJ, Barros AP (2004): Winter storms in the central Himalayas. J Meteorol Soc Jpn 82:829-844

Lutz AF, Immerzeel WW, Gobiet A, Pellicciotti F, Bjerkens MFP (2013) Comparison of climate change signals in CMIP3 and CMIP5 multi-model ensembles and implications for central Asian glaciers. Hydrol Earth Syst Sci 17:3661-3677

Madden R, Julian P (1972) Description of global-scale circulation cells in the tropics with a 40-50 day period. J Atmos Sci 29:1109-1123

Maussion F, Scherer D, Molg T, Collier E, Curio J, Finkelnburg R (2014) Precipitation seasonality and variability over the Tibetan Plateau as resolved by the High Mountain Asia Reanalysis. J Climate 27:1910-1927

Martin GM, et al. (2011) The HadGEM2 family of Met Office unified model climate configurations. Geosci Model Dev 4:723-757

Mass C, Ovens D, Albright M, Westrick K (2002) Does increasing horizontal resolution produce better forecasts?: The results of two years of real-time numerical weather prediction in the Pacific Northwest. Bull Amer Meteor Soc 83:407–430.

Medina S, Houze R (2003) Air motions and precipitation growth in alpine storms. Quart J Roy Meteor Soc 129:345-371

Miller JD, Immerzeel WW, Rees G (2012) Climate change impacts on glacier hydrology and river discharge in the Hindu Kush-Himalayas: A synthesis of the scientific basis. Mountain Res Dev 32:461-467

Mlawer EJ, Taubman SJ, Brown PD, Iacono MJ, Clough SA (1997) Radiative transfer for inhomogeneous atmospheres: RRTM, a validated correlated-k model for the longwave. J Geophys Res – Atmos 16663-16682.

Monin AS, Obukhov AM (1954) Basic laws of turbulent mixing in the surface layer of the atmosphere, TR AKad Nauk SSSR Geofiz Inst 24:163-187

Niu GY, et al. (2011) The community Noah land surface model with multiparameterization options (Noah-MP): 1. Model description and evaluation with local-scale measurements. J Geophys Res 116 doi:10.1029/2010JD015139

Norris J, Carvalho LMV, Jones C, Cannon F (2015) WRF simulations of two extreme snowfall events associated with contrasting extratropical cyclones over the Himalayas. J Geophys Res doi:10.1002/2014JD022592

Norris J, Carvalho LMV, Jones C, Cannon F, Bookhagen B (2015) The spatiotemporal variability of precipitation in the Himalaya: Validation of a one-year WRF model simulation. Clim Dyn (*submitted)*

Palazzi E, von Hardenberg J, Provenzale A (2013) Precipitation in the Hindu-Kush Karakoram Himalaya: Observations and future scenarios. J Geophys Res-Atmos 118:85-100

Palazzi E, von Hardenberg J, Terzago S, Provenzale A (2014) Precipitation in the Karakoram-Himalaya: a CMIP5 view. Clim Dyn 45:21-45

Palazzi E, Tahir AA, Cristofanelli P, Vuillermoz E, Provenzale A (2015) Climatic characterization of Baltoro Glacier (Karakoram) and northern Pakistan from in-situ stations. *Engineering Geology for Society and Territory*. Springer, Switzerland

Park S, Schowengerdt R (1983) Image reconstruction by parametric cubic convolution. Comput Vis Graph Im Proc. 23;258-272

Rasmusson EM, Carpenter TH (1982) Variations in tropical sea surface temperature and wind fields associated with the southern oscillation/El Nino. Mon Wea Rev 111:517-528

Ridley J, Wiltshire A, Mathison C (2013) More frequent occurrence of westerly disturbances in Karakoram up to 2100. Sci Total Environ 468-469:S31-S35

Roe GH (2005) Orographic Precipitation. Annu Rev Earth Planet Sci 33:647-671

Saha S et al (2010) The NCEP Climate Forecast System Reanalysis. B Am Meteorol Soc 91:1015-1057

Shea JM, Immerzeel WW, Wagnon P, Vincent C, Bajracharya S (2015) Modelling glacier change in the Everest region, Nepal Himalaya. The Cryosphere 9:1105-1128

Singh P, Ramasastri KS, Kumar N (1995) Topographical influence on precipitation distribution in different ranges of western Himalayas. Nord Hydrol 26:259-284

Skamarock WC, Klemp BJ, Dudhia J, Gill DO, Barker DM, Duda MG, Huang XY, Wang W, Powers JG (2008) A description of the Advanced Research WRF Version 3. NCAR Technical Note – 4751STR

Soncini A, Bocchiola D, Confortola G, Nana E, Bianchi A, Rosso R, Diolaiuti G, Smiraglia C, von Hardenberg J, Palazzi E, Provenzale A, Vuillemoz E (2015) Hydrology of the upper Indus Basin under potential climate change scenarios. *Engineering Geology for Society and Territory*. Springer, Switzerland pp43-49

Su F, Zhang L, Ou T, Chen D, Yao T, Tong K, Qi Y (2016) Hydrological response to future climate changes for the major upstream river basins in the Tibetan Plateau. Glob Planet Change 136:82-95

Tahir AA, Chevallier P, Arnaud Y, Ahmad B (2011) Snow cover dynamics and hydrological regime of the Hunza River basin, Karakoram Range, Northern Pakistan. Hydrol Earth Syst Sci 15:2275-2290

Thompson g, Field PR, Rasmussen RM, Hall WD (2008) Explicit forecasts of winter precipitation using an improved bulk microphysics scheme. Part II: Implementation of a new snow parameterization. Mon Wea Rev 136:5095-5115

Wehner M (2013) Methods of projecting future changes in extremes. *Extremes in a Changing Climate*. 223-237 Springer, Netherlands

Wenygand SS, Seaman NL (1994) Quantification of predictive skill for mesoscale and synoptic scale meteorological features as a function of horizontal grid resolution. Mon Wea Rev 122:57-71

Wilks DS (2006) Statistical methods in the atmospheric sciences. Elsevier, Burlington

Wulf H, Bookhagen B, Scherler D (2016) Differentiating between rain, snow, and glacier contributions to river discharge in the western Himalaya using remote-sensing data and distributed hydrological modeling. Adv Water Resour 88:152-169

World Climate Research Program Coupled Model Intercomparison Project – Phase 5 (CMIP5), CLIVAR Exchanges 56, Vol 16, 32pp, 2011

Yorgun MS, Rood RB (2015) An object-based approach for quantification of GCM biases of the simulation of orographic precipitation. Part I: Idealized simulations. J Climate 27:9139-9154

Conclusion

The current state and future fate of High Mountain Asia's glaciers and snowpack are of central importance for water, food, and power supply of densely populated regions in south, east, and central Asia. In addition to the highly seasonal summer rainfall, winter snowpack accumulation from westerly disturbances (WD) is important for discharge during dry periods in spring and fall. However, observation, understanding, and prediction of regional climate remain poorly understood. ***This dissertation provides novel insight and improves understanding of High Mountain Asia climate through three interconnected research objectives:***

1) Investigate the dynamics of WD and define how these systems generate extreme precipitation events in High Mountain Asia (Chapter 1).
2) Establish the relationships between WD and global atmospheric variability, emphasizing the role of tropical forcing in event-to-event variability (Chapter 2).
3) Use a mesoscale model to evaluate the importance of resolving High Mountain Asia's topography in simulating the relationships between orographic precipitation, WD and global circulation (Chapter 3).

The individual studies that comprise this dissertation represent a thorough investigation of KH climate with numerous unique and important findings that have contributed to the scientific understanding of High Asia's hydroclimate.

A novel wave-tracking algorithm was developed in Chapter 1 of this dissertation to provide an inventory of location, timing, intensity, and duration of WD events, allowing for a comprehensive study of the mechanisms within WD that drive orographic precipitation, on an individual event basis and in the aggregate. This work identified the relationship between

the strength of disturbances, the state of the background environment during their propagation, and precipitation totals in western High Asia. The study demonstrated significant differences in convective (thermodynamic) and mechanical (dynamic) instability contributions to orographic precipitation as a function of the intensity of WD and background temperature and moisture. Dynamic forcing is the most important driver of orographic precipitation during intense WD with strong cross-barrier winds, while weaker WD with similar precipitation totals are observed to benefit from relatively more available moisture and enhanced instability, occurring primarily in the late winter/premonsoon. These results indicated that changes in the frequency or intensity of WD alone were not sufficient to infer changes in winter orographic precipitation. Variability in the influence of these factors on a case-by-case basis is also attributable to natural variability, including tropical-extratropical interactions, as identified in Chapter 2.

The second chapter of this dissertation focused on the role of tropical forcing in modifying the background state of the atmosphere through which WD propagate. On interannual time-scales, El Niño related changes in tropical diabatic heating induce a Rossby wave response over southwest Asia that is linked with enhanced dynamical forcing of WD and available moisture. Consequently, extreme orographic precipitation events are more frequent during El Niño than La Niña or neutral conditions. A similar spatial pattern of tropical diabatic heating is produced by the Madden Julian Oscillation (MJO) at intraseasonal scales. In comparison to El Niño, the Rossby wave response to MJO activity is less spatially uniform over southwest Asia and varies on shorter time-scales. This research found that the MJO's relationship with WD and High Asia precipitation is more complex than that of the El Nino Southern Oscillation. Phases of the MJO propagation cycle that favor the dynamical

enhancement of WD simultaneously suppress available moisture over southwest Asia, and vice versa. As a result, extreme precipitation events in the KH occur with similar frequency in most phases of the MJO, however, there is a transition in the relative importance of dynamical forcing and moisture availability in WD to orographic precipitation in High Asia as the MJO evolves. This research is unique relative to previous studies because of its focus on extreme events, rather than monthly or seasonal averages. The study's findings give insight into the dynamics and predictability of extreme precipitation events in the KH through their relationship with global atmospheric variability, and are an important consideration in evaluating Asia's water resources.

The final chapter of this dissertation built on previous efforts to develop regional downscaling of reanalysis data over High Asia (Norris et al. 2015; 2016). Downscaling of extreme precipitation event case studies benefits the investigation of High Mountain Asia hydroclimate by more realistically representing regional orographic precipitation processes and meteorological forcing than is possible with reanalyses. The optimal model configuration from research by Norris et al. (2015; 2016) was utilized to perform a set of modified topography experiments in which WD-generated extreme precipitation events in High Mountain Asia were simulated at 6.7km resolution with the model's original topography, and then using smoothed topography taken from a 1.875°x1.25° resolution global circulation model. The experiments' objective was to evaluate the importance of resolving High Mountain Asia's topography in simulating the relationships between orographic precipitation and WD.

Modified topography experiments illustrated that topographic smoothing fundamentally alters the mechanisms in westerly disturbances that produce orographic

precipitation. Smooth topography simulations exhibited stronger cross-barrier winds and intensified WD dynamics. Topographic smoothing also reduced mountain blocking and enabled enhanced vapor transport to high elevations of High Mountain Asia, which increased available moisture and reduced stability during extreme precipitation events. However, smooth topography experiments generated only a fraction of the orographic ascent observed in original topography simulations of WD over the Karakoram and western Himaalaya, thus precipitation rates and total precipitation for these specific regions were drastically reduced. Contrastingly, the entire study region's area-averaged precipitation increased in smoothed topography simulation of WD. This increase indicated that the effects of enhanced moisture transport and thermodynamics in generating precipitation over a broad and moderate slope outweigh the negative effect of smoothing the most pronounced orographic features. These findings identify an important source of bias in coarse-resolution simulated precipitation in High Asia and are an important consideration for the application of global circulation models toward projecting regional hydroclimate in the 21st century.

Collectively, the three chapters of this dissertation give novel insight into the dynamics of extreme precipitation events in High Mountain Asia, their relationships with global atmospheric variability, and the ability of global circulation models to simulate them. These findings advance the scientific community's understanding of weather and climate in High Mountain Asia and improve the potential for evaluating the current state and future fate of regional water resources.

Suggestions for Future Work

The research presented in this dissertation emphasized the relationship between westerly disturbances and extreme precipitation events in High Mountain Asia. A notable limitation to this research is the lack of available precipitation measurements in the region and the lack of confidence in extant data. Station precipitation measurements are biased toward low elevation, populated river valleys, while the few instruments placed at high elevations experience issues ranging from undercatch, to data gaps that arise due to the difficulty of maintaining remote stations in that part of the world. Precipitation estimates from satellites are also problematic. In this work we evaluated precipitation from the multisatellite TRMM 3B42 V7 product, which has documented difficulties in estimating light and solid-state precipitation (Lang and Barros, 2006).

Future work would benefit greatly from higher quality precipitation data. While there is little confidence in available station data and a general lack of availability, investigating the ability of new remote sensing platforms, including the Global Precipitation Measurement mission (GPM), could prove exceptionally useful for improving precipitation and snowfall estimates in High Mountain Asia. GPM's dual-frequency precipitation radar (DPR) is capable of accurately estimating snowfall, and its application in High Mountain Asia should yield an improvement over TRMM. Comparisons of GPM-DPR overpasses during snowfall events with mesoscale model output would help to understand the abilities and shortfalls of both models and GPM in representing regional precipitation.

With respect to mesoscale modeling in High Mountain Asia, preliminary work indicated that WRF could be improved by replacing lower boundary initial conditions with satellite-derived estimates of the land surface, including; snow water equivalent, soil moisture and surface temperature. More realistic lower boundary conditions were observed to

modify meteorological simulation, including convective precipitation in the Himalaya. Continued effort should be invested toward maximizing the ability of remote sensing to garner the best possible near real-time estimates of the land surface for WRF initialization. Furthermore, validation should be extended to include various satellite sensors that provide vertical profiles of the atmosphere, including CloudSat and GPM-DPR. Previous analyses only evaluated WRF against 2D surface fields from remote sensing platforms, including snowcover, precipitation and surface temperature. Improved mesoscale model simulation in these regions could benefit hazard forecasting and resource management, as local agencies rely on their output for daily operations.

Additionally, more should be done to evaluate the 35 years of dynamically downscaled data that the CLIVAC group has produced at 6.7km horizontal resolution. This dataset has the potential to illuminate spatial gradients in climate variability and trends across High Asia, and is sufficiently high-resolution to evaluate the simulated climate of individual glaciers. Downscaled meteorological data is essential to investigating the role of climate in glacier trends across High Mountain Asia in recent decades. This work would further benefit from collaboration with field scientists working on Karakoram glaciers that have documented positive mass-balance trends, such as the Batura Glacier (Boerst et al. 2013).

At the regional scale, Coupled Model Intercomparisson Project (CMIP) simulations of future climate scenarios over High Mountain Asia should be evaluated based on the findings of this dissertation. The analyses presented in Chapters 1 and 2 of this dissertation should be applied toward global climate model simulations under representative control pathway 8.5 forcing. Furthermore, individual models to be included in future work should be selected based on the evaluation presented in Chapter 3. Investigating future changes in the

dynamic and thermodynamic precipitation mechanisms that are associated with WD, at coarse resolution, will yield a basic idea of future changes in the primary drivers of winter precipitation in High Mountain Asia, independent of any individual model's simulation of precipitation. Furthermore, results from CMIP analyses should be evaluated against the findings of the present dissertation to better understand possible sources of error or bias in global circulation models. Identifying bias in the representation of key components of High Mountain Asia's climate in CMIP models will benefit their application toward projecting High Mountain Asia's water resources through the 21st century.

Additional effort should also be invested toward discussing the results of this dissertation, and future work, with hydrologists and glaciologists working in High Mountain Asia. Ultimately, the goal of this research is to provide climate information and products that are useful to the scientific community, as a whole, and that will improve the understanding of the current state and future fate of water resources in High Mountain Asia.

References

Barros AP, Chiao S, Lang TJ, Burbank D, Putkonen J (2006) From weather to climate – Seasonal and interannual variability of storms and implications for erosion processes in the Himalaya. Geol Soc Am Spec Pap 398:17-38

Cannon F, Carvalho LMV, Jones C, Bookhagen B (2014) Multi-annual variations in winter westerly disturbance activity affecting the Himalaya. Clim Dyn 44:441-455

Cannon F, Carvalho LMV, Jones C, Norris J (2015) Winter westerly disturbance dynamics and precipitation in the western Himalaya and Karakoram: a wave-tracking approach. Theor Appl Climatol doi:10.1007/s00704-015-1489-8

Cannon F, Carvalho LMV, Jones C, Hoell A, Norris J, Kiladis G, Tahir AA (2016) The influence of tropical forcing on extreme winter precipitation in the western Himalaya. Clim Dyn doi:10.1007/s00382-016-3137-0

Dimri AP, Niyogi D, Barros AP, Ridley J, Mohanty UC, Yasunari T, Sikka DR (2015) Western disturbances: a review. Rev Geophys 53:225-246

Norris J, Carvalho LMV, Jones C, Cannon F (2015) WRF simulations of two extreme snowfall events associated with contrasting extratropical cyclones over the Himalayas. J Geophys Res doi:10.1002/2014JD022592

Norris J, Carvalho LMV, Jones C, Cannon F, Bookhagen B (2015) The spatiotemporal variability of precipitation in the Himalaya: Validation of a one-year WRF model simulation. Clim Dyn (*submitted)*